USING VINCULIN MUTANTS TO ASCERTAIN THE ROLE OF VINCULIN IN CELLULAR MOTILITY AND MECHANOTRANSDUCTION

by

Leilani M. Sharpe

A dissertation submitted to Johns Hopkins University in conformity with the requirements for the degree of Doctor of Philosophy

Baltimore, MD

February 2014

Thesis Abstract:

Vinculin is a 117kDa soluble cytoplasmic protein that localizes to focal adhesions. Biochemical studies show that vinculin tail binds actin and vinculin head binds talin. These ligand binding interactions imply a role for vinculin as a mechanical linker between the actin cytoskeleton and the extracellular matrix. The consensus within the field is that expression of vinculin increases the adhesion of cells to the extracellular matrix and slows cellular migration speed. Vinculin is also implicated in the cellular mechanotransduction response because focal adhesion size is positively correlated with increased traction force between a cell and its substrate and because vinculin is recruited to focal adhesions with the application external force to a cell. The binding sites for many of vinculin's ligands are regulated by an autoinhibition mechanism inherent to the structure of vinculin. However, it is unknown how vinculin's autoinhibition and vinculin's interactions with its ligands regulate vinculin's role in cellular migration and mechanotransduction. To study vinculin's role in these processes, a panel of vinculin ligand binding and autoinhibition mutants were expressed in an embryonic fibroblast line isolated from a *Vcl*-null mouse. I used timelapse microscopy to quantify the effect of vinculin and vinculin mutants on the speed of randomly migrating cells. My data shows that the presence of vinculin has no significant effect on cell speed. This result was unexpected, but it is in agreement with one other publication on the random migration of *Vcl*-null versus vinculin-expressing cells. To investigate another phenotype of vinculin-expressing cells, I developed a device capable of introducing uniaxial stretch to silicone-based cell culture chambers. This device was used to apply stretch to live cells in order to quantify mechanoresponsive change in mature vinculin-containing focal adhesions.

My data shows that mature focal adhesions do not increase in size or number with greater frequency than unpaired, timelapse controls. This lack of force-dependent change in mature focal adhesions suggests the hypothesis that effects of external forces are restricted to a different subpopulation of focal adhesions, possibly nascent focal adhesions.

Research Advisor: Susan W. Craig, Ph.D.

Thesis Reader: Douglas Robinson, Ph.D.

Foreword:

This thesis would not have been possible without the support and generous intellectual input of many people, all of whom I would profusely thank if Johns Hopkins would let me write another thesis-length manuscript. First and foremost, I would like to thank my advisor, Dr. Susan Craig. She took me on as a graduate student and allowed me to pursue a degree in her laboratory.

My work would not have been possible without the many tools left to me by previous students of the Craig Lab. Dr. Daniel Cohen and Dr. Hui Chen, in particular, created many of the vinculin constructs that I used in my project. Many thanks are extended to the current Craig Lab members, including Dr. Suman Nanda, Thuy Hoang, and Priya Patel. Each of them shared tirelessly of their skillsets, knowledge, and unflagging support.

I must also extend thanks to the members of my thesis committee, Drs. Douglas Robinson, Joy Yang, Andrew Ewald, and Daniel Raben. Particular thanks go to Dr. Robinson, who worked with me on the computational limitations of our analysis software, kindly extended the use of his microscopy setup for several of my analyses, and agreed to serve as a reader for this thesis.

To my friends: You know I am not an overly demonstrative person. So I would just like to acknowledge publicly that this work could not have been completed without the endless support of my family and friends. My parents unwaveringly supplied support

through an educational process they did not quite understand. Through it all, they reminded of my goals when I came to Hopkins and offered whatever help they could to make sure I would make it one more day. My friends were tirelessly generous with their time, feedback, and emotional support. Each of you, every single one of you, helped to make sure that I completed this thesis.

Table of Contents

List of Tables

List of Figures

Chapter 1:

Introduction

Vinculin was originally isolated serendipitously from chicken gizzard smooth muscle and characterized as a cytosolic protein that localizes to regions where microfilament bundles meet membrane attachment sites to the extracellular matrix (Geiger, 1979; Burridge and Feramisco, 1980; Geiger *et al.*, 1980). As a novel protein with unknown function, it was named vinculin from the Latin word *vinculum*, meaning a bond signifying a union or unity (Geiger, 1979; Peng *et al.*, 2011), because its localization supported the proposal that the function of vinculin might be to participate in the linkage of the termini of microfilament bundles to cell membranes. In the 30 years since its discovery, the study of vinculin has expanded to include animal, biochemical, structural and *in vivo* functional studies to determine the role of vinculin in biology.

The function of vinculin in animals:

Vinculin is an actin cytoskeleton-associated protein that is expressed in most cells and tissues (Geiger *et al.*, 1980; Otto, 1990) and is enriched in numerous cell-matrix or cell-cell adhesion junctions (Geiger *et al.*, 1980), including the dense plaques of smooth muscle (Geiger *et al.*, 1980), subsarcolemmal lattices, and costameres of skeletal and cardiac muscle (Pardo *et al.*, 1983a; Pardo *et al.*, 1983b; Craig and Pardo, 1983; Shear and Bloch, 1985; Danowski *et al.*, 1992; Ervasti, 2003), myotendinous junctions (Shear and Bloch, 1985), and intercalated discs (Pardo *et al.*, 1983a; Koteliansky and Gneushev, 1983). Vinculin is highly conserved and is necessary for embryonic development (Bakolitsa *et al.*, 2004) in mice (Xu *et al.*, 1998a) and worms (Barstead and Waterston, 1991), but not in *Drosophila* (Alatortsev *et al.*, 1997). *C. elegans* carrying mutant copies of vinculin are paralyzed and have disorganized muscle. *Vcl*-null C. *elegans* fail to

connect their myofibrils to the plasma membrane and die at an early larval stage because they cannot move to feed (Barstead and Waterston, 1991). Mice heterozygous for vinculin expression are predisposed to stress-induced cardiomyopathy (Zemljic-Harpf *et al.*, 2004) while *Vcl*-null mice have an embryonic lethal phenotype with severe heart and brain abnormalities (Xu *et al.*, 1998a). Mice with cardiac myocyte specific excision of the vinculin gene die due to sudden cardiac death secondary to disruption of cell:cell junctions (Zemljic-Harpf *et al.*, 2007). Analyses of human tissue samples from patients with dilated cardiomyopathy (Maeda *et al.*, 1997; Olson *et al.*, 2002) show a correlation with hereditary mutations in a muscle specific splice-variant of vinculin, metavinculin (Byrne *et al.*, 1992). Cholinergic contraction of canine tracheal smooth muscle tissue results in localization of vinculin to the cell membrane (Opazo Saez *et al.*, 2004; Huang *et al.*, 2011). Furthermore, there is decreased tracheal smooth muscle contractility when mutants of vinculin that prevent the appropriate activation or ligand binding of endogenous vinculin are expressed (Huang *et al.*, 2011). Combined, these studies indicate that vinculin is involved in the assembly or maintenance of transmembrane linkages that allow the intracellular cytoskeleton to transmit force.

Vinculin is recruited to newly forming focal adhesions:

Vinculin localizes to dynamic connections called focal adhesions that link the actin cytoskeleton of a cell to the extracellular matrix (Bloch and Geiger, 1980; Geiger *et al.*, 1980; Alenghat *et al.*, 2000; Ziegler *et al.*, 2006). It is known that vinculin is recruited to focal adhesions as they mature (DePasquale and Izzard, 1987; Izzard, 1988; Ezzell *et al.*, 1997). Recent advances in our understanding of focal adhesion development indicate

that vinculin is present throughout focal adhesion maturation (Choi *et al.*, 2008). Before focal adhesion formation, the leading edge of migrating cells, also called the lamellipodium, contains dendritic actin, Arp 2/3, and cofilin. Within the lamellipodium, nascent focal adhesions assemble in an actin-dependent, myosin-independent manner, and contain vinculin, paxillin, FAK, zyxin, and GlT1. These nascent focal adhesions are short lived (60s) and typically dissemble as the wave of depolymerizing actin at the rear of the lamellipodium passes them by (Choi *et al.*, 2008). However, if the leading edge of a cell pauses, some nascent adhesions grow and elongate along actin filaments anchored to the focal complexes (Choi *et al.*, 2008) in a Rac-dependent manner (Nobes and Hall, 1995; Galbraith *et al.*, 2002) to form focal complexes. Focal complexes are twice as large as nascent focal adhesions, myosin activity dependent, and found mainly at the lamellipodium-lamellum interface (Choi *et al.*, 2008). Focal complexes continue to mature along centripetally-oriented stress fibers in a Rho-dependent manner (Izzard, 1988) as actin filaments become increasingly crosslinked by alpha-actinin and myosin II (Choi *et al.*, 2008; Oakes *et al.*, 2012) and provide a template for the hierarchical addition of additional focal adhesion components (Choi *et al.*, 2008). Vinculin's presence throughout focal adhesion maturation indicates that vinculin may play a key role in the function of focal adhesions within cells.

Studies on the structure and biochemistry of vinculin provide insight on vinculin's function:

Structural (Bakolitsa *et al.*, 2004) and biochemical studies (Coutu and Craig, 1988; Price *et al.*, 1989; Cohen *et al.*, 2005) show that vinculin is a 117kD modular protein with a

head domain (Vh) and a tail domain (Vt) that are linked by a flexible proline-rich region (Bakolitsa *et al.*, 2004) (Figure 1-1).

Figure 1-1: Structure of full-length vinculin in its autoinhibited state. Domains are shown in different colors: D1, residues 6–252; D2, 253–485; D3, 493–717; D4, 719–835; D5 (Vt), 896–1066. A short N-terminal strand ('N', residues 1–5) precedes D1. The proline-rich region (838–878) is partly disordered and precedes a 'strap' (residues 878–890), that lies across the surface of Vt and the C terminus ('C'). The known ligands for each domain are indicated and the text color matches the color of the domain of vinculin to which the particular ligand binds. (Modified from Bakolitsa 2004).

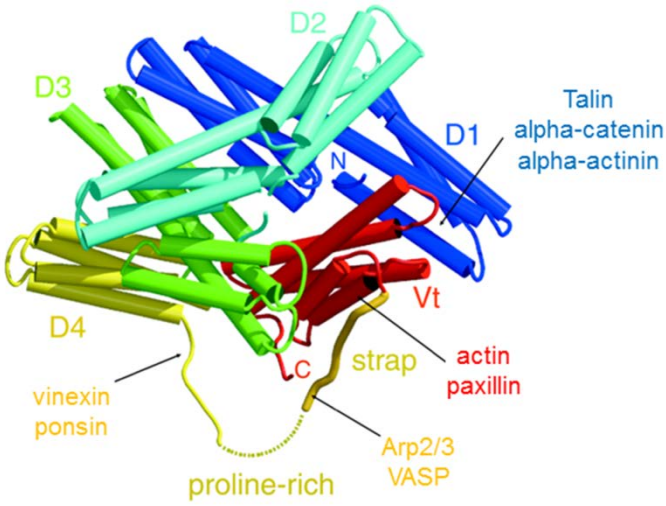

The function of vinculin is highly autoinhibited by the coupled interaction of two relatively low affinity interfaces between its head and tail domains (Johnson and Craig, 1994; Johnson and Craig, 1995b; Bakolitsa *et al.*, 2004). The flexible hinge region between Vh and Vt aids in this autoinhibition by preventing the diffusion of Vh from Vt. As a result, vinculin must be activated before it can bind to known ligands (Cohen *et al.*, 2005), and models of vinculin activation depend on the interruption of head-tail interactions (Cohen *et al.*, 2006). Activation can occur through simultaneous binding of two of vinculin's ligands talin and F-actin (Chen *et al.*, 2006). However, purified intact vinculin is tightly autoinhibited (Johnson and Craig, 1994; Johnson and Craig, 1995b) and does not bind its ligands in solution, with the exception of IpaA, a *Shigella flexneri* bacterial invasin protein (Bourdet-Sicard *et al.*, 1999). The ability of IpA to activate vinculin may reside in the presence of three vinculin binding sites (VBSs) in the C-terminus of the IpaA protein that molecularly mimic that sites for in talin for vinculin:talin interaction (Izard *et al.*, 2006; Park *et al.*, 2011) and in the presence of more than one IpA binding site on vinculin (Nhieu and Izard, 2007).

Since vinculin has no intrinsic enzymatic ability, activated vinculin must accomplish its functions through binding of its ligands. Purified domains of vinculin have been shown to bind *in vitro* to several components of focal adhesions complexes (FACs); including talin (Burridge and Mangeat, 1984), alpha-actinin (Belkin and Koteliansky, 1987) paxillin (Turner *et al.*, 1990), F-actin (Jockusch and Isenberg, 1981; Jockusch *et al.*, 1993; Menkel *et al.*, 1994; Johnson and Craig, 1995b), VASP (Brindle *et al.*, 1996; Reinhard *et al.*, 1996), Arp 2/3 (DeMali *et al.*, 2002), and vinexin/ponsin (Kioka *et al.*,

1999). Vinculin also binds acid phospholipids (Johnson and Craig, 1995a), with highest selectivity for PIP_2 (Palmer *et al.*, 2009). The role of these ligand interactions with vinculin in the cell and how they regulate vinculin function has not been tested.

FRET studies have shown vinculin's conformation is variable at focal adhesions, with lower autoinhibition conformations present in peripheral focal adhesions and higher autoinhibition conformations present in the cytoplasm and retracting areas of the cell (Chen *et al.*, 2005). This indicates that vinculin activation is involved with both the formation of nascent focal adhesions and recruitment of vinculin to existing focal adhesions.

Suggested functions for vinculin in cells:

It has been difficult to pinpoint precisely how vinculin performs its function in cells. Vinculin's presence in focal adhesions, its highly autoinhibited nature, and its many binding partners has challenged researchers to determine how the structure of vinculin and its ligand binding state may contribute to its cellular functions. Their findings suggest that vinculin may play a variety of roles within the cell.

Evidence that vinculin regulates cell adhesion and motility:

Vinculin head (Vh) co-localizes with talin, which localizes to cell-matrix adhesions (Burridge and Mangeat, 1984; Gilmore *et al.*, 1992). Vinculin (Vt) binds F-actin (Menkel *et al.*, 1994; Johnson and Craig, 1995b). These binding partners combined with vinculin's localization to sites of actin-filament associated cell adhesion indicate that one

role of vinculin may be as a mechanical linker between the actin cytoskeleton and talin (Geiger, 1979; Geiger *et al.*, 1980; Johnson and Craig, 1995b; Humphries *et al.*, 2007).

As a mechanical linker, vinculin may regulate focal adhesion formation. As an example, vinculin's interaction with talin activates transmembrane integrin heterodimers (Ohmori *et al.*, 2010). These activated integrins may then cause the phosphorylation of Focal Adhesion Kinase (FAK) (Guan *et al.*, 1991; Kornberg *et al.*, 1991) or bind directly to FAK (Schaller *et al.*, 1995; Schaller and Parsons, 1995). FAK functions as a scaffolding protein shown to interact with talin (Chen *et al.*, 1995), paxillin (Turner and Miller, 1994; Schaller and Parsons, 1995), and when autophosphorylated, generates docking sites for various Src-kinases (Cobb *et al.*, 1994; Schlaepfer *et al.*, 1994; Xing *et al.*, 1994). These studies indicate that vinculin may regulate focal adhesion formation through involvement in talin-mediated integrin activation and affecting the localization of additional focal adhesion protein to initial ECM:integrin attachment sites. By regulating focal adhesion assembly, vinculin could regulate cell adhesion and motility.

The effect of *Vcl* knockout on cellular adhesion and motility has been studied extensively in both *Vcl*-null embryonal carcinoma and fibroblast cell-lines (Table 1-1). Vinculin-deficient F9 mouse embryonal carcinoma (EC) cells adhere less well to their substrates, contain smaller focal adhesions, and extend fewer lamellipodia than wild-type F9 cells (Samuels *et al.*, 1993; Goldmann *et al.*, 1995; Volberg *et al.*, 1995). When plated on a micropatterned substrate to separate effects of cell spreading from measurements of cell adhesive strength, *Vcl*-null F9 EC cells have 20% lower adhesion than wild type cells

(Gallant *et al.*, 2005). *Vcl*-null fibroblasts isolated from primary sources and from culture lines also show less adherence on fibronectin-coated substrates (Xu *et al.*, 1998a; Xu *et al.*, 1998b), a more rounded morphology (Rodriguez Fernandez *et al.*, 1993) and higher migration rates than wild type cells in both wound healing and Boyden chamber assays (Rodriguez Fernandez *et al.*, 1993; Xu *et al.*, 1998a; DeMali *et al.*, 2002). However, of two recent publications studying vinculin's effect on cell speed in random migration (Mierke *et al.*, 2010; Fraley *et al.*, 2010), only one found a speed difference between *Vcl*-null and vinculin-expressing cells (Mierke *et al.*, 2010).

Table 1-1: Summary of previously published studies on the role of vinculin on cellular motility and/or speed.

First Author	Year	Cell Type	Cells Compared	Assay	Result
Fernandez	1992	Balb/C 3T3 clone A31	*WT* cells, endogenous vinculin level *WT*+20%, overexpressed chicken vinculin	1. Wound Healing 2. Phagokinetic tracks on colloidal gold surfaces	1. WT+20% were 3-4x slower closing wound and had 3-4x shorter tracks than WT 2. WT cells moved 4x less randomly
Fernandez	1993	Balb/C 3T3 clone A31	*WT:* endogenous vinculin levels *Null*: transfect vinculin antisense DNA (incomplete knockdown)	1. Wound Healing 2. Phagokinetic tracks on colloidal gold surfaces	1. Cells with reduced vinculin migrate at least 2x further into wound 2. Cells with reduced vinculin have tracks 2x longer than WT cells
Goldmann	1995	Parental F9 EC	*WT*: endogenous vinculin levels *Null*: obtained by EMS mutagensis of the WT cells.	Filopodia extension	WT cells extended filopodia at 58 nm/s while vinculin deficient cells extended at 48.5 nm/s
Coll	1995	Parental F9 EC	*WT*: endogenous vinculin levels *Null*: obtained by homologous recombination with a vinculin targeting vector	1. Phagokinetic tracks on colloidal gold surfaces 2. Wound Healing	1. Null cells had a 2.4x longer track than WT 2. 2.4x more null cells migrated into scratch wound
Xu	1998a	Parental F9 EC	*WT*: vinculin transfected into isolated null line *Null*: isolated from *Vcl*-null mouse pups (homologous recombination)	1. Boyden Chambers 2. Migration away from a cell aggregate	1. Null cells had 2x more migration across the membrane. Vh had 3-4x the migration 2. Confirmed that Vh alone increased migration over Vh+Vt
Xu	1998b	MEFs	Cells isolated from +/+ or -/- mice that spontaneously immortalized in culture (Adamson cell-lines)	1. Boyden Chambers 2. Wound Healing	1. Nulls moved 3-9-fold more than WT across membrane 2. Nulls filled 50% of the gap by 6 hrs, while WT only filled 10%
DeMali	2002	MEFs	*WT*: gift of the Adamson lab *Null*: gift of the Adamson lab	Transwell chambers	Null cells had 2x more migration across the membrane.
Mills	2005	F9 PE	*WT*: F9 teratocarcinoma line *Null*: F9 vin -/-, gift of the Adamson lab	Migration away from cell aggregate	Loss of vinculin promotes a 2x increase in outgrowth
Mierke	2010	MEFs	Adamson WT or vin-/- lines or similar lines derived from vin-/- or WT littermates by immortalization with large T-antigen (Mierke)	1. Timelapse photography 2. Collagen invasion assay	1. Nulls move 3x faster than WT on collagen 2. WT show 9-fold increase in invasive cells compared to null cells
Marg	2010	MEFs	Isolated from embryos and immortalized with large T-antigen	Collagen invasion assay	WT show 6-fold increase in the % of invasive cells compared to *Vcl*-nulls
Fraley	2010	HT1080	*WT*: untransfected cells *Null*: transfect with shRNA vinculin	Timelapse photography	No speed difference between the knockdown and WT in 2D or 3D

Footnotes:

a. Wound healing: Cell migration into a scratch wound on a confluent layer
b. EMS: ethyl methanesulfonate
c. EC: embryonic carcinoma
d. PE: parietal endoderm (made by treating EC with retinoic acid, causing differentiation into parietal endoderm)
e. MEF: mouse embryo-derived fibroblast cell-line
f. HT1080: human fibrosarcoma cell-line

Truncation mutants of vinculin have been expressed in cells and analyzed for changes in motility compared to *Vcl*-null and wild-type cells. *Vcl*-null mouse embryonic fibroblasts (MEFs) expressing only vinculin head (Vh) have a distinctly different migration pattern than cells expressing only vinculin tail (Vt). Vh-expressing cells are more adherent than *Vcl*-null cells, have a more rounded shape, and are more motile than *Vcl*-null cells. In contrast, Vt cells are less adherent than *Vcl*-null cells and have 6-fold less migration than vinculin cells (Xu *et al.*, 1998b). However, Vt localizes to actin stress fibers whereas Vh and vinculin does not (Humphries *et al.*, 2007), and so the observed motility differences may also be due to differences in the localization of Vh versus Vt. To date, no study has investigated how vinculin regulates cell adhesion and motility using mutants of vinculin that contain specific point mutations that affect binding to particular ligands, rather than using truncation mutants of vinculin.

Mutants of vinculin with lowered autoinhibition have been reported (Cohen *et al.*, 2005). Expression of autoinhibition mutants in *Vcl*-null cells results in more numerous and longer focal adhesions (Cohen *et al.*, 2005; Humphries *et al.*, 2007). Furthermore, FRAP studies have shown that autoinhibition mutants of vinculin are turned over more slowly within focal adhesions (Cohen *et al.*, 2006; Humphries *et al.*, 2007). From this data, one could hypothesize that expressing an autoinhibition mutant of vinculin would result in increased focal adhesion formation and increased cell adhesion. One recent, unpublished study (Dumbauld, 2013) supports this hypothesis. The author investigated the of vinculin, Vh and T12 (a vinculin autoinhibition mutant; Cohen *et al.*, 2005) expression on cellular adhesion, and found that vinculin and Vh increase cellular adhesion 25% over

Vcl-null cells, while T12 increases cellular adhesion 50%. Together, these studies suggest that expression of autoinhibition mutants in cells may affect cellular motility by affecting how a cell interacts with the extracellular matrix.

The effect of vinculin loss on cell adhesion and migration is typically attributed to the presence of vinculin in focal adhesions and vinculin's ability to modulate the strength cell-matrix adhesions, presumably by reinforcement of integrin:ECM connections to the actin cytoskeleton. It should be noted that vinculin is also present at the leading edge of migrating cells in nascent focal adhesions and focal adhesion formation itself is dependent on polymerization of the actin cytoskeleton causing lamellipodial advancement (Choi *et al.*, 2008). Localized actin polymerization is thought to generate and sustain the necessary membrane protrusion of new lamellipodia (Le Clainche and Carlier, 2008) where nascent adhesions form (Choi *et al.*, 2008). Vinculin binds to two key proteins in this process, Arp 2/3 (DeMali *et al.*, 2002) and VASP (Brindle *et al.*, 1996; Reinhard *et al.*, 1996). The Arp2/3 complex is a key component in regulating nucleation of actin polymerization and protrusion at the leading edge of migrating cells (Mullins *et al.*, 1998; DeMali *et al.*, 2002) and nucleates actin polymerization by binding to the sides of existing cytoskeletal actin filaments (Svitkina and Borisy, 1999), causing the formation of the highly branched, dendritic network (Pantaloni *et al.*, 2000; Bailly *et al.*, 2001) essential for lamellopodial extension (Bailly *et al.*, 2001). Vasodilator-stimulated phosphoprotein (VASP) plays a role in determining actin architecture by preventing actin capping and promoting actin elongation (Bear *et al.*, 2002; Barzik *et al.*, 2005; Pasic *et al.*, 2008). VASP expression increases the rate of lamellipodial protrusion,

but also results in faster lamellipodial retraction, leading to a global negative effect on cell motility. VASP null cells have lamellipodia that protrude more slowly, but persist longer (Bear *et al.*, 2002; Krause *et al.*, 2003). Vinculin's ability to bind both Arp 2/3 and VASP provides an alternative mechanism for vinculin to affect cell speed and adhesion. Vinculin could play a role in directing dendritic polymerization and cellular protrusion within the cell through its interaction with Arp2/3 and VASP. This potential function of vinculin has not been tested.

Finally, a more recent study indicates that the phosphorylation state of vinculin may dictate the timing of vinculin's turnover within focal adhesions (Kupper *et al.*, 2010). From this, one could hypothesize that vinculin's phosphorylation state may affect cellular adhesion and therefore speed. To date, no studies have been conducted to determine how vinculin's phosphorylation state affects cellular motility.

Evidence for a role for vinculin in force transduction:

While there is a consistent body of work on the assembly and maturation of focal adhesions (DePasquale and Izzard, 1987; Izzard, 1988; Nobes and Hall, 1995; Ezzell *et al.*, 1997; Galbraith *et al.*, 2002; Choi *et al.*, 2008; Oakes *et al.*, 2012), the results of studies on how external forces affect focal adhesion growth have been less consistent. A number of studies show a positive, linear correlation between increased focal adhesion size and increased traction force exerted by the cell onto its growth substrate (Pelham and Wang, 1997; Balaban *et al.*, 2001; Beningo *et al.*, 2001; Tan *et al.*, 2003; Goffin *et al.*, 2006; Stricker *et al.*, 2011), with some studies showing data that there are outlier focal

adhesions to this trend (Balaban *et al.*, 2001; Tan *et al.*, 2003; Goffin *et al.*, 2006). To date, there have been five key studies (Riveline *et al.*, 2001; Galbraith *et al.*, 2002; Sawada and Sheetz, 2002; Sniadecki *et al.*, 2007; Stricker *et al.*, 2011) on the effect of applying external force on focal adhesions. Each study has used a different approach and these studies have had only partially consistent results. Despite this, the consensus within the field has been that the application of external force to cells causes an increase in focal adhesion number and size. It is currently unknown whether external force has different effects on focal adhesions in different stages of focal adhesion maturation.

Evidence that vinculin regulates cell survival:

A single study proposes that an alternative function of vinculin is as a regulator of cell viability. Comparison of parental F9 cells to *Vcl*-null cells created by EMS mutagenesis revealed that *Vcl*-null cells have increased resistance to apoptosis and that this resistance was reversed by expression of vinculin tail. These findings implied a role for vinculin in cell survival. Further studies showed that *Vcl*-null cells reduced cleavage of Caspase-9, an initiator protease for apoptosis whose cleavage is downregulated by ERK1/2. Additional immunoprecipitation studies showed that *Vcl*-null cells have increased paxillin:FAK interaction and increased phosphorylation of paxillin and FAK. Together, Subauste's findings suggest that a function of vinculin could be to sequester paxillin from interacting with FAK, limiting activation of FAK, resulting in lowered activity of ERK1/2 signaling and functional Caspase-9 mediated apoptosis (Subauste *et al.*, 2004).

Use of vinculin mutants to ascertain the role of vinculin in cellular motility and mechanotransduction:

In this thesis, I use wild-type vinculin and a panel of vinculin mutants introduced into a previously characterized (Xu *et al.*, 1998a; Xu *et al.*, 1998b) *Vcl*-null cell-line to study the role of vinculin, its autoinhibition, and its specific ligand binding abilities on 1) cell speed and 2) the response of mature focal adhesions to external stretch. My results in two different cell systems and two different motility assays show that the expression of vinculin has no statistically significant effect on the speed of *Vcl*-null cells. In contrast to previous studies reporting a difference in cell speed between *Vcl*-null and vinculin-expressing cells, my results show that the presence of vinculin is not sufficient to affect cellular motility in these cells under the conditions of my experiments. Furthermore, while stretching vinculin-expressing cells can result in impressive changes in mature focal adhesion number or size, these changes do not occur with greater frequency in stretched cells than in unpaired controls. A re-examination of the literature in light of these results suggests the hypothesis that growth of nascent focal adhesions may be responsible for the previously reported findings that application of external force results in increased focal adhesion size and suggests an avenue of research that would further clarify the conditions under which external force affects focal adhesion assembly.

References:

Alatortsev, V.E., I.A. Kramerova, M.V. Frolov, S.A. Lavrov, and E.D. Westphal. 1997. Vinculin gene is non-essential in Drosophila melanogaster. *FEBS letters*. 413:197-201.

Alenghat, F.J., B. Fabry, K.Y. Tsai, W.H. Goldmann, and D.E. Ingber. 2000. Analysis of cell mechanics in single vinculin-deficient cells using a magnetic tweezer. *Biochemical and biophysical research communications*. 277:93-99.

Bailly, M., I. Ichetovkin, W. Grant, N. Zebda, L.M. Machesky, J.E. Segall, and J. Condeelis. 2001. The F-actin side binding activity of the Arp2/3 complex is essential for actin nucleation and lamellipod extension. *Curr Biol*. 11:620-625.

Bakolitsa, C., D.M. Cohen, L.A. Bankston, A.A. Bobkov, G.W. Cadwell, L. Jennings, D.R. Critchley, S.W. Craig, and R.C. Liddington. 2004. Structural basis for vinculin activation at sites of cell adhesion. *Nature*. 430:583-586.

Balaban, N.Q., U.S. Schwarz, D. Riveline, P. Goichberg, G. Tzur, I. Sabanay, D. Mahalu, S. Safran, A. Bershadsky, L. Addadi, and B. Geiger. 2001. Force and focal adhesion assembly: a close relationship studied using elastic micropatterned substrates. *Nature cell biology*. 3:466-472.

Barstead, R.J., and R.H. Waterston. 1991. Vinculin is essential for muscle function in the nematode. *The Journal of cell biology*. 114:715-724.

Barzik, M., T.I. Kotova, H.N. Higgs, L. Hazelwood, D. Hanein, F.B. Gertler, and D.A. Schafer. 2005. Ena/VASP proteins enhance actin polymerization in the presence of barbed end capping proteins. *The Journal of biological chemistry*. 280:28653-28662.

Bear, J.E., T.M. Svitkina, M. Krause, D.A. Schafer, J.J. Loureiro, G.A. Strasser, I.V. Maly, O.Y. Chaga, J.A. Cooper, G.G. Borisy, and F.B. Gertler. 2002. Antagonism between Ena/VASP proteins and actin filament capping regulates fibroblast motility. *Cell*. 109:509-521.

Belkin, A.M., and V.E. Koteliansky. 1987. Interaction of iodinated vinculin, metavinculin and alpha-actinin with cytoskeletal proteins. *FEBS letters*. 220:291-294.

Beningo, K.A., M. Dembo, I. Kaverina, J.V. Small, and Y.L. Wang. 2001. Nascent focal adhesions are responsible for the generation of strong propulsive forces in migrating fibroblasts. *The Journal of cell biology*. 153:881-888.

Bloch, R.J., and B. Geiger. 1980. The localization of acetylcholine receptor clusters in areas of cell-substrate contact in cultures of rat myotubes. *Cell*. 21:25-35.

Bourdet-Sicard, R., M. Rudiger, B.M. Jockusch, P. Gounon, P.J. Sansonetti, and G.T. Nhieu. 1999. Binding of the Shigella protein IpaA to vinculin induces F-actin depolymerization. *The EMBO journal*. 18:5853-5862.

Brindle, N.P., M.R. Holt, J.E. Davies, C.J. Price, and D.R. Critchley. 1996. The focal-adhesion vasodilator-stimulated phosphoprotein (VASP) binds to the proline-rich domain in vinculin. *The Biochemical journal*. 318 (Pt 3):753-757.

Burridge, K., and J.R. Feramisco. 1980. Microinjection and localization of a 130K protein in living fibroblasts: a relationship to actin and fibronectin. *Cell*. 19:587-595.

Burridge, K., and P. Mangeat. 1984. An interaction between vinculin and talin. *Nature*. 308:744-746.

Byrne, B.J., Y.J. Kaczorowski, M.D. Coutu, and S.W. Craig. 1992. Chicken vinculin and meta-vinculin are derived from a single gene by alternative splicing of a 207-base pair exon unique to meta-vinculin. *The Journal of biological chemistry*. 267:12845-12850.

Chen, H., D.M. Choudhury, and S.W. Craig. 2006. Coincidence of actin filaments and talin is required to activate vinculin. *The Journal of biological chemistry*. 281:40389-40398.

Chen, H., D.M. Cohen, D.M. Choudhury, N. Kioka, and S.W. Craig. 2005. Spatial distribution and functional significance of activated vinculin in living cells. *The Journal of cell biology*. 169:459-470.

Chen, H.C., P.A. Appeddu, J.T. Parsons, J.D. Hildebrand, M.D. Schaller, and J.L. Guan. 1995. Interaction of focal adhesion kinase with cytoskeletal protein talin. *The Journal of biological chemistry*. 270:16995-16999.

Choi, C.K., M. Vicente-Manzanares, J. Zareno, L.A. Whitmore, A. Mogilner, and A.R. Horwitz. 2008. Actin and alpha-actinin orchestrate the assembly and maturation of nascent adhesions in a myosin II motor-independent manner. *Nature cell biology*. 10:1039-1050.

Cobb, B.S., M.D. Schaller, T.H. Leu, and J.T. Parsons. 1994. Stable association of pp60src and pp59fyn with the focal adhesion-associated protein tyrosine kinase, pp125FAK. *Molecular and cellular biology*. 14:147-155.

Cohen, D.M., H. Chen, R.P. Johnson, B. Choudhury, and S.W. Craig. 2005. Two distinct head-tail interfaces cooperate to suppress activation of vinculin by talin. *The Journal of biological chemistry*. 280:17109-17117.

Cohen, D.M., B. Kutscher, H. Chen, D.B. Murphy, and S.W. Craig. 2006. A conformational switch in vinculin drives formation and dynamics of a talin-

vinculin complex at focal adhesions. *The Journal of biological chemistry*. 281:16006-16015.

Coutu, M.D., and S.W. Craig. 1988. cDNA-derived sequence of chicken embryo vinculin. *Proceedings of the National Academy of Sciences of the United States of America*. 85:8535-8539.

Craig, S.W., and J.V. Pardo. 1983. Gamma actin, spectrin, and intermediate filament proteins colocalize with vinculin at costameres, myofibril-to-sarcolemma attachment sites. *Cell motility*. 3:449-462.

Danowski, B.A., K. Imanaka-Yoshida, J.M. Sanger, and J.W. Sanger. 1992. Costameres are sites of force transmission to the substratum in adult rat cardiomyocytes. *The Journal of cell biology*. 118:1411-1420.

DeMali, K.A., C.A. Barlow, and K. Burridge. 2002. Recruitment of the Arp2/3 complex to vinculin: coupling membrane protrusion to matrix adhesion. *The Journal of cell biology*. 159:881-891.

DePasquale, J.A., and C.S. Izzard. 1987. Evidence for an actin-containing cytoplasmic precursor of the focal contact and the timing of incorporation of vinculin at the focal contact. *The Journal of cell biology*. 105:2803-2809.

Dumbauld, D.W., T.T. Lee, A. Singh, J. Scrimgeour, C.A. Gersbach, E.A. Zamir, J. Fu, C.S. Chen, J.E. Curtis, S.W. Craig, and A.J. Garcia. 2013. How vinculin regulates force transmission. *Proceedings of the National Academy of Sciences of the United States of America*. 110:9788-9793.

Ervasti, J.M. 2003. Costameres: the Achilles' heel of Herculean muscle. *The Journal of biological chemistry*. 278:13591-13594.

Ezzell, R.M., W.H. Goldmann, N. Wang, N. Parashurama, and D.E. Ingber. 1997. Vinculin promotes cell spreading by mechanically coupling integrins to the cytoskeleton. *Experimental cell research*. 231:14-26.

Fraley, S.I., Y. Feng, R. Krishnamurthy, D.H. Kim, A. Celedon, G.D. Longmore, and D. Wirtz. 2010. A distinctive role for focal adhesion proteins in three-dimensional cell motility. *Nature cell biology*. 12:598-604.

Galbraith, C.G., K.M. Yamada, and M.P. Sheetz. 2002. The relationship between force and focal complex development. *The Journal of cell biology*. 159:695-705.

Gallant, N.D., K.E. Michael, and A.J. Garcia. 2005. Cell adhesion strengthening: contributions of adhesive area, integrin binding, and focal adhesion assembly. *Molecular biology of the cell*. 16:4329-4340.

Geiger, B. 1979. A 130K protein from chicken gizzard: its localization at the termini of microfilament bundles in cultured chicken cells. *Cell*. 18:193-205.

Geiger, B., K.T. Tokuyasu, A.H. Dutton, and S.J. Singer. 1980. Vinculin, an intracellular protein localized at specialized sites where microfilament bundles terminate at cell membranes. *Proceedings of the National Academy of Sciences of the United States of America*. 77:4127-4131.

Gilmore, A.P., P. Jackson, G.T. Waites, and D.R. Critchley. 1992. Further characterisation of the talin-binding site in the cytoskeletal protein vinculin. *Journal of cell science*. 103 (Pt 3):719-731.

Goffin, J.M., P. Pittet, G. Csucs, J.W. Lussi, J.J. Meister, and B. Hinz. 2006. Focal adhesion size controls tension-dependent recruitment of alpha-smooth muscle actin to stress fibers. *The Journal of cell biology*. 172:259-268.

Goldmann, W.H., M. Schindl, T.J. Cardozo, and R.M. Ezzell. 1995. Motility of vinculin-deficient F9 embryonic carcinoma cells analyzed by video, laser confocal, and reflection interference contrast microscopy. *Experimental cell research*. 221:311-319.

Guan, J.L., J.E. Trevithick, and R.O. Hynes. 1991. Fibronectin/integrin interaction induces tyrosine phosphorylation of a 120-kDa protein. *Cell regulation*. 2:951-964.

Huang, Y., W. Zhang, and S.J. Gunst. 2011. Activation of vinculin induced by cholinergic stimulation regulates contraction of tracheal smooth muscle tissue. *The Journal of biological chemistry*. 286:3630-3644.

Humphries, J.D., P. Wang, C. Streuli, B. Geiger, M.J. Humphries, and C. Ballestrem. 2007. Vinculin controls focal adhesion formation by direct interactions with talin and actin. *The Journal of cell biology*. 179:1043-1057.

Izard, T., G. Tran Van Nhieu, and P.R. Bois. 2006. Shigella applies molecular mimicry to subvert vinculin and invade host cells. *The Journal of cell biology*. 175:465-475.

Izzard, C.S. 1988. A precursor of the focal contact in cultured fibroblasts. *Cell motility and the cytoskeleton*. 10:137-142.

Jockusch, B.M., and G. Isenberg. 1981. Interaction of alpha-actinin and vinculin with actin: opposite effects on filament network formation. *Proceedings of the National Academy of Sciences of the United States of America*. 78:3005-3009.

Jockusch, B.M., C. Wiegand, C.J. Temm-Grove, and G. Nikolai. 1993. Dynamic aspects of microfilament-membrane attachments. *Symposia of the Society for Experimental Biology*. 47:253-266.

Johnson, R.P., and S.W. Craig. 1994. An intramolecular association between the head and tail domains of vinculin modulates talin binding. *The Journal of biological chemistry*. 269:12611-12619.

Johnson, R.P., and S.W. Craig. 1995a. The carboxy-terminal tail domain of vinculin contains a cryptic binding site for acidic phospholipids. *Biochemical and biophysical research communications*. 210:159-164.

Johnson, R.P., and S.W. Craig. 1995b. F-actin binding site masked by the intramolecular association of vinculin head and tail domains. *Nature*. 373:261-264.

Kioka, N., S. Sakata, T. Kawauchi, T. Amachi, S.K. Akiyama, K. Okazaki, C. Yaen, K.M. Yamada, and S. Aota. 1999. Vinexin: a novel vinculin-binding protein with multiple SH3 domains enhances actin cytoskeletal organization. *The Journal of cell biology*. 144:59-69.

Kornberg, L.J., H.S. Earp, C.E. Turner, C. Prockop, and R.L. Juliano. 1991. Signal transduction by integrins: increased protein tyrosine phosphorylation caused by clustering of beta 1 integrins. *Proceedings of the National Academy of Sciences of the United States of America*. 88:8392-8396.

Koteliansky, V.E., and G.N. Gneushev. 1983. Vinculin localization in cardiac muscle. *FEBS letters*. 159:158-160.

Krause, M., E.W. Dent, J.E. Bear, J.J. Loureiro, and F.B. Gertler. 2003. Ena/VASP proteins: regulators of the actin cytoskeleton and cell migration. *Annual review of cell and developmental biology*. 19:541-564.

Kupper, K., N. Lang, C. Mohl, N. Kirchgessner, S. Born, W.H. Goldmann, R. Merkel, and B. Hoffmann. 2010. Tyrosine phosphorylation of vinculin at position 1065 modifies focal adhesion dynamics and cell tractions. *Biochemical and biophysical research communications*. 399:560-564.

Le Clainche, C., and M.F. Carlier. 2008. Regulation of actin assembly associated with protrusion and adhesion in cell migration. *Physiological reviews*. 88:489-513.

Maeda, M., E. Holder, B. Lowes, S. Valent, and R.D. Bies. 1997. Dilated cardiomyopathy associated with deficiency of the cytoskeletal protein metavinculin. *Circulation*. 95:17-20.

Menkel, A.R., M. Kroemker, P. Bubeck, M. Ronsiek, G. Nikolai, and B.M. Jockusch. 1994. Characterization of an F-actin-binding domain in the cytoskeletal protein vinculin. *The Journal of cell biology*. 126:1231-1240.

Mierke, C.T., P. Kollmannsberger, D.P. Zitterbart, G. Diez, T.M. Koch, S. Marg, W.H. Ziegler, W.H. Goldmann, and B. Fabry. 2010. Vinculin facilitates cell invasion into three-dimensional collagen matrices. *The Journal of biological chemistry*. 285:13121-13130.

Mullins, R.D., J.A. Heuser, and T.D. Pollard. 1998. The interaction of Arp2/3 complex with actin: nucleation, high affinity pointed end capping, and formation of

branching networks of filaments. *Proceedings of the National Academy of Sciences of the United States of America*. 95:6181-6186.

Nhieu, G.T., and T. Izard. 2007. Vinculin binding in its closed conformation by a helix addition mechanism. *The EMBO journal*. 26:4588-4596.

Nobes, C.D., and A. Hall. 1995. Rho, rac, and cdc42 GTPases regulate the assembly of multimolecular focal complexes associated with actin stress fibers, lamellipodia, and filopodia. *Cell*. 81:53-62.

Oakes, P.W., Y. Beckham, J. Stricker, and M.L. Gardel. 2012. Tension is required but not sufficient for focal adhesion maturation without a stress fiber template. *The Journal of cell biology*. 196:363-374.

Ohmori, T., Y. Kashiwakura, A. Ishiwata, S. Madoiwa, J. Mimuro, S. Honda, T. Miyata, and Y. Sakata. 2010. Vinculin activates inside-out signaling of integrin alphaIIbbeta3 in Chinese hamster ovary cells. *Biochemical and biophysical research communications*. 400:323-328.

Olson, T.M., S. Illenberger, N.Y. Kishimoto, S. Huttelmaier, M.T. Keating, and B.M. Jockusch. 2002. Metavinculin mutations alter actin interaction in dilated cardiomyopathy. *Circulation*. 105:431-437.

Opazo Saez, A., W. Zhang, Y. Wu, C.E. Turner, D.D. Tang, and S.J. Gunst. 2004. Tension development during contractile stimulation of smooth muscle requires recruitment of paxillin and vinculin to the membrane. *American journal of physiology*. 286:C433-447.

Otto, J.J. 1990. Vinculin. *Cell motility and the cytoskeleton*. 16:1-6.

Palmer, S.M., M.P. Playford, S.W. Craig, M.D. Schaller, and S.L. Campbell. 2009. Lipid binding to the tail domain of vinculin: specificity and the role of the N and C termini. *The Journal of biological chemistry*. 284:7223-7231.

Pantaloni, D., R. Boujemaa, D. Didry, P. Gounon, and M.F. Carlier. 2000. The Arp2/3 complex branches filament barbed ends: functional antagonism with capping proteins. *Nature cell biology*. 2:385-391.

Pardo, J.V., J.D. Siliciano, and S.W. Craig. 1983a. Vinculin is a component of an extensive network of myofibril-sarcolemma attachment regions in cardiac muscle fibers. *The Journal of cell biology*. 97:1081-1088.

Pardo, J.V., J.D. Siliciano, and S.W. Craig. 1983b. A vinculin-containing cortical lattice in skeletal muscle: transverse lattice elements ("costameres") mark sites of attachment between myofibrils and sarcolemma. *Proceedings of the National Academy of Sciences of the United States of America*. 80:1008-1012.

Park, H., C. Valencia-Gallardo, A. Sharff, G. Tran Van Nhieu, and T. Izard. 2011. Novel vinculin binding site of the IpaA invasin of Shigella. *The Journal of biological chemistry*. 286:23214-23221.

Pasic, L., T. Kotova, and D.A. Schafer. 2008. Ena/VASP proteins capture actin filament barbed ends. *The Journal of biological chemistry*. 283:9814-9819.

Pelham, R.J., Jr., and Y. Wang. 1997. Cell locomotion and focal adhesions are regulated by substrate flexibility. *Proceedings of the National Academy of Sciences of the United States of America*. 94:13661-13665.

Peng, X., E.S. Nelson, J.L. Maiers, and K.A. DeMali. 2011. New insights into vinculin function and regulation. *International review of cell and molecular biology*. 287:191-231.

Price, G.J., P. Jones, M.D. Davison, B. Patel, R. Bendori, B. Geiger, and D.R. Critchley. 1989. Primary sequence and domain structure of chicken vinculin. *The Biochemical journal*. 259:453-461.

Reinhard, M., M. Rudiger, B.M. Jockusch, and U. Walter. 1996. VASP interaction with vinculin: a recurring theme of interactions with proline-rich motifs. *FEBS letters*. 399:103-107.

Riveline, D., E. Zamir, N.Q. Balaban, U.S. Schwarz, T. Ishizaki, S. Narumiya, Z. Kam, B. Geiger, and A.D. Bershadsky. 2001. Focal contacts as mechanosensors: externally applied local mechanical force induces growth of focal contacts by an mDia1-dependent and ROCK-independent mechanism. *The Journal of cell biology*. 153:1175-1186.

Rodriguez Fernandez, J.L., B. Geiger, D. Salomon, and A. Ben-Ze'ev. 1993. Suppression of vinculin expression by antisense transfection confers changes in cell morphology, motility, and anchorage-dependent growth of 3T3 cells. *The Journal of cell biology*. 122:1285-1294.

Samuels, M., R.M. Ezzell, T.J. Cardozo, D.R. Critchley, J.L. Coll, and E.D. Adamson. 1993. Expression of chicken vinculin complements the adhesion-defective phenotype of a mutant mouse F9 embryonal carcinoma cell. *The Journal of cell biology*. 121:909-921.

Sawada, Y., and M.P. Sheetz. 2002. Force transduction by Triton cytoskeletons. *The Journal of cell biology*. 156:609-615.

Schaller, M.D., C.A. Otey, J.D. Hildebrand, and J.T. Parsons. 1995. Focal adhesion kinase and paxillin bind to peptides mimicking beta integrin cytoplasmic domains. *The Journal of cell biology*. 130:1181-1187.

Schaller, M.D., and J.T. Parsons. 1995. pp125FAK-dependent tyrosine phosphorylation of paxillin creates a high-affinity binding site for Crk. *Molecular and cellular biology*. 15:2635-2645.

Schlaepfer, D.D., S.K. Hanks, T. Hunter, and P. van der Geer. 1994. Integrin-mediated signal transduction linked to Ras pathway by GRB2 binding to focal adhesion kinase. *Nature*. 372:786-791.

Shear, C.R., and R.J. Bloch. 1985. Vinculin in subsarcolemmal densities in chicken skeletal muscle: localization and relationship to intracellular and extracellular structures. *The Journal of cell biology*. 101:240-256.

Sniadecki, N.J., A. Anguelouch, M.T. Yang, C.M. Lamb, Z. Liu, S.B. Kirschner, Y. Liu, D.H. Reich, and C.S. Chen. 2007. Magnetic microposts as an approach to apply forces to living cells. *Proceedings of the National Academy of Sciences of the United States of America*. 104:14553-14558.

Stricker, J., Y. Aratyn-Schaus, P.W. Oakes, and M.L. Gardel. 2011. Spatiotemporal constraints on the force-dependent growth of focal adhesions. *Biophysical journal*. 100:2883-2893.

Subauste, M.C., O. Pertz, E.D. Adamson, C.E. Turner, S. Junger, and K.M. Hahn. 2004. Vinculin modulation of paxillin-FAK interactions regulates ERK to control survival and motility. *The Journal of cell biology*. 165:371-381.

Svitkina, T.M., and G.G. Borisy. 1999. Arp2/3 complex and actin depolymerizing factor/cofilin in dendritic organization and treadmilling of actin filament array in lamellipodia. *The Journal of cell biology*. 145:1009-1026.

Tan, J.L., J. Tien, D.M. Pirone, D.S. Gray, K. Bhadriraju, and C.S. Chen. 2003. Cells lying on a bed of microneedles: an approach to isolate mechanical force. *Proceedings of the National Academy of Sciences of the United States of America*. 100:1484-1489.

Turner, C.E., J.R. Glenney, Jr., and K. Burridge. 1990. Paxillin: a new vinculin-binding protein present in focal adhesions. *The Journal of cell biology*. 111:1059-1068.

Turner, C.E., and J.T. Miller. 1994. Primary sequence of paxillin contains putative SH2 and SH3 domain binding motifs and multiple LIM domains: identification of a vinculin and pp125Fak-binding region. *Journal of cell science*. 107 (Pt 6):1583-1591.

Volberg, T., B. Geiger, Z. Kam, R. Pankov, I. Simcha, H. Sabanay, J.L. Coll, E. Adamson, and A. Ben-Ze'ev. 1995. Focal adhesion formation by F9 embryonal carcinoma cells after vinculin gene disruption. *Journal of cell science*. 108 (Pt 6):2253-2260.

Xing, Z., H.C. Chen, J.K. Nowlen, S.J. Taylor, D. Shalloway, and J.L. Guan. 1994. Direct interaction of v-Src with the focal adhesion kinase mediated by the Src SH2 domain. *Molecular biology of the cell*. 5:413-421.

Xu, W., H. Baribault, and E.D. Adamson. 1998a. Vinculin knockout results in heart and brain defects during embryonic development. *Development (Cambridge, England)*. 125:327-337.

Xu, W., J.L. Coll, and E.D. Adamson. 1998b. Rescue of the mutant phenotype by reexpression of full-length vinculin in null F9 cells; effects on cell locomotion by domain deleted vinculin. *Journal of cell science*. 111 (Pt 11):1535-1544.

Zemljic-Harpf, A.E., J.C. Miller, S.A. Henderson, A.T. Wright, A.M. Manso, L. Elsherif, N.D. Dalton, A.K. Thor, G.A. Perkins, A.D. McCulloch, and R.S. Ross. 2007. Cardiac-myocyte-specific excision of the vinculin gene disrupts cellular junctions, causing sudden death or dilated cardiomyopathy. *Molecular and cellular biology*. 27:7522-7537.

Zemljic-Harpf, A.E., S. Ponrartana, R.T. Avalos, M.C. Jordan, K.P. Roos, N.D. Dalton, V.Q. Phan, E.D. Adamson, and R.S. Ross. 2004. Heterozygous inactivation of the vinculin gene predisposes to stress-induced cardiomyopathy. *The American journal of pathology*. 165:1033-1044.

Ziegler, W.H., R.C. Liddington, and D.R. Critchley. 2006. The structure and regulation of vinculin. *Trends in cell biology*. 16:453-460.

Chapter 2:

The Effect of Vinculin Activation and Vinculin Ligand Binding Mutants on Cellular Migration

Abstract:

Published studies show that vinculin inhibits cellular migration. Since vinculin has no intrinsic enzymatic activity, vinculin's effect on cell migration is likely mediated by vinculin's interaction with particular binding partners. Studies have been conducted comparing the motility of *Vcl*-null versus vinculin-expressing cells, and a single study has explored how vinculin head and tail domains affect cellular motility. No studies have been performed using vinculin autoinhibition mutants or mutants of full-length vinculin that specifically disrupt vinculin-ligand interactions. Studies using these mutants would help clarify the protein:protein interactions involved in vinculin regulated cellular motility. In this study, eGFP-labeled wild-type and mutant vinculin constructs are used to test for changes in cellular motility using timelapse microscopy. My results in two different cell systems and two different assays show that the introduction of vinculin into *Vcl*-null cells has no effect on cell speed. While these results do not agree with the majority of published work in the field, these results indicate that the presence of vinculin is not sufficient to slow cell speed in assays monitoring the random migration of individual cells and the haptotaxis of cells through a fibronectin-coated substrate.

Introduction:

Mutants of vinculin have been developed for a variety of purposes. Vinculin head (Vh) and vinculin tail (Vt) mutants were initially developed to study vinculin head-tail interactions and vinculin's mechanism of autoinhibition (Johnson and Craig, 1994;

Johnson and Craig, 1995) before the crystal structure of vinculin had been determined (Bakolitsa *et al.*, 2004). Speculation on the precise intermolecular interactions responsible for the tight (10^{-9} K_d) interface between vinculin head and tail (Bakolitsa *et al.*, 2004) prompted the development of two charge-to-alanine mutants that alter sites on vinculin head (D4) and vinculin tail (T12) to cause a 100-fold decrease in vinculin's autoinhibition (Cohen *et al.*, 2005). Other vinculin mutants have been developed that ablate binding to VASP (Brindle *et al.*, 1996), Arp 2/3 (DeMali *et al.*, 2002), talin (Bakolitsa *et al.*, 2004), and mimic various phosphorylation states of vinculin (Kupper *et al.*, 2010). The Craig lab has created a library of these mutants, each of them fused to eGFP (Table 2-1). Expression of these mutants in *Vcl*-null cells would clarify how vinculin's autoinhibition and specific ligand binding abilities affect vinculin's proposed functions in cells.

In collaboration with the Garcia lab at the Georgia Institute of Technology, several of these eGFP-fused mutants were introduced into a previously characterized *Vcl*-null mouse embryonic fibroblast (MEF) parental line (Xu *et al.*, 1998a) using a tetracycline-regulated retroviral system. This strategy has major advantages over a transient transfection system in that 1) it eliminates batch-to-batch variability in transfection efficiency, 2) the high transduction efficiency of this system results in a polyclonal population and eliminates issues found with clonal lines, and 3) tetracycline-regulated expression provides ideal negative controls since the eGFP-tagged vinculin mutants can be to be turned on or off at will in the same population. These cell-lines were used in

recent studies to show that vinculin and Vh increase cellular adhesion 25% over *Vcl*-null cells, while T12 increases cellular adhesion 50% over *Vcl*-null cells (Dumbauld, 2013).

Name	AA Composition	Specific Mutations	Comments
Vin -/-	*Vcl*-null	NA	Parent Cell Type
WT	GFP: 1-1066	NA	Wild Type
Vh	GFP: 1-851	NA	Head domain only; Does not bind actin or paxillin
D4	GFP : 1-1066	N773;E775:A	100-fold decrease in strength of autoinhibition
T12	GFP : 1-1066	D974;K975; R976;R978:A	100-fold decrease in strength of autoinhibition
A50I	GFP: 1-1066	A50I	Blocks binding of talin rod domain and alpha-actinin
Arp 2/3	GFP: 1-1066	P878A	Blocks Arp2/3 binding
VASP	GFP: 1-1066	F842A	Blocks VASP binding
Y1065E	GFP: 1-1066	Y1065E	Mimics phosphorylated state
Y1065A	GFP: 1-1066	Y1065A	Mimics dephosphorylated state

Table 2-1: Reference table of available vinculin mutants, their mutation sites, and altered functions.

In this study, I used both cell-lines created with a tetracycline-regulated retroviral system and transiently transfected cells to test the effect of vinculin autoinhibition and vinculin ligand binding mutants on cell speed. Cell speed was measured by tracking individual cells undergoing random migration and by measuring haptotaxis across a transwell. Neither cell system or migration assay reproduced previously published results showing

that vinculin slows cell speed. The tetracycline-regulated retroviral system showed that Vh reduces the speed of *Vcl*-null cells by 14% ($p<0.001$), but this finding is not reproduced with transiently transfected cells.

Materials and Methods:

Cell culture, transduction, and transfection: Vinculin-null mouse embryonic fibroblasts (MEFs) were a gift from Eileen Adamson and have been previously described (Xu *et al.*, 1998a). These fibroblasts were engineered to express eGFP-fused vinculin constructs as previously described (Dumbauld, 2013). Stated briefly, these lines were designed with the eGFP-fused vinculin constructs downstream of a tetracycline-regulated promoter. Incubation of the cell-lines with tetracyline results in repression of construct expression. All MEF lines were plated on 0.1% gelatin coated cell culture plastic and maintained using high glucose Dulbecco's Modified Eagle Medium (DMEM, Gibco 31053) supplemented with 10% FBS (Hyclone) and 2 mM glutamine (Gibco 25030) at 37°C and 5% CO_2. Cells were enzymatically lifted from the culture dish using 0.04% trypsin (Gibco 15090). For transient transfections, $2x10^6$ cells were combined with 100 uL of Ingenio Electroporation Solution (Mirus MIR 50117) and 15 μg of appropriate DNA. Cells were electroporated using setting T-20 on an Amaxa electroporation machine. Cells were them transferred to RPMI with 10% FBS and incubated for 10 min at 37°C to aid membrane closure. Transfected cells were then transferred to 4 mL of phenol-free, high glucose DMEM (Gibco 31053) supplemented with 10% FBS (Hyclone) and 2 mM glutamine (Gibco 25030) and allowed to recover for at least 48 hrs before use.

Migration Assay: $2x10^5$ cells were plated on Lab-Tek II Chambered #1.5 Coverglass Chambers (Nalge Nunc 155342) coated with 20 μg/μL human plasma fibronectin (Gibco 33016) diluted in water and blocked with 0.2% BSA. Cell were allowed to recover for 24 hrs, and then placed in a microscope incubation chamber (Tokai) at 37°C and 5% CO_2. Phase contrast or DIC images at 20x magnification were taken using a Nikon Eclipse Ti every 2 min for 4 hrs and compiled into films using Nikon Elements software. Migration speeds, cell area, and directional persistence were calculated using either Nikon Elements (tetracycline-regulated lines) or Metamorph (transient lines). The data are expressed as the mean values ± SE unless otherwise indicated. Statistical analysis was performed using Kaleidagraph or Graphpad Prism. A Student t-test was used for two population comparisons and a one-way ANOVA was used to compare 3 or more populations. $p<0.05$ was considered to be statistically significant.

Transwell Haptotaxis Migration Assay: Cells were harvested with 0.4% trypsin (Gibco) and plated on 24-well cell-culture inserts containing polyethylene terephthalate membrane (PET), 8.0 mm pore size, $1.0x\ 10^5$ pore density (Corning 3422). The lower surface of the PET membrane was coated with 20 μg/mL human plasma fibronectin (Gibco) diluted in Dulbecco's Phosphate-Buffered Saline (DPBS) and then blocked for 30 min in 0.2% BSA (Sigma 9418) diluted in DPBS that had been heat denatured for 30 min at 65°C. The lower chamber was filled with 1 mL of phenol free DMEM containing 10% FBS, and cells were plated in 1 mL of phenol free, serum free DMEM. Cells were allowed to migrate for 8 hrs at 37°C and 5% CO2. The upper surface of the membrane was then wiped with a cotton swab to mechanically remove nonmigratory cells and the

migrant cells attached to the lower surface were fixed in 10% formalin at room temperature for 30 min, stained for 15min with 0.1% crystal violet in a 100 mM borate buffer, pH 9.0, containing 2% ethanol. The number of stained cells per 20x field were photographed and counted. At least three fields were analyzed per condition per experiment. Background migration was determined using BSA coated PET membranes and this number was subtracted from all data.

Results:

My first experiment compared the speed of the *Vcl*-null parental cell-line to the virally transduced vinculin, Vh, and D4 cell-lines. The cell-lines were used immediately after recovery from freeze down, and plated onto German coverglass chambers coated with 20 μg/μL fibronectin. To analyze cell speed, each cell was treated as a single experiment. Thirty fluorescent cells from each cell-line were analyzed in each experiment. The results showed no reproducible differences in cell speed between any of the cell-lines (Figure 2-2, Experiment 1). I hypothesized that the lack of speed differences was due to the relatively short time (4 hrs) the cells were given to recover between trypsinization/plating and filming. To address this, I repeated the experiment but filmed the cells at 4 and 15 hrs after plating. However, this time both experiments showed significant differences in cell speed between the different lines. The experiment filmed 4 hrs after plating (Figure 2-2, Experiment 2) showed the Vh-expressing cells move significantly more slowly than the other lines, but the expression of vinculin had no effect on cell speed. In contrast, the experiment filmed 15 hrs after plating (Figure 2-2,

Experiment 3) showed that expression of Vh had no effect on cell speed, but expression of vinculin slowed cell speed.

Because filming the same cell-lines at two different times after plating had resulted in conflicting results (Figure 2-2, Experiments 2 and 3), I decided that I needed to determine whether the different cell-lines were expressing similar amounts of eGFP-labeled construct. Furthermore, I needed to gain a sense of what proportion of cells in each cell-line were expressing the eGFP-tagged construct. I hypothesized that my experiments were showing conflicting results because different platings from a single cell-line could result in different subpopulations of cells expressing different levels of eGFP-tagged construct to be observed. An initial western blot comparing the expression of eGFP-tagged vinculin constructs showed there was no expression of eGFP without an attached vinculin construct. However, while the bands for the three vinculin constructs were detectable, they showed varying levels of expression (Figure S2-1). To explore this further, I analyzed each cell-line by Fluorescence Activated Cell Sorting (FACS). This showed that each line contained cells that expressed eGFP-tagged constructs over a comparable range of fluorescence (Figure 2-1A). Comparison of vinculin-expressing cultures at different passages showed that eGFP fluorescence (and therefore vinculin expression) could be lost with continued culture (Figure 2-1B). Based on this FACS data, I decided to FACS sort each cell-line every two weeks for cells expressing 100-1000 FU. This would ensure that every cell-line used for future experiments would express comparable levels of eGFP-tagged construct. FACS sorted cell-lines were always allowed to recover at least 48 hrs before being used for an experiment.

Figure 2-1: **FACS analysis of virally transduced cell-lines to evaluate eGFP-tagged construct expression and stability.** Each cell-line was stained with propidium iodide (PI), a DNA intercalating agent that marks dead cells. Live cells have a PI fluorescence between 0-10 FU. A) FACS analysis of *Vcl*-null cells and cells virally transduced with eGFP-tagged vinculin, D4 or Vh. The *Vcl*-null line was eGFP negative and the virally tranduced lines expressed comparable levels of eGFP-tagged construct. B) Analysis of the vinculin-expressing cell-line after time in culture showed that eGFP-expression could be lost with continued passaging. For this reason, each cell-line was FACS sorted every two weeks to maintain eGFP-expression between 100-1000 FU.

A

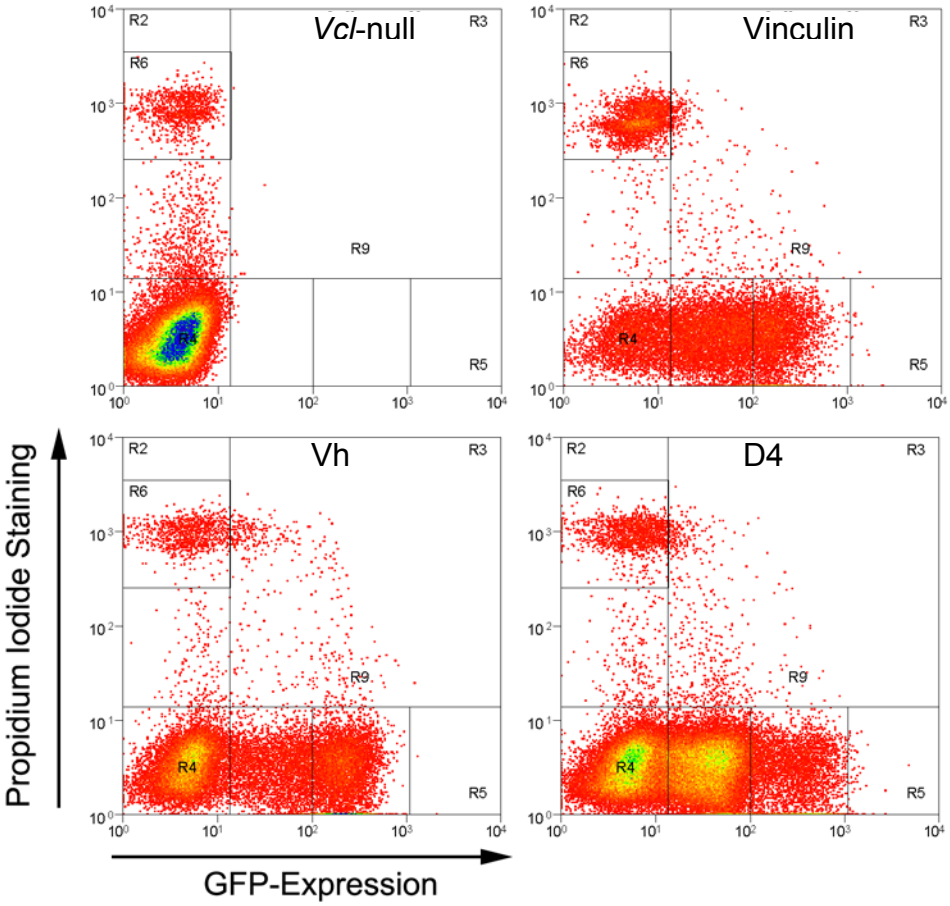
Vcl-null
Vinculin
Vh
D4
R2
R3
R6
R9
R4
R5
Propidium Iodide Staining
GFP-Expression

B

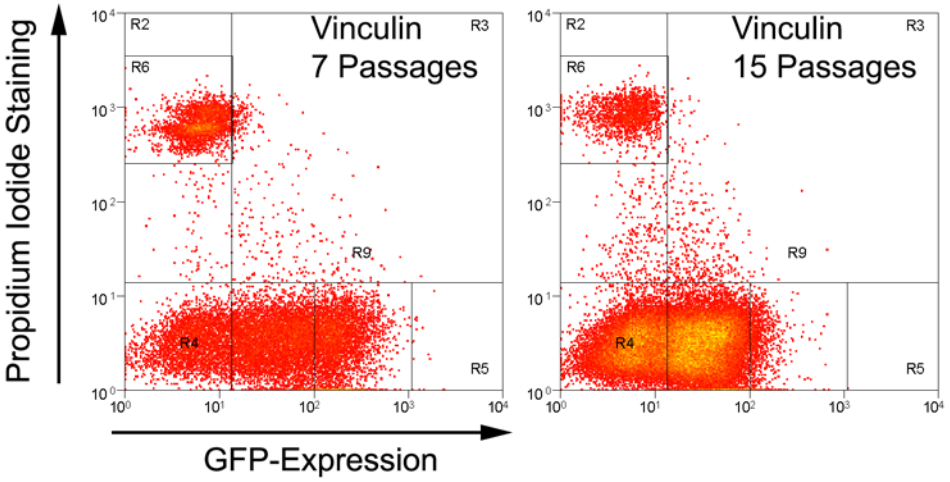
Vinculin
7 Passages
Vinculin
15 Passages
R2
R3
R6
R9
R4
R5
Propidium Iodide Staining
GFP-Expression

After deciding to FACS sort each of my cell-lines to ensure similar expression levels of eGFP-tagged constructs, I repeated my random motility assay using FACS sorted cell-lines and filmed the cells 4 hrs after plating. There was no speed difference between any of the cell-lines (Figure 2-2, Experiment 4).

I hypothesized that the motility phenotype was still not being observed because I had FACS sorted the cell-lines for inappropriately high expression levels of eGFP-tagged construct (100-1000 FU). I resorted the cell-lines for cells 50-100 FU. These cell-lines became infected from the FACS sorting process. After consultation with my laboratory, I decided to treat these cells with a combination of penicillin, streptomycin, and gentamycin for 12 hrs. I then filmed the lines 4 hrs and 15 hrs after plating. Neither experiment showed significant differences in cell speed between the various lines (Figure 2-2, Experiments 5 and 6).

I attempted two final random motility experiments using these lines. The cells were again FACS sorted for between 100-1000 FU, and I decided to revisit the effect of time after plating on cell speed using the FACS sorted cell-lines. The experiment filmed 4 hrs after plating showed no differences in cell speed between the lines (Figure 2-2, Experiment 7). The experiment filmed 15 hrs after plating showed that expression of vinculin increased cell speed (Figure 2-2, Experiment 8). This was in conflict with the effect of vinculin expression observed in Experiment 3 (also taken 15 hrs after filming) and opposite to the trend published in the literature.

In total, thirteen experiments comparing the transduced cell-lines were completed (Table S2-1). I have described eight in detail in this manuscript, and they are summarized in Figure 2-2. Two additional experiments were completed using cells that had not been FACS sorted. These experiments were conducted because there was a period of time when our lab did not have access to a FACS sorting facility. I chose not to analyze this data because FACS analysis of my cell-lines showed that expression of eGFP-tagged constructs could decrease with continued passage (Figure 2-1B), and I could not be confident the cells were expressing similar levels of eGFP-tagged constructs during those experiments. I also completed two experiments where I worked briefly in collaboration with both the Garcia lab and Intelligent Substrates™ to test different potential coatings for the German coverglass chambers. The Garcia lab suggested modifying the protocol to coat the chambers with fibronectin to match their protocol for fibronectin coating that had been previously established for use in their various cell adhesion studies (Michael, 2003). Briefly, German coverslips are first coated by successive thin films of titanium, and gold, and then incubated with hexadecanethiol (HDT) followed by human plasma fibronectin. In collaboration with the Garcia lab, the chambers were treated to create a thin film of titanium and gold, and then subsequently incubated with HDT and fibronectin in the Craig lab. Our cell-lines began apoptosis within 4 hrs after being plated on this substrate and did not survive long enough to be filmed. Additionally, we worked in collaboration with Intelligent Substrates™ to determine whether using a proprietary method for patterning the fibronectin growth substrate would limit the direction of cellular motility and result in differences in cell speed. The cell-lines tolerated these patterned substrates initially, but apoptosed during the course of filming.

Since we had been able to successfully culture the transduced cell-lines using the fibronectin coating protocol established in the Craig lab, these alternative coating procedures were not further pursued and the data from these films was not analyzed.

Figure 2-2: **Eight experiments comparing the random migration speed of** *Vcl*-null **cells to cell-lines expressing different eGFP-tagged vinculin constructs.** *Vcl*-null MEF cells virally transduced with eGFP-tagged constructs for vinculin, Vh, and D4 were plated on fibronectin-coated german coverglass chambers. To determine the effect of filming at different timepoints after plating, Experiments 1, 2, 4, 5, and 7 were filmed 4 hrs after plating and Experiments 3, 6, and 8 were filmed 15 hrs after plating. FACS sorting ensured comparable expression levels of eGFP-tagged construct between cell-lines. Experiments 3, 4, 7, and 8 were FACS sorted for cells between 100-1000 FU. Experiments 5 and 6 were FAC sorted for cells between 50-100 FU. For filming, the chambers were moved to an onstage incubator and imaged using 20x DIC or Phase objectives. The resulting films were analyzed by tracking the nucleus of 30 GFP-positive cells from each cell-line every 2 min over 4 hrs using Nikon Elements tracking software. The resulting data was analyzed by ANOVA. Red line indicates average cell speed. * implies $p<0.01$, ** implies $p<0.001$.

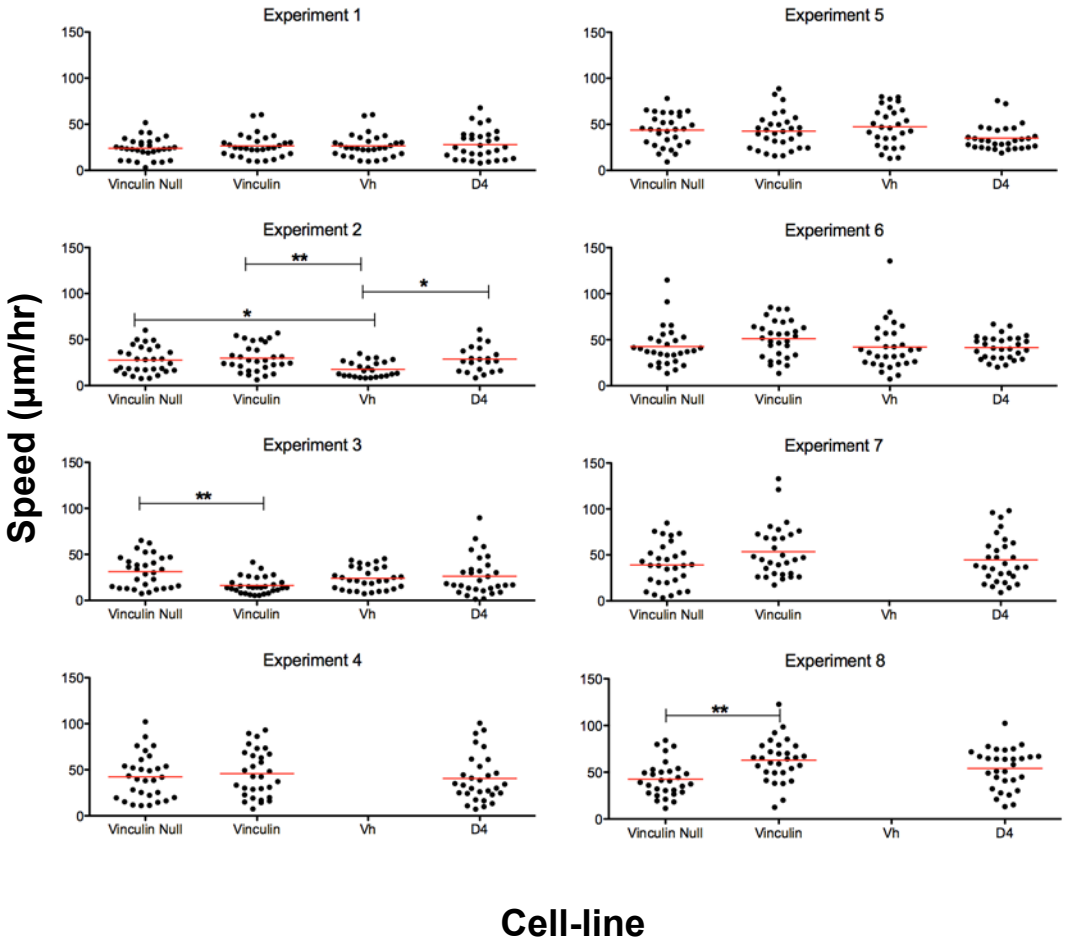
Experiment 1
Experiment 5
Experiment 2
Experiment 6
Experiment 3
Experiment 7
Experiment 4
Experiment 8
Speed (µm/hr)
Cell-line
Vinculin Null
Vinculin
Vh
D4
150
100
50
0
**
*
*
**

Of my timelapse films, eight experiments contained 4 hrs of motility data on healthy, fluorescent cells. I decided to pool the data from these experiments, treat each cell as an experiment in cellular motility, and determine whether the larger sample number and increased statistical power would detect small differences in cell speed between the lines. Pooling the data showed a small (36.6 μm/hr versus 31.9 μm/hr) speed difference between *Vcl*-null cells and the Vh cell-line (Figure 2-3). However, there was no speed difference between *Vcl*-null and vinculin-expressing lines. This result was not in agreement with previous publications showing that vinculin expression slows cell speed (Table 1-1).

Figure 2-3: **When the data from 8 individual experiments is pooled, there is no speed difference between** *Vcl*-null **and vinculin-expressing cells.** *Vcl*-null MEF cells virally transduced with eGFP-tagged constructs for vinculin, Vh, and D4 were plated on fibronectin-coated german coverglass chambers and allowed to recover at least 4 hrs. The chambers were then moved to an onstage incubator and imaged using 20x DIC or Phase objectives. The resulting films were analyzed by tracking the nucleus of 30 GFP-positive cells from each cell-line every 2 min over 4 hrs using Nikon Elements tracking software. The resulting pooled data was analyzed by ANOVA. Red line indicates average cell speed. *** implies p<0.0001.

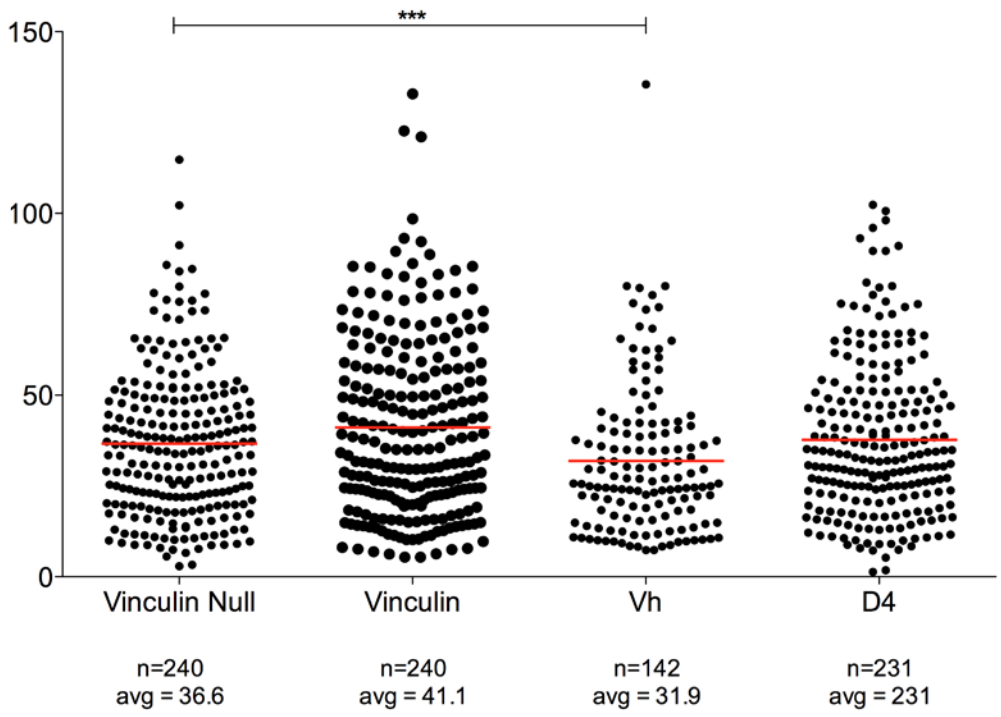

The inability to reproduce previously published differences in cell speed prompted me to study whether the substrate extracellular matrix (ECM) concentration affected cell speed. Palecek *et al.* had shown that CHO cells have a biphasic migration speed dependence on substrate fibronectin concentration. At low fibronectin concetrations, cell speed increased as fibronectin concentration on the substrate increased. However at high fibronectin concentrations, cell speed decreased as fibronectin concentration on the substrate increased (Palecek *et al.*, 1997). Our collaborators in the Garcia lab had preliminary data that the adhesiveness of our construct lines changed with fibronectin concentration. Additionally, I conducted a preliminary enzyme-linked immunosorbent assay (ELISA) to analyze the adsorption of fibronectin to the German coverglass chambers used in my assays. This ELISA data showed that incubation of the German coverglass chambers with 20 μg/mL fibronectin was near saturating while incubation of the German coverglass chambers with 5 μg/mL fibronectin reduced fibronectin binding 67% (data not shown). Based on this information, I hypothesized that my experiments were conducted at a saturating concentration of fibronectin (20 μg/ml) that limited cell speed and prevented detection of speed differences between the different cell-lines. To address concerns about whether the amount of fibronectin bound to the coverslips was responsible for the lack of motility differences observed between the virally transduced cell-lines, I conducted another random migration experiment where cell speed was analyzed at two different concentrations of fibronectin, 20 μg/mL and 2 μg/mL. Lowering the concentration of fibronectin used to coat the growth substrate increased overall migration speed, but this increase was not significant. Lowering the

concentration of fibronectin did not result in speed differences between *Vcl*-null and vinculin-expressing cells (Figure 2-4).

Figure 2-4: **Substrate fibronectin concentration has no effect on cell speed.** *Vcl*-null and vinculin-expressing cells were plated onto German coverglass chambers coated with either saturating (20 µg/mL) or minimal (2 µg/mL) fibronectin and allowed to recover for 48 hrs. Cells were filmed as described above with images collected every 6 min for 5 hrs. The resulting films were analyzed by tracking the nucleus of 30 GFP-positive cells from each cell-line every 6 min over 5 hrs using Nikon Elements tracking software. The resulting data was analyzed by ANOVA. Red bars indicate the mean cell speed.

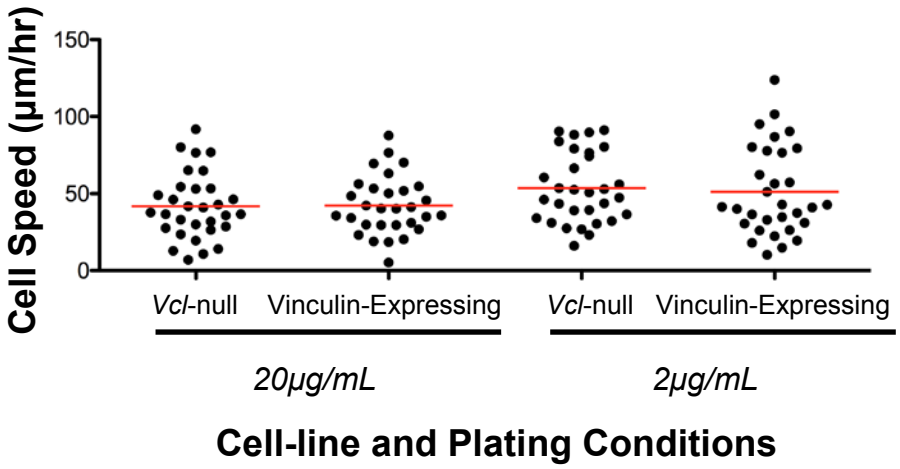

Although two studies have been published (Mierke *et al.*, 2010; Fraley *et al.*, 2010) that analyze random cell motility, the majority of studies on vinculin's effect on cell migration were performed using scratch wound healing assays and transwell systems

(Table 1-1). To determine whether the assay itself was the cause for not being able to replicate results published in previous studies, I used the virally transduced lines in a haptotaxis assay on transwells. An initial experiment did show a significant difference in migration between Vcl-null and vinculin-expressing cells. However, this migration was not a fold change as previously reported (Xu *et al.*, 1998a; Xu *et al.*, 1998b; DeMali *et al.*, 2002). Furthermore, this small but significant difference in cell speed between *Vcl*-null and vinculin-expressing did not replicate in an additional experiment (Figure 2-5).

Figure 2-5: An initial small but significant migration differences between *Vcl*-null and vinculin- expressing cells. Polyethylene terephthalate (PET) transwells were coated with either 20 µg/mL BSA (BSA) or 20 µg/mL fibronectin (FN). *Vcl*-null or vinculin-expressing cells were plated on the transwell, allowed to migrate through transwell for 8 hrs, fixed with paraformaldehyde, and stained with 0.1% crystal violet. For each experiment, three 20x fields were counted to determine relative cell migration. Bars represent standard deviation.

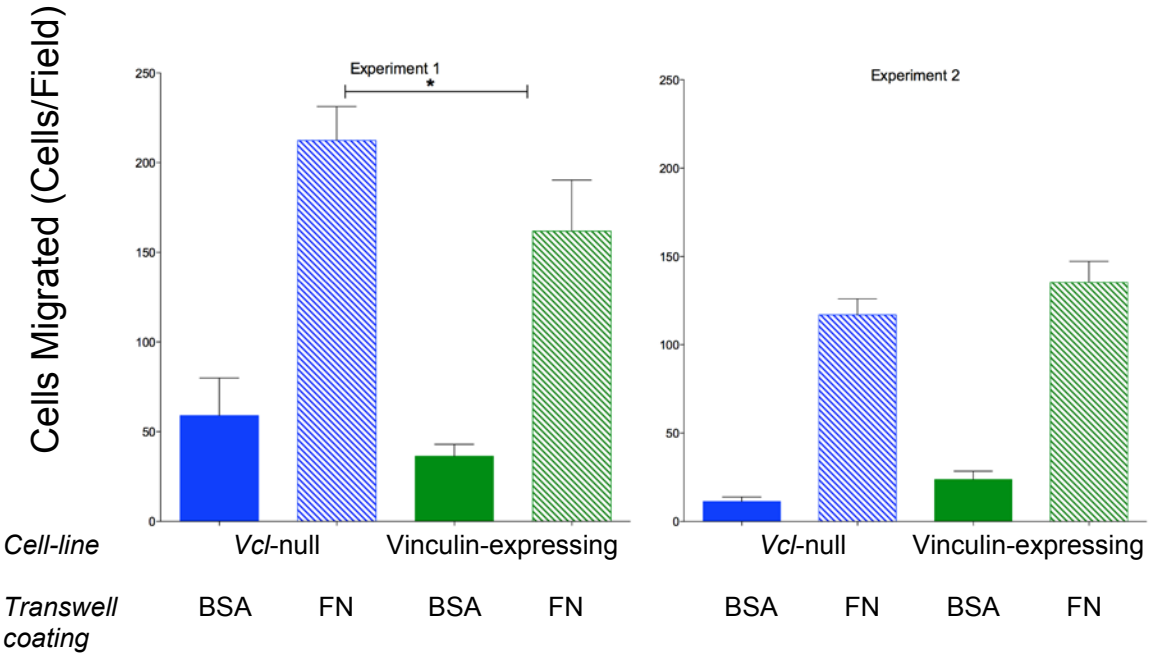

While my data did not show differences in cell speed between *Vcl*-null and vinculin-expressing cells, it was still possible that there were gross morphological differences between *Vcl*-null and vinculin-expressing cells. Previously published data shows that *Vcl*-null F9 cells have decreased cell area compared to wild-type F9 cells (Xu *et al.*, 1998b). To determine whether vinculin expression affected the average cell areas of the different virally transduced cell-lines, I randomly selected two of the previously collected timelapse microscopy experiments (Experiment 2 and Experiment 6) and reanalyzed the images to quantify cell area. Thirty cells from each cell-line were analyzed from each of these experiments, and the two experiments show similar trends in relative cell area. When the data was pooled across the two experiments, *Vcl*-null cells were found to be significantly smaller than any other cell-line studied (Figure 2-6). There was no difference in area between any of the lines expressing eGFP-labeled constructs. However, it should be noted that the negative control in these experiments, the parental *Vcl*-null MEFs, had not undergone the viral transduction process. Early discussions between our lab and the lab of our collaborator's had decided that the *Vcl*-null line would be an adequate initial negative control. The data in Figure 2-6 caused me to revisit how I would use the virally tranduced cell-lines in future experiments.

Figure 2-6: The parental *Vcl*-null MEFs have a consistently smaller cell area than all the cell-lines created with virally transduced vinculin constructs. Two previously collected timelapse experiments were reanalyzed to quantify the cell area of 30 GFP-positive cells in each cell-line. The data for the two experiments was pooled for statistical analysis. Each bar represents the mean area of 60 cells from two experiments. Analysis of the resulting data by ANOVA shows significant differences in area between the parental *Vcl*-null cell-line and all other cell-lines.

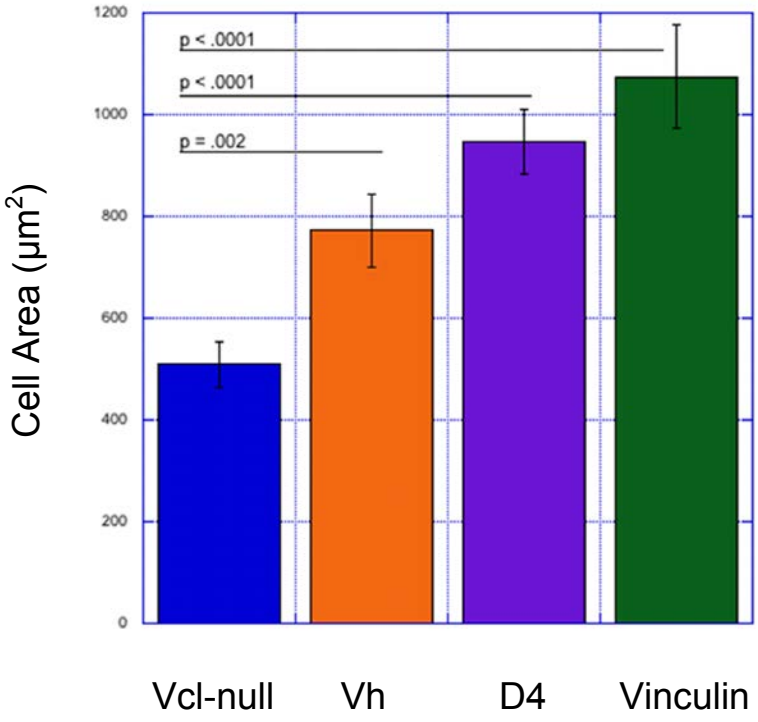

Since the only area differences occurred between the parental *Vcl*-null cell-line and virally transduced cell-lines, I began to question whether the parental *Vcl*-null cells were the appropriate negative control for my experiments. At this point, I decided to use the fact that the virally transduced lines were originally designed to allow tetracycline regulation of eGFP-construct expression to determine whether, in these cell-lines, *Vcl*-null cells have decreased cell area compared to cells expressing eGFP-tagged vinculin or eGFP-tagged vinculin mutants. Failure to reproduce my previous results showing that *Vcl*-null cells were significantly smaller than any other cell-line studied (Figure 2-6) with paired, tetracycline-regulated lines would indicate that the finding was due the parental *Vcl*-null cell-line being an inappropriate negative control for my previous experiments. Furthermore, it would stand as evidence that I should instead move towards a transient transfection system.

Prior to my joining the Craig lab, our collaborators in the Garcia lab had sent a library of cell-lines that had been virally transduced to have tetracycline-regulated expression of wild-type eGFP-vinculin and eGFP-tagged vinculin mutants. Each virally transduced cell-line used in this study was created with the eGFP-tagged vinculin construct downstream of a tetracycline-downregulated promoter. Culture of the virally transduced cell-lines in 10ng/mL tetracycline should repress expression of the eGFP-tagged constructs (Dumbauld, 2013). Therefore, treatment with tetracycline allows creation of a matched *Vcl*-null control cell-line for every virally transduced cell-line. To date, I had only used three of these lines (vinculin, D4, and Vh). Conversations with the Garcia lab had indicated that two of these lines were not able to be tetracycline-regulated: vinculin and D4.

Since I was going to invest the effort to create paired, tetracycline lines, I decided to examine the entirety of the cell-line library for the effect of vinculin and vinculin mutants on cell area. This would allow me to work with a new mutant of vinculin (A50I) as well as provide a cell-line containing a vinculin autoinhibition mutant (T12) that (according to the Garcia lab) could be tetracycline-regulated. FACS analysis of the A50I and T12 lines showed that these lines had similar baseline fluorescence to previously studied cell-lines (Figure 2-7a).

To provide a paired *Vcl*-null control for the vinculin line (which, according to the Garcia lab, could not be tetracycline-regulated), I purposefully FACS sorted GFP negative cells from the vinculin-expressing line. These cells were cultured as a separate line named "*Vcl*-null 2". These cells were maintained in culture for three weeks and showed no expression eGFP vinculin when analyzed three weeks later (Figure 2-7a). The *Vcl*-null 2 line would also allow me to test whether eGFP-fluorescence was truly linked to vinculin expression in the virally transduced lines. *Vcl*-null 2 cells should not contain tetracycline-regulated eGFP-tagged vinculin construct. Therefore, they should be resistant to any effects of tetracycline treatment.

Four cell-lines were initially treated with 10ng/mL tetracycline to determine by Western blot whether expression of the eGFP-tagged vinculin constructs could be repressed. As expected, the vinculin-expressing line showed no change with treatment. Treatment of the Vh-expressing and T12-expressing lines showed undetectable levels of eGFP-tagged protein by 7 days of treatment (Figure 2-7b). Based on conversations with the Garcia lab,

I did not test the regulation of the A50I and D4 cell-lines by Western blot. Instead, I considered the A50I cell-line tetracycline-regulated and the D4 cell-line incapable of tetracycline regulation. I then created paired cell-lines for every eGFP-tagged vinculin construct. To create negative controls (Tet +), each virally transduced line was treated with 10ng/mL tetracycline for at least 16 days to achieve maximum repression of construct expression. To ensure that construct-expressing cell-lines (Tet -) would continue to express comparable levels of fluorescence for future experiments, I continued to FACS sort these lines every two weeks for cells expressing 100-1000 FU.

Figure 2-7: **Testing the effect of vinculin and vinculin mutants on cell area required the use of additional cell-lines and testing the tetracycline regulation of the virally transduced lines.** A) The A50I and T12 lines showed comparable levels of baseline fluorescence to previously studied virally transduced cells lines. The T12 line provided a virally transduced line expressing a tetracycline-regulated autoinhibition mutant of vinculin. The *Vcl*-null 2 line isolated from the eGFP-vinculin line by FACS sorting showed no signs of spontaneous eGFP-vinculin expression 3 weeks after isolation. These cells were subsequently used as a negative control for the eGFP-vinculin line. B) The parental *Vcl*-null, vinculin, Vh, and T12 cell-lines were treated with 10ng/mL tetracycline. “Day” indicates the number of days the cells were treated with tetracycline. “Tet” indicates the presence or absence of tetracycline. The vinculin-expressing line is not regulated by tetracycline treatment. The Vh and T12 lines show undetectable levels of eGFP-tagged protein by 7 days.

A

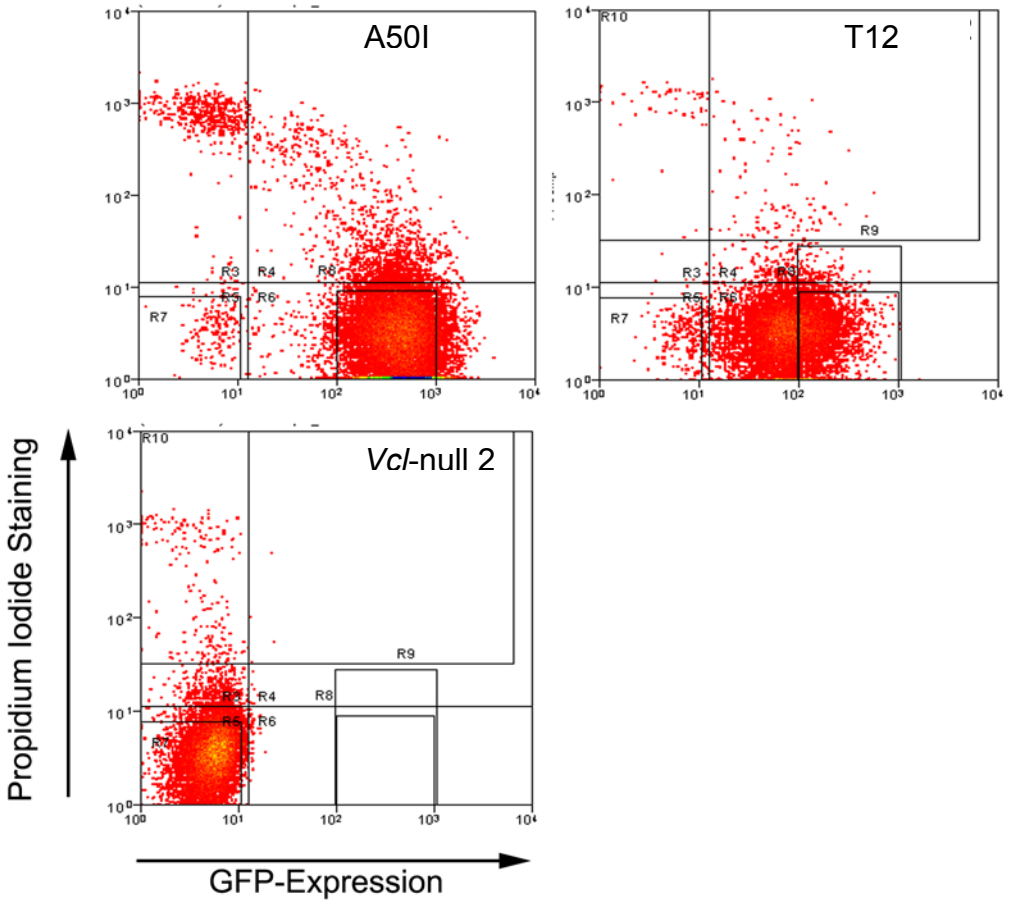
A50I
T12
Vcl-null 2
Propidium Iodide Staining
GFP-Expression

B

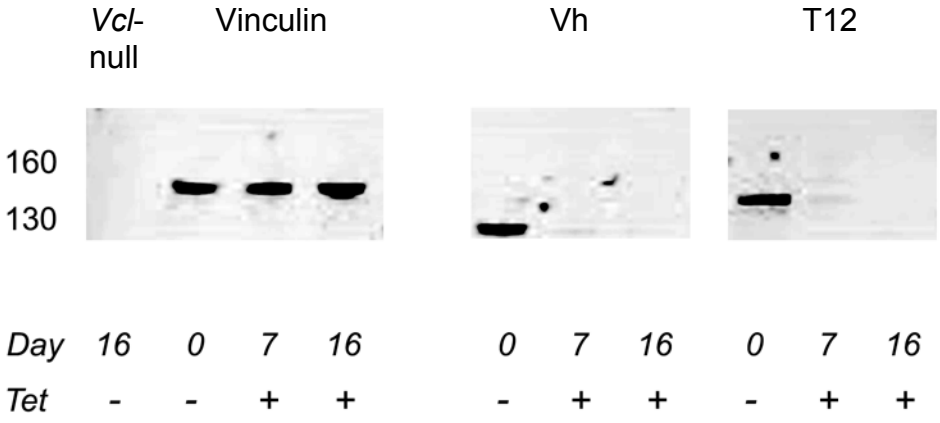
Vcl-null
Vinculin
Vh
T12
160
130
Day 16 0 7 16 0 7 16 0 7 16
Tet - - + + - + + - + +

All the construct-expressing lines and their paired negative control cell-lines were plated and imaged as described above. Two experiments were completed, and for each experiment thirty cells were analyzed for each cell-line. Since the trends in each individual experiment were similar, the data collected from the two experiments was pooled to give a larger sample number and increased statistical power. Of the cell-lines that could be tetracycline-regulated (A50I, Vh, and T12), only the Vh-expressing line showed a greater average cell area than its tetracycline-downregulated negative control ($p=0.001$) (Figure 2-8). This indicated that my previous findings (Figure 2-6) were likely the result of the parental *Vcl*-null cell-line being an inappropriate negative control for the virally transduced cell-lines. More significantly, the GFP-negative cells that had been FACS sorted from the vinculin line (*Vcl*-null 2) showed significant ($p=0.002$) changes in cell area with tetracycline treatment (Figure 2-8). This indicated that there was a disconnect between tetracycline regulation and eGFP-construct expression in these virally transduced cell-lines.

Figure 2-8: **Providing the virally transduced cell-lines with individual negative controls ablated most differences in cell area.** Two experiments were conducted using all the construct-expressing lines and their paired negative control cell-lines. Cells from each line were plated and filmed as previously described. For each experiment, 30 GFP-positive cells were analyzed for total cell area using Nikon Elements. The two separate experiments showed similar trends, so the data was pooled to increase sample number and statistical power. Each bar represents the average area of 60 analyzed cells for each condition. Solid bars indicate cell-lines expressing the construct listed. Bars with a hash mark pattern indicate the tetracycline treated paired control cells lines. *Vcl*-null 2 is a line created by FACS sorting the eGFP-vinculin-expressing line (Vinculin). Error bars indicate S.D. Data was analyzed by ANOVA. Of the lines that could be regulated (A50I, Vh, and T12), only the Vh-expressing line showed a greater average cell area than its tetracycline-downregulated negative control ($p=0.001$). The *Vcl*-null 2 cells should contain no tetracycline-regulated eGFP-vinculin construct but show significant changes ($p=0.002$) in cell area with tetracycline treatment.

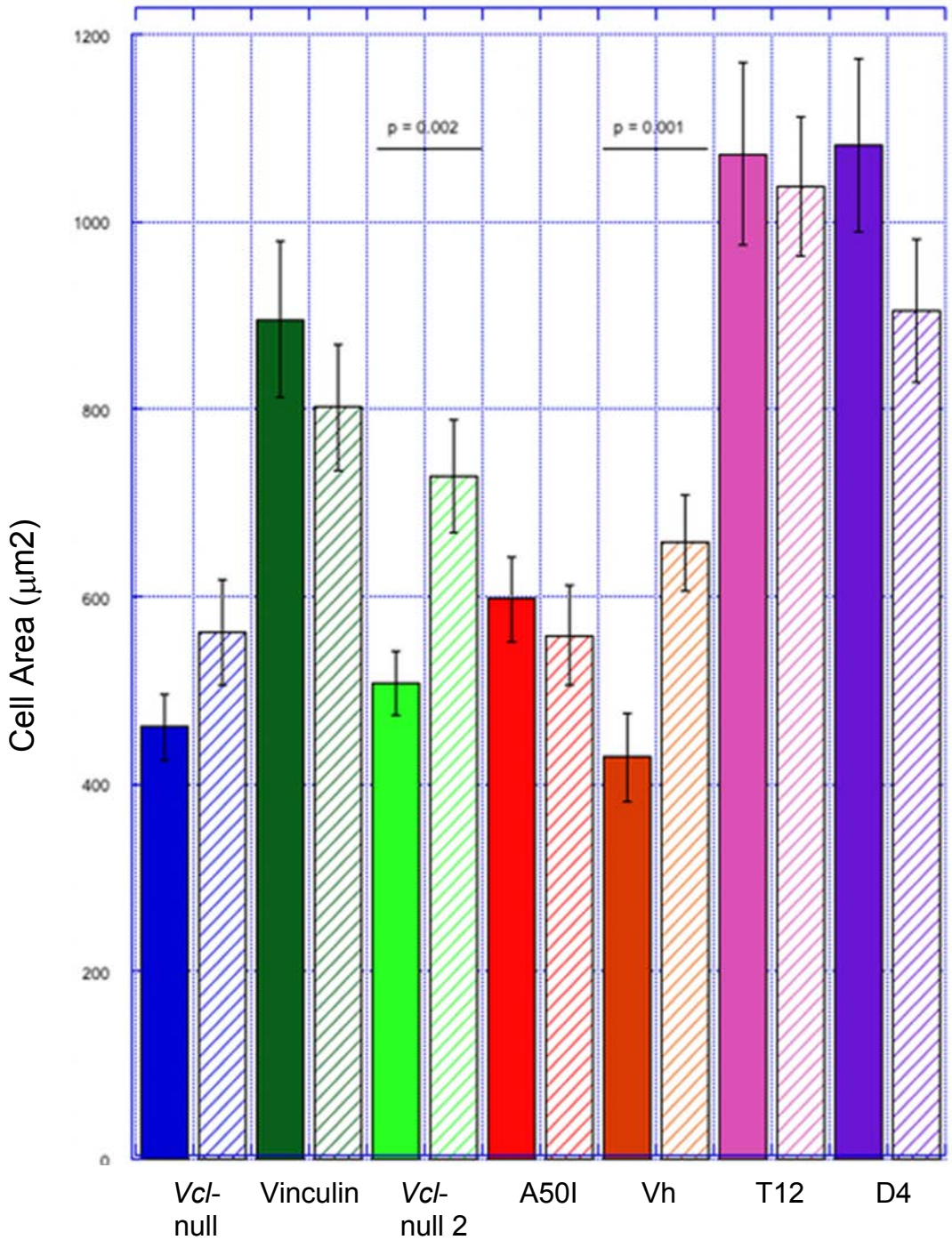
Cell Area (μm2)
1200
1000
800
600
400
200
0
p = 0.002
p = 0.001
Vcl-null
Vinculin
Vcl-null 2
A50I
Vh
T12
D4

Overall, using the paired, tetracycline-regulated lines showed me that my previous data showing that vinculin and vinculin mutants affect cell area were likely only due to an inappropriate negative control. Furthermore, this data indicated that I would have to address the caveat of using separate cell-lines to test phenotypic differences between *Vcl*-null and vinculin-expressing cells: Separate cell-lines, despite being generated from the sample parental cell-line, can diverge from each other when maintained separately in culture. As a result, attempts to compare phenotypic differences between the cell-lines may reflect differences between the lines that result from divergence and not from the expression of different eGFP-tagged constructs.

The caveats of using separate cell-lines to test for speed differences between *Vcl*-null cells and cells expressing various eGFP-tagged constructs could be addressed in several ways. One option would be to use the parental line as a negative control. However, my data shows that attempting to use the parental *Vcl*-null cell-line as a negative control does not produce the previously published result that expression of vinculin decreases cell speed. Another option would be to create a negative control cell-line by virally transducing the parental *Vcl*-null cell-line with an empty vector. Our collaborators in the Garcia lab attempted to virally transduce the parental *Vcl*-null cell-line with an empty vector but were not successful. Additionally, one could test multiple versions of each cell-line to ensure that observed phenotypic differences are dependent on the construct being expressed and not on divergence of the cell-lines being studied. However, this results in the need to maintain an onerous number of cell-lines. Finally, one could attempt to knockdown expression of endogenous vinculin with siRNA before expressing

the desired eGFP-tagged construct. However, previous studies in the Craig lab (unpublished data) showed that while siRNA attempts can significantly reduce vinculin expression levels on Western blot, the vinculin that is expressed in cells transfected with siRNA constructs against vinculin localizes to focal adhesions. Based on these options, and previous attempts to created alternative negative controls for vinculin expression in both the Craig lab and the Garcia lab, I decided that I would stop using the virally transduced cell-lines and repeat the random motility assays using transiently transfected cells.

One final experiment was conducted to confirm the presence of systemic errors in the virally transduced cell-lines. Timelapse microscopy was performed to compare cell speed between the vinculin line and the line obtained by FACS sorting the vinculin line for GFP-negative cells (*Vcl*-null 2). Thirty cells from each line were analyzed and there was no difference in speed (Figure 2-9).

Figure 2-9: A virally transduced vinculin-expressing lines compared to the most appropriate negative control failed to produce expected speed differences. The vinculin line and the line obtained by FACS sorting the vinculin line for GFP-negative cells (*Vcl*-null 2) were imaged as described above to determine the comparative cell speed of these cell-lines during random migration. The resulting film was analyzed by tracking the nucleus of 30 GFP-positive cells from each cell-line every 2 min over 4 hrs using Nikon Elements tracking software. The resulting data was analyzed by ANOVA. Red line indicates average cell speed. There was no speed difference between the two groups.

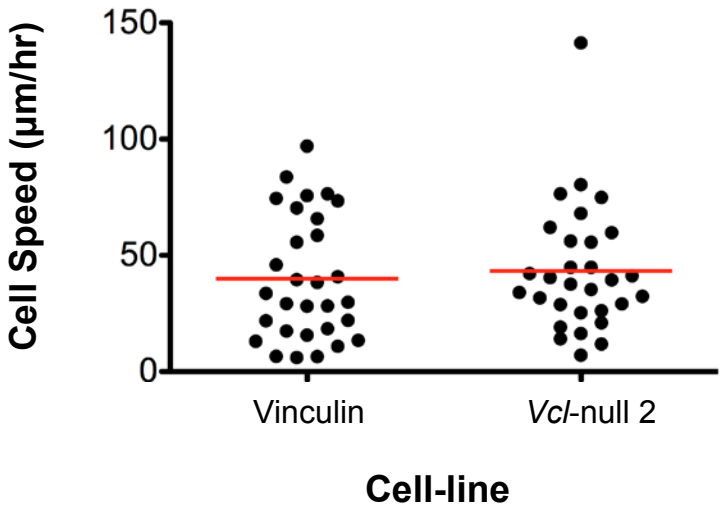

Since the virally transduced cell-lines had failed to produce a vinculin-dependent cell speed phenotype and since there was evidence that the tetracycline regulation in these lines was questionable, I deemed transient transfection necessary for any further studies on the effect of vinculin on cellular motility. Originally, transient transfection had been avoided because *Vcl*-null MEFs have a particularly low transfection rate of 1-2% using conventional lipofectamine. However, I was able to develop an electroporation protocol that had sufficient transfection efficiencies (20% - 40%) and the motility studies were repeated.

Five experiments using transiently transfected cells were conducted (Figure 2-10). The culture, plating, and microscopy conditions were identical to those described previously. As a negative control, *Vcl*-null cells were underwent an "empty transfection", *i.e.* they were electroporated in solution lacking a construct. There was no speed difference between empty transfections and cells that had been transiently transfected with eGFP alone (Figure 2-10, Experiment 1). There were no differences in cell speed between the negative controls and cells expressing any vinculin construct. However, the difficulty in transfecting certain constructs lead to small sample numbers in individual experiments. For this reason, the data was pooled to yield larger sample numbers and increase statistical power. The pooled data also showed no difference in cell speed between the negative controls and cells expressing vinculin or any vinculin mutant (Figure 2-11).

Figure 2-10: **Cells transiently transfected with different eGFP-vinculin mutant constructs showed no difference in cell speed compared to negative controls.** *Vcl*-null cells were transiently transfected with eGFP-tagged vinculin or vinculin mutant constructs, then plated and filmed as described above. As a negative control, *Vcl*-null cells were underwent an "empty transfection", *i.e.* they were electroporated in solution lacking a construct. Data on cell speed was analyzed by ANOVA. Red bars indicate average cell speed. Over five experiments, each evaluating slightly different groups of constructs, there was no difference in cell speed between the negative controls and any vinculin construct.

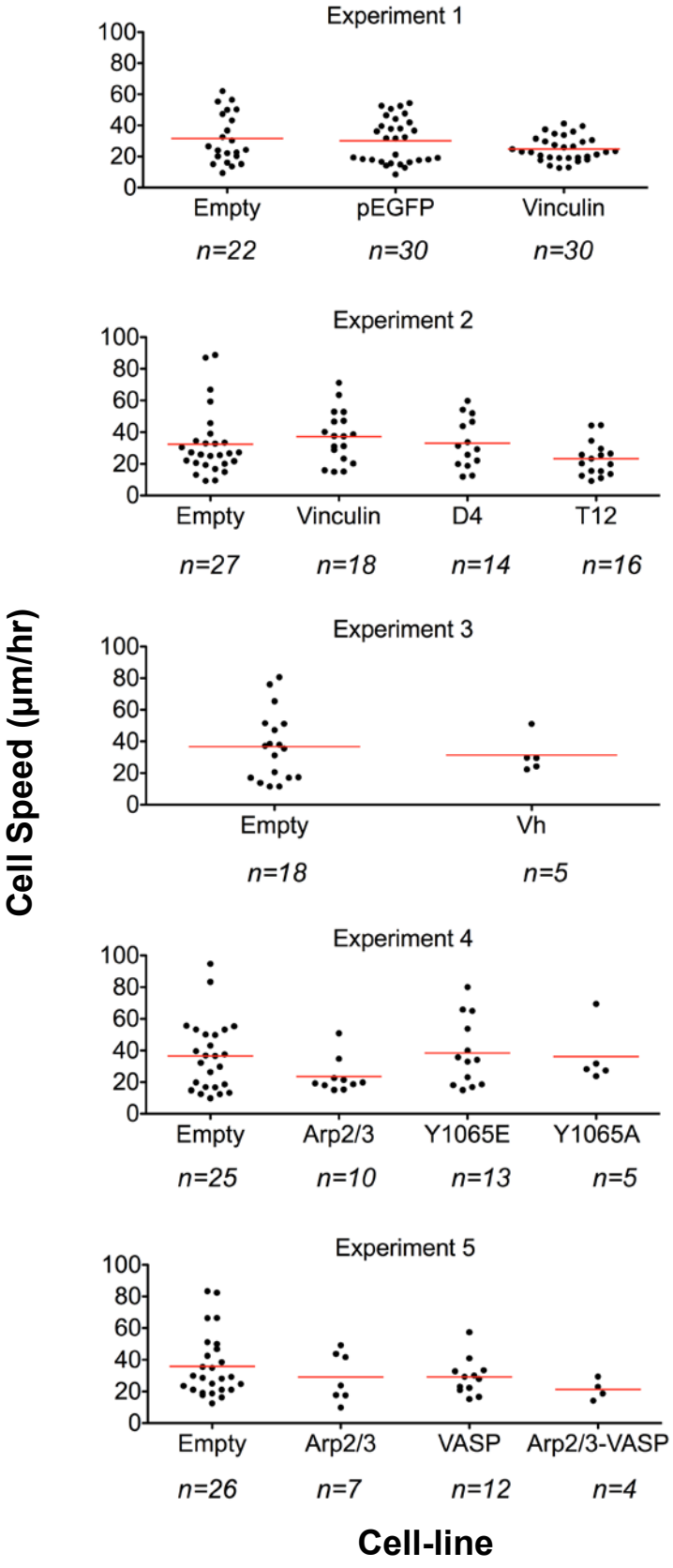
Experiment 1
100
80
60
40
20
0
Empty
pEGFP
Vinculin
n=22
n=30
n=30
Experiment 2
Empty
Vinculin
D4
T12
n=27
n=18
n=14
n=16
Experiment 3
Empty
Vh
n=18
n=5
Experiment 4
Empty
Arp2/3
Y1065E
Y1065A
n=25
n=10
n=13
n=5
Experiment 5
Empty
Arp2/3
VASP
Arp2/3-VASP
n=26
n=7
n=12
n=4
Cell Speed (µm/hr)
Cell-line

Figure 2-11: Pooled data across all transient transfection experiments show that the presence of vinculin, or any of its mutants, has no effect on cell speed. *Vcl*-null cells were transiently transfected with eGFP-tagged vinculin or vinculin mutant constructs, then plated and filmed as described above. As a negative control, *Vcl*-null cells underwent an "empty transfection", *i.e.* they were electroporated in solution lacking a construct. "Double Mutant" is a construct containing both the Arp2/3 and VASP mutations. Data on cell speed was analyzed by ANOVA. Red bars indicate average cell speed. There were no differences in cell speed between the negative controls and any vinculin construct.

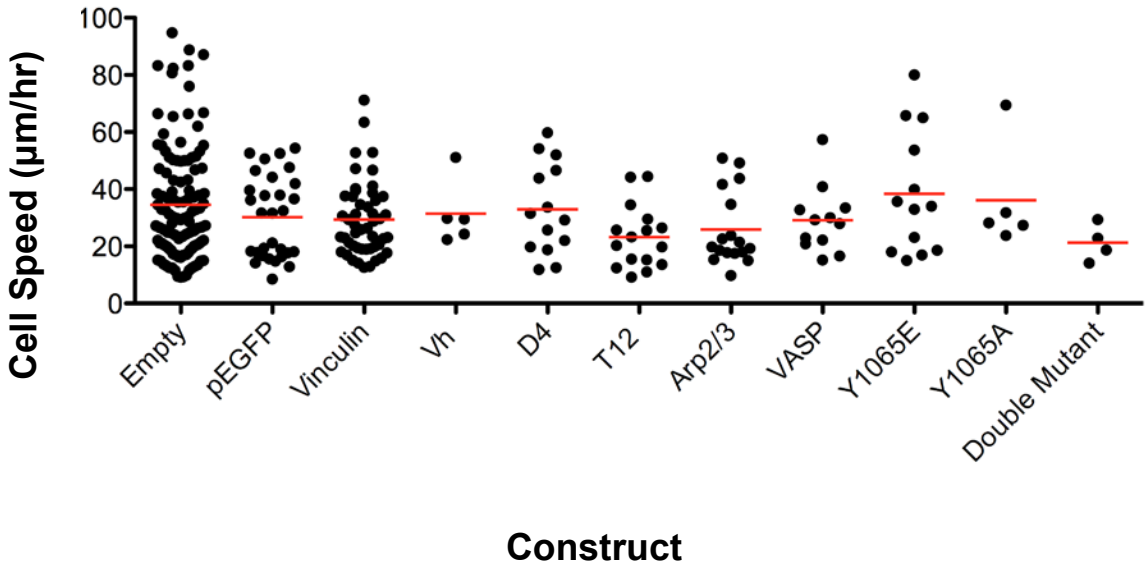

Discussion:

I began this study hoping to use virally transduced cell-lines expressing eGFP-tagged vinculin constructs to explore the effect of vinculin, its autoinhibition, and its ligand binding abilities on cell speed. These cells lines had been created in collaboration with the Garcia lab to have the eGFP-tagged constructs downstream of a tetracycline-downregulated promoter. Ideally, these lines could be treated with tetracycline to create a paired negative control cell-line. I also anticipated that they would be a superior system for generating a high level of reproducibility between experiments not achievable through transient transfection.

Prior to beginning my experiments, the Garcia lab had collected preliminary data that the vinculin and D4 lines were not under complete regulation by the tetracycline-downregulated promoter. They were, at the time, still trying to generate tetracycline-regulated lines for eGFP alone, eGFP-tagged vinculin, and eGFP-tagged D4. For this reason, after several discussions with both my lab and the Garcia lab, I decided to use the parental line used to create each of these cell-lines, *Vcl*-null MEFS from the Adamson lab, as negative control for my experiments. Figures 2-6, 2-8, and 2-9 together indicate that there is a distinct difference between using the parental line as a negative control and using a negative control that had been created by tetracycline downregulation of construct expression. When using the *Vcl*-null MEF parental line as a negative control, I found that vinculin, D4, and Vh had no effect on cell speed but significantly increased cell area.

These differences did not reproduce when a paired, tetracycline-downregulated negative control was created for each cell-line.

Despite these systemic and technical issues, this study did gather a large amount of data regarding the effect of vinculin on cellular motility. Since I used timelapse microscopy instead of population migration studies, I could treat each analyzed cell as an experiment on how the expression of a particular vinculin construct effects random motility. However, despite large sample numbers (Figure 2-3), I did not observe the previously reported finding that vinculin-expressing cells have a slower migration speed than *Vcl*-null cells (Table 1-1). Despite this, I do feel confident that these engineered lines are able to report phenotypic differences due to the expression of vinculin or its mutants. Our collaborators in the Garcia lab were able to use these lines to detect adhesion differences between cells expressing vinculin, Vh, and T12. However, the parental *Vcl*-null MEFs line served as the negative control in many of their experiments (Dumbauld, 2013). I have interpreted this to indicate that while the lines created were appropriate for the adhesion studies used in that paper, they were not appropriate for timelapse migration studies. Furthermore, I am confident that any shortcomings of the engineered lines were addressed when my experiments were repeated using transiently transfected *Vcl*-null MEFs (Figures 2-10 and 2-11) derived from vinculin null mouse embryos and wild type littermates.

A critical review of previous studies comparing the motility of *Vcl*-null to vinculin-expressing cells reveals that the majority of these studies were population migration

studies. There are only two published studies that use timelapse microscopy of individual cells instead of population migration studies. These studies had conflicting results. While Mierke (Mierke *et al.*, 2010) confirmed previous results showing a 3-fold speed difference, Fraley (Fraley *et al.*, 2010) reports no speed difference at all. I interpret these studies, in addition to my own, as indicating that the actual effect of vinculin on cell speed may not be dependent on its role in adhesiveness and that timelapse photography highlights this in a way that population studies do not. Although, if that were the case, I expect to have had similar results to previously published studies in at least in my haptotaxis assays (Figure 2-5). Additionally, only a single published study attempts to rescue a *Vcl*-null line with expression of a vinculin construct (Xu *et al.*, 1998b). In this study, the author published an image of a single haptoxis field that was analyzed in her study and states the expression of vinculin in *Vcl*-null cells decreased cell speed. There is no quantitation of the data presented. The remaining studies (Table 1-1) compare the relative cell speeds of separate cell-lines. After a review of my data and the conditions of previously published studies on the effect of vinculin on cell speed, I hypothesize that there is a difference in motility that is present in primary lines or newly immortalized *Vcl*-null lines that has been lost in my *Vcl*-null cells with passage. I have not repeated the motility studies in another cell-line to explore this.

References:

Bakolitsa, C., D.M. Cohen, L.A. Bankston, A.A. Bobkov, G.W. Cadwell, L. Jennings, D.R. Critchley, S.W. Craig, and R.C. Liddington. 2004. Structural basis for vinculin activation at sites of cell adhesion. *Nature*. 430:583-586.

Brindle, N.P., M.R. Holt, J.E. Davies, C.J. Price, and D.R. Critchley. 1996. The focal-adhesion vasodilator-stimulated phosphoprotein (VASP) binds to the proline-rich domain in vinculin. *The Biochemical journal*. 318 (Pt 3):753-757.

Cohen, D.M., H. Chen, R.P. Johnson, B. Choudhury, and S.W. Craig. 2005. Two distinct head-tail interfaces cooperate to suppress activation of vinculin by talin. *The Journal of biological chemistry*. 280:17109-17117.

DeMali, K.A., C.A. Barlow, and K. Burridge. 2002. Recruitment of the Arp2/3 complex to vinculin: coupling membrane protrusion to matrix adhesion. *The Journal of cell biology*. 159:881-891.

Dumbauld, D.W., T.T. Lee, A. Singh, J. Scrimgeour, C.A. Gersbach, E.A. Zamir, J. Fu, C.S. Chen, J.E. Curtis, S.W. Craig, and A.J. Garcia. 2013. How vinculin regulates force transmission. *Proceedings of the National Academy of Sciences of the United States of America*. 110:9788-9793.

Fraley, S.I., Y. Feng, R. Krishnamurthy, D.H. Kim, A. Celedon, G.D. Longmore, and D. Wirtz. 2010. A distinctive role for focal adhesion proteins in three-dimensional cell motility. *Nature cell biology*. 12:598-604.

Johnson, R.P., and S.W. Craig. 1994. An intramolecular association between the head and tail domains of vinculin modulates talin binding. *The Journal of biological chemistry*. 269:12611-12619.

Johnson, R.P., and S.W. Craig. 1995. F-actin binding site masked by the intramolecular association of vinculin head and tail domains. *Nature*. 373:261-264.

Kupper, K., N. Lang, C. Mohl, N. Kirchgessner, S. Born, W.H. Goldmann, R. Merkel, and B. Hoffmann. 2010. Tyrosine phosphorylation of vinculin at position 1065 modifies focal adhesion dynamics and cell tractions. *Biochemical and biophysical research communications*. 399:560-564.

Michael, K.E., Vernekar, V.N., Garcia A.J. 2003. Adsorption-Induced Conformational Changes in Fibronectin Due to Interactions with Well-Defined Surface Chemistries. *Langmuir*. 19:8033-8040.

Mierke, C.T., P. Kollmannsberger, D.P. Zitterbart, G. Diez, T.M. Koch, S. Marg, W.H. Ziegler, W.H. Goldmann, and B. Fabry. 2010. Vinculin facilitates cell invasion

into three-dimensional collagen matrices. *The Journal of biological chemistry*. 285:13121-13130.

Palecek, S.P., J.C. Loftus, M.H. Ginsberg, D.A. Lauffenburger, and A.F. Horwitz. 1997. Integrin-ligand binding properties govern cell migration speed through cell-substratum adhesiveness. *Nature*. 385:537-540.

Xu, W., H. Baribault, and E.D. Adamson. 1998a. Vinculin knockout results in heart and brain defects during embryonic development. *Development (Cambridge, England)*. 125:327-337.

Xu, W., J.L. Coll, and E.D. Adamson. 1998b. Rescue of the mutant phenotype by reexpression of full-length vinculin in null F9 cells; effects on cell locomotion by domain deleted vinculin. *Journal of cell science*. 111 (Pt 11):1535-1544.

Chapter 2 Supplementary Information:

Figure S2-1: An initial Western blot comparing the expression levels of eGFP-constructs in the virally transduced cell-lines. Lanes are as follows: 1) eGFP alone 2) Benchmark ladder 3) eGFP-Vh line 4) eGFP-vinculin line 5) eGFP-D4 line 6) *Vcl*-null parental line This image is a scanned reproduction of a printed image. The scanned image was imported into Photoshop and converted to black and white. Western blot samples were prepared by lysing $2x10^7$ cells from each line in 500 uL of lysis buffer. 5 uL of this sample was run a 4-12% Bis-Tris gel and transferred to nitrocellulose. Antibodies: eGFP (C22, 1:2000), actin (C4, 1:4000). The Vh, vinculin, and D4 lines all express eGFP-labelled vinculin construct, but at varying levels. No detectable eGFP alone is expressed in these cell-lines.

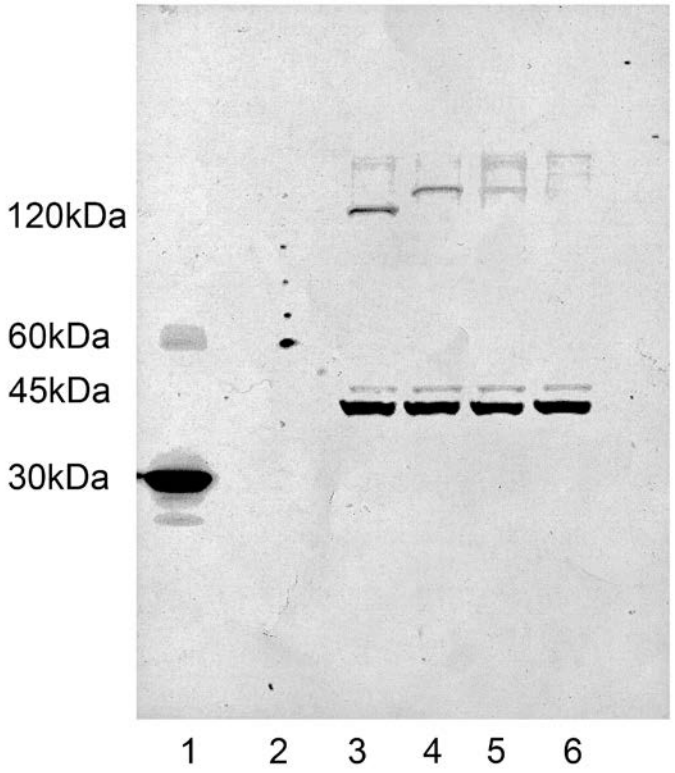

Table S2-1: **Summary of all motility experiments conducted.** Thirteen experiments comparing the cell speed of the virally transduced cell-lines were completed. “a” indicates a film taken 4 hrs after plating cells and “b” indicates a film taken 15 hrs after plating cells. Small changes in experimental conditions were made with each experiment (described in detail in the text) to determine if there were technical reasons I was not able to reproduce previously published differences in the cell speeds of *Vcl*-null versus vinculin-expressing cells. As no single experiment was able to do this, each experiment that filmed cells every 2 min for at least 4 hrs was analyzed both individually and included in a pooled analysis (Figure 2-2 and Figure 2-3). These experiments are marked “Yes” in the Data Analyzed column and are listed as Experiments 1-8 chronologically in Figure 2-3.

Date of Experiment	Cell-lines				FACS Sorted?	Condition of Cells?	Data Analyzed?	Results
	vin -/-	WT	Vh	D4				
8/20/09	x	x	x	x	No	Good	Yes	No differences in average speed. *Vcl*-null line has a greater distribution of velocities
9/15/2009a	x	x	x	x	No	Good	Yes	Vh significantly slower
9/15/2009b	x	x	x	x	No	Good	Yes	*Vcl*-null has a smaller spread in cell speeds. Vinculin-expressing slowest, then Vh.
10/22/2009b	x	x		x	Yes	Good	Yes	FACS sorted for 100-1000 FU. No differences in average cell speed.
11/6/2009a	x	x	x	x	No*	Good	No	Film not analyzed. Cells FACS analyzed but not sorted and microscope's fluorescent bulb broken.
11/6/2009b	x	x	x	x	No*	Good	No	Film not analyzed. Cells FACS analyzed but not sorted and microscope's fluorescent bulb broken.
11/16/2009a	x	x	x	x	Yes	Poor	No	Garcia lab HDT substrate. Cells are spiky and many die during filming. Film not analyzed.
11/16/2009b	x	x	x	x	Yes	Not ideal	No	Garcia lab HDT substrate. Cells more spiky than usual and have low motility. Film not analyzed.
11/20/09	x		x	x	No	Good	No	Biowrite (Intelligent Substrates™) substrate. Cells initially looked healthy but died during filming. Film not analyzed.
12/3/2009a	x	x	x	x	Yes	Good	Yes	FACS sorted for 50-100 FU. Cells infected and grown for 12 hrs in Pen/Strep/Gent. Experiments conducted in Pen/Strep. Occasional Vh cell is blebby.
12/3/2009b	x	x	x	x	Yes	Poor	Yes	FACS sorted for 50-100 FU. Cells infected and grown for 12 hrs in Pen/Strep/Gent. Experiment conducted in Pen/Strep. All lines contain a few blebby cells.
12/4/2009a	x	x		x	Yes	Not ideal	Yes	FACS sorted for 100-1000 FU. Cells infected and grown for 24 hrs in Pen/Strep/Gent. Experiment conducted in Pen/Strep/Gent. A few blebby cells in all lines, but fewer than on 12/3/2009.
12/4/2009b	x	x		x	Yes	Good	Yes	FACS sorted for 100-1000 FU. Cells infected and grown for 24 hrs in Pen/Strep/Gent. Experiment conducted in Pen/Strep/Gent. A few blebby cells in all lines, but fewer than on 12/3/2009.

Chapter 3:

A Simple Benchtop Device to Study the Effects of Acute Uniaxial Stretch Applied to Mature Focal Adhesions

Abstract:

Studies showing a positive correlation between the size of a focal adhesion and the traction force exerted by that focal adhesion on the cell substrate prompted questions about how focal adhesions would respond to the application of external force. Over the last decade, several studies have tried various approaches to applying external force to living cells. The methods and results have been varied, but together they have led to the consensus within the field that the application of external force to living cells leads to an increase in focal adhesion size. In order to determine the role of vinculin, its autoinhibition, and its ligand binding abilities on the focal adhesion response to external force, I developed a simple, manual device capable of applying uniaxial stretch to living cells. I then applied acute, uniaxial stretch to living cells expressing two markers of focal adhesions: vinculin and paxillin. Surprisingly, while stretched cells could show impressive changes in focal adhesion size and number, I found that these changes did not occur with greater frequency in stretched cells than in unpaired timelapse controls. This result prompted me to examine published studies on the effects of external force on living cells for conditional aspects of the assays that might explain why I could not produce the expected result of uniaxial stretch causing increased focal adhesion size. In doing so, I found evidence that previous studies may have been conducted under conditions that weigh the observations toward the effect of external force on the growth of nascent focal adhesions. Furthermore, I did not find a single study that was conducted to parse how the application of external force affects nascent versus mature focal adhesions. In light of this information, I hypothesize that external force may have different effects on different

populations of focal adhesions. Furthermore, I believe that my data is in accordance with two more recent studies indicating that established focal adhesions respond differently than nascent focal adhesions to external force. My assay, with several clearly described modifications, could in the future be used to determine the effects of external force on different populations of focal adhesions. Once such a study is completed, then one would be able to probe the role of vinculin in the focal adhesion response to force.

Introduction:

Studies characterizing the interaction between cells and their substrates led to the discovery that cells are capable of exerting traction forces upon their substrates. Cells in culture are capable of generating traction forces sufficient to cause gross deformation of rubber or collagen artificial substrates (Harris *et al.*, 1981; Stopak *et al.*, 1985; Lee *et al.*, 1994; Oliver *et al.*, 1995). *In vivo*, the cells of a developing embryo exert sufficient traction forces to rearrange injected, fluorescently labeled collagen according to the needs of developing embryo (Stopak *et al.*, 1985). More recent advances in microfabrication and imaging technology have allowed analysis of how individual focal adhesions generate traction forces. These studies have shown that cells can sense the rigidity of their growth substrate (Pelham and Wang, 1997) and increase focal adhesion number and size in response to increased substrate stiffness (Pelham and Wang, 1997; Choquet *et al.*, 1997). Subsequent research quantifying the traction forces exerted by individual focal adhesions on a cell's growth substrate has led to the consensus within the field that increasing traction force upon a substrate is correlated with increasing focal adhesion size (Beningo *et al.*, 2001; Balaban *et al.*, 2001; Tan *et al.*, 2003; Goffin *et al.*, 2006). However, there is evidence that the relationship between focal adhesion size and traction force is complex. Very small (Tan *et al.*, 2003) and very large focal adhesions have been shown to exert traction forces disproportionate to their size (Goffin *et al.*, 2006). Furthermore, locomoting cells show an inverse relationship between traction force and focal adhesion length at the leading edge of cells, but not in their retracting tails (Beningo *et al.*, 2001). Clearly, how a cell modifies focal adhesions to generate various traction

forces, and what dictates the strength of traction forces generated, has not been completely parsed. However, studies on the maturation of focal adhesions indicate that myosin II-dependent contractility is necessary for focal adhesion growth (Riveline *et al.*, 2001; Choi *et al.*, 2008). To mimic cellular contractility, several studies have intentionally applied force to living cells to study the focal adhesion response to external force. These studies have used the focal adhesion proteins vinculin (Riveline *et al.*, 2001; Galbraith *et al.*, 2002; Sniadecki *et al.*, 2007) and paxillin (Sawada and Sheetz, 2002) as reporters of focal adhesion growth and provided evidence that there is also a correlation between applied external force (as opposed to traction force) and focal adhesion size. While each study used slightly different methods and had slightly varied results, together these studies have led to the consensus within the field that application of external force to cells results in increased focal adhesion size.

Vinculin could potentially play a role in regulating traction forces. Vinculin is recruited early in the process of focal adhesion maturation (DePasquale and Izzard, 1987; Izzard, 1988; Ezzell *et al.*, 1997; Choi *et al.*, 2008) and could potentially regulate the assembly of new adhesions. Since one of vinculin's proposed functions within a cell is to act as a mechanical linker between the cytoskeleton and the extracellular matrix, a role for vinculin in regulating the focal adhesion growth and traction forces would provide a mechanism for mechanosensing in focal adhesions.

This potential role for vinculin is supported by data generated using *Vcl*-null cells. Loss of vinculin in most cells decreases lamellipodial protrusion (Rodriguez Fernandez *et al.*,

1993; Xu *et al.*, 1998; DeMali *et al.*, 2002), decreases focal adhesion size (Rodriguez Fernandez *et al.*, 1993; Xu *et al.*, 1998), and decreases overall cell adhesion (Xu *et al.*, 1998; Dumbauld, 2013), while increasing cell speed (Table 1-1). Since cellular motility is dependent on the strength of adhesions generated between the cell and the extracellular matrix (Palecek *et al.*, 1997), together these findings indicate that cellular motility may be partly regulated by altering cellular traction forces through focal adhesions. These studies also indicate that information on how the autoinhibition and ligand binding abilities of vinculin affect focal adhesion responses to external force would illuminate how vinculin regulates cell adhesion and motility. Previous studies have shown that expression of vinculin autoinhibition mutants (Cohen *et al.*, 2005; Humphries *et al.*, 2007) or VD1 increase focal adhesion size and number. It has also been shown that autoinhibition mutants of vinculin increase cellular adhesion (Dumbauld, 2013). However, no study has expressed vinculin autoinhibition or ligand binding mutants in cells to ascertain their effect on how focal adhesions respond to external force.

In this study I first develop a simple, manually operated device to apply uniaxial stretch commercial, silicone-based cell culture chambers. After characterization, the device is used to apply acute, uniaxial stretch to cells expressing YFP-Paxillin, eGFP-vinculin, or eGFP-Vh. Despite each focal adhesion marker showing instances of marked focal adhesion change in stretched cells, analysis of all peripheral focal adhesions, regardless of focal adhesion marker, showed no difference in focal adhesion number or area between stretched cells and their unpaired timelapse controls.

Materials and Methods:

Cell culture: *Vcl*-null mouse embryo fibroblasts (MEFs), a kind gift from Eileen Adamson, have been previously described (Xu *et al.*, 1998) and were maintained in phenol-free, high glucose DMEM (Gibco 31053) supplemented with 10% FBS (Hyclone) and 2 mM glutamine (Gibco 25030). HEK293 cells were provided by Dr. Peter Devreotes at Johns Hopkins University and were maintained in high glucose DMEM supplemented with 10% FBS (Hyclone). Cells were cultured at 37°C and 5% CO_2 on tissue culture plastic coated with 0.1% gelatin. For transfer onto other growth substrates, cells were enzymatically lifted from the culture dish using 0.04% trypsin (Gibco 15090).

Cell transfection: 2 x 10^6 cells were combined with 100 µL of Ingenio Electroporation Solution (Mirus MIR 50117) and 15 µg of appropriate DNA. Cells were electroporated using setting T-20 on an Amaxa electroporation machine. Electroporated cells were transferred to RPMI with 10% FBS and incubated for 10 min at 37°C to aid membrane closure. Transfected cells were then transferred to 4 mL of phenol-free, high glucose DMEM (Gibco 31053) supplemented with 10% FBS (Hyclone) and 2 mM glutamine (Gibco 25030) and allowed to recover for 48 hrs before use in experiments.

YFP-paxillin lysate for cytoskeletal experiments: HEK 293 cells were seeded on 0.1% gelatin-coated 100 mm dishes at 3 x 10^6 per plate; transfection was performed the next day with 3 µg of plasmid DNA using Lipofectamine/Plus reagent (Invitrogen). HEK 293 cells were lysed 2.5-5 days after transfection with Stretch Assay Buffer (SAB) (20 mM

HEPES, 150 mM NaCl, 4 mM $MgCl_2$, 0.05 mM $CaCl_2$, 0.5 mM ATP, 1 mM PMSF, 1 mM DTT, 0.02% BSA). SAB+ refers to SAB with 2x protease inhibitor cocktail I (PIC I) and protease inhibitor cocktail II (PIC II)) from 1000x stocks . 1000x PIC I stock contained 1 mg/mL leupeptin, 2 mg/mL antipain, 10 mg/mL benzamidine, 10 KIU/mL aprotinin in H_2O. 1000x PIC II contained 1 mg/mL chymostatin, and 1 mg/mL pepstatin in dimethyl sulfoxide. Lysates were evaluated for fluorescence using a fluorimeter and a standard curve for EGFP/YFP concentration.

Construction of the uniaxial stretch device: The device is made from 6-gauge aluminum (base plate), stainless steel screws, and Teflon (slider bars and stabilizing plate), all of which are durable, easily cut, and inexpensive. The base plate and slider bars are threaded, which allows the thumbscrews to stabilize the entire setup securely. The device is resistant to ethanol and isopropanol, allowing it to be sterilized for use in cell-culture applications. Coating of the aluminum base plate with a standard, matte, water-based paint was necessary to prevent corrosion in live-cell, incubated conditions. Milling was use to cut exactly vertical lines in which the sliding screws could move, ensuring that each silicone chamber was stretched in exactly the same manner as the one next to it. The dimensions of the base plate and the spacing of the slider bar and secured screws were chosen to be compatible with a silicone chamber system already in use. The entire device was manufactured using a standard workbench drill and (for the larger device) lathe. The cost of a single, reusable device, excluding the silicone chambers, can be approximated at <$100, the bulk of which is manual labor costs. In order to modify the device for live cell imaging, the base plate was manufactured on a smaller scale to be

compatible with a Tokai Hit INUBTFP-WSKM-F1 onstage incubator mounted on a Nikon Eclipse Ti with a motorized stage.

Cytoskeletal stretch assay: Silicone stretch chambers (B-Bridge) were coated with human plasma fibronectin at 20 μg/ml (Gibco 33016) diluted in Dulbecco's Phosphate-Buffered Saline (DPBS) and plated with $0.25x10^6$ *Vcl*-null cells in DMEM supplemented with 10% FBS (Hyclone), 2 mM glutamine (Gibco 25030), penicillin (μg/mL), and gentamycin (20 μg/mL) After 2 days (~80% confluency), the cells were rinsed twice with warm DPBS (37°C) and crosslinked to the fibronectin substrate using the cell impermeable reversible crosslinker 3,3´-Dithiobis(sulfosuccinimidylpropionate) (Sigma) at 1 mM in DPBS for 15 min at 37°C. The cells were rinsed 2x and the crosslinking reaction quenched with 50 mM Tris-HCl pH 7.5 in DPBS for 15 min at 37°C. The cells were then rinsed 2x with Stretch Assay Buffer (SAB) (20 mM HEPES, 150 mM NaCl, 4 mM $MgCl_2$, 0.05 mM $CaCl_2$, 0.5 mM ATP, 1 mM PMSF, 1 mM DTT, 0.02% BSA) before being incubated with 0.003% digitonin in SAB+ to create digitonin-insoluble cytoskeletons. The resulting cytoskeletons were rinsed once with SAB+ and stretched 15% uniaxially on a Strex mechanical strain instrument (B-Bridge). Exogenous proteins diluted in SAB+ were immediately added and the system was stretched for 5 min at 37°C. Stretched cytoskeletons were then rinsed with SAB+ before adding 100 μL 0.1% Triton X-100 diluted in SAB+. Samples were scraped from the silicone substrate using the rounded edge of a pipette tip and stored at 0°C. Live images of cell stretch were taken using the custom-built stretch device engineered to be compatible with a TokaiHit WSKM onstage incubator.

Immunoblotting: Western blots were developed with species-specific infrared secondary antibodies (Li-Cor) per the manufacturer's instructions. YFP-labelled paxillin was detected with a lab developed, affinity-purified primary antibody EGFP-A (1:1300). G-11 anti-vinculin was obtained from Sigma and used at a 1:250 dilution. Anti-actin C4 (1:4000) was a kind gift from Dr. Jim Lessard.

Microscopy of immunostained cytoskeletons: *Vcl*-null cells were plated onto either poly-L-lysine treated coverslips coated with 20 μg/mL human plasma fibronectin or fibronectin-coated stretch chambers and allowed to reach ~80% confluency. Cytoskeletons were created as above and fixed using 4% paraformaldyhyde in ddH_20 pH 7.3 at room temperature for 30 min and blocked using 2% goat serum. Rabbit anti-EGFP affinity purified antibody (EGFP-A) was made in lab and used at 1:1300 dilution , anti-talin 8D4 was used 1:50 (Sigma T3287) or used neat from a monoclonal supernatant. Coverslips were mounted in Prolong Gold Anti-Fade solution with DAPI. Confocal images were acquired on an upright LSM 510 (Carl Zeiss, Germany) microscope using Zeiss AIM software. Digital images were imported into Adobe Photoshop for figure preparation. All other images were acquired on a Nikon Eclipse Ti using Elements software.

Live imaging: Transfected cells were plated on a silicone chamber (Strex ST-CH-10) coated with 20 μg/mL human plasma fibronectin (Gibco), and incubated at 37°C and 5% CO_2 to recover for 48 hrs. For experiments, chambers were mounted onto a manual

stretch device fitted to a Tokai Hit INUBTFP-WSKM-F1on-stage incubator mounted to a Nikon Ti Eclipse Microscope. In order to stabilize the relatively thin bottom of the silicone chamber, a 22x50 mm No.1 cover glass was placed beneath the chamber in the unstretched state and removed for visualization during stretches. Images were taken with a 40x CFI Plan Fluor ELWD NA 0.6 ELWD objective and a Photometrics HQ2 Coolsnap camera.

Image Analysis: All images were segmented and quantified using Nikon Elements software. Fluorescent images collected using a 40x extra long working distance phase objective were first segmented to minimize cytoplasmic signal while preserving signal from focal adhesions using the Image Detect Peaks tool. The resulting secondary images were inverted and then thresholded to create a binary that reflected only cellular focal adhesions. This binary was then analyzed in Elements to report every focal adhesion as an object, without additional conversion of each object into a smooth ellipse. Focal adhesion length is reported as the longest axis of each object. Circularity is reported as the ratio of the length and width axes (a perfect circle = 1) using the formula Circularity = $4* \pi *\text{Area}/\text{Perimeter}^2$ to include non-elliptical objects. The perimeter is reported as the length of the outside boundary of an object and calculated using Elements' application of Crofton's formula where for a given object, the total perimeter = $n *(Pr_0 + Pr_{45} + Pr_{90} + Pr_{135})/4$ using *n* as a given curve and *Pr* as a defined projection through space. The focal adhesion angle was taken from the Elements output of Orientation, calculated by determining the angle between the long axis of an object and the horizon (set to be parallel with the direction of stretch). Negative angles of orientation were avoided by

limiting all focal adhesions to occurring between 0 and 179 degrees from the horizon, with orientations greater than 90 degrees indicating that the focal adhesion extended in a direction opposite that of stretch. A focal adhesion was categorized as perpendicular to stretch if the orientation was between 45 and 135 degrees. All other orientations were considered parallel to the direction of stretch.

Statistics: All statistics were performed using Prism 5 by GraphPad software. The statistical tests used are as listed in figure legends.

Results:

This project began with a need to simultaneously apply external force and image living cells in order to detect focal adhesion change over time. Previous labs have published their assays, but after much deliberation I chose to avoid the potential technical pitfalls of trying to recreate the highly specialized assays of other labs using our available equipment. Investigation into more widely available methods for applying external force to cells introduced me to two commercial systems designed to study the effect of externally generated tension on adherent cells or cytoskeletons, Flexcell® and B-Bridge Strex®. These systems apply biaxial (Flexcell) or uniaxial (Strex) stretch to silicone-based cell culture chambers and the tension generated on the chamber is transmitted to adherent cells. While these commercial systems are available for purchase, I needed a device that was affordable and easily accessible to my lab. I considered an ideal device one that would cost a fraction of what the commercial systems cost and yet be compatible

with commercially available, silicone-based cell-culture chambers. To this end, I chose to purchase silicone-based cell culture chambers, but design my own device to generate tension on the chamber.

After examination of how a Strex machine applies uniaxial stretch to a chamber, I realized I could construct a similar, manually operated device that depended on a sliding bar system secured with thumbscrews rather than automated pistons. This manual device is constructed with a 6-gauge aluminum base plate for tensile strength, resistance to corrosion, and the ability to withstand autoclave conditions if necessary. All other parts were constructed out of stainless steel to prevent corrosion in a humidified incubator.

Operation of the device is simple. The base plate has two sides. One side has secured screws and the other has pre-drilled grooves that allow the center-to-center movement of the sliding screws to be exactly 5 mm. Each silicone-based cell culture chamber sold by B-Bridge has a cell culture area of 3.2 mm x 3.2 mm and comes prefabricated with four holes for mounting onto the Strex machine. On my device, one side of the chamber is immobilized by the secured screws on the baseplate. The other side is sandwiched between the slider bar and the stabilization plate. The sliding screws move the sliding bar from the unstretched position to the stretched position by traveling the complete distance of the grooves in the base plate. This causes the sandwiched end of the chamber to move uniaxially 5 mm (Figure 3-1a). This basic design was later turned into two different manual stretch devices. One is designed to hold five chambers and is intended for use in *in vitro* cytoskeletal experiments (Figure 3-1b). The other is designed on a smaller scale

and is only capable of holding one chamber, but the smaller device is compatible with the dimensions of a Tokai onstage incubator (Figures 3-1c and 3-1d). On the smaller device, the slider bar is constructed out of Teflon to ease smooth transition from the unstretched to stretched state.

Figure 3-1: Design of two simple, manually operated devices to study the effect of uniaxial stretch on cytoskeletons and live cells. A. Basic mechanism of both devices. A silicone chamber is immobilized at one end while a sliding pull bar is moved to achieve the desired uniaxial stretch. Thumbscrews are used to anchor the stretch for the desired amount of time. B. The large device designed to stretch multiple chambers at once. C. The small-scale device, designed using the same principles, allows live imaging of stretched cells. D. Small-scale device mounted in a Tokai on-stage incubator.

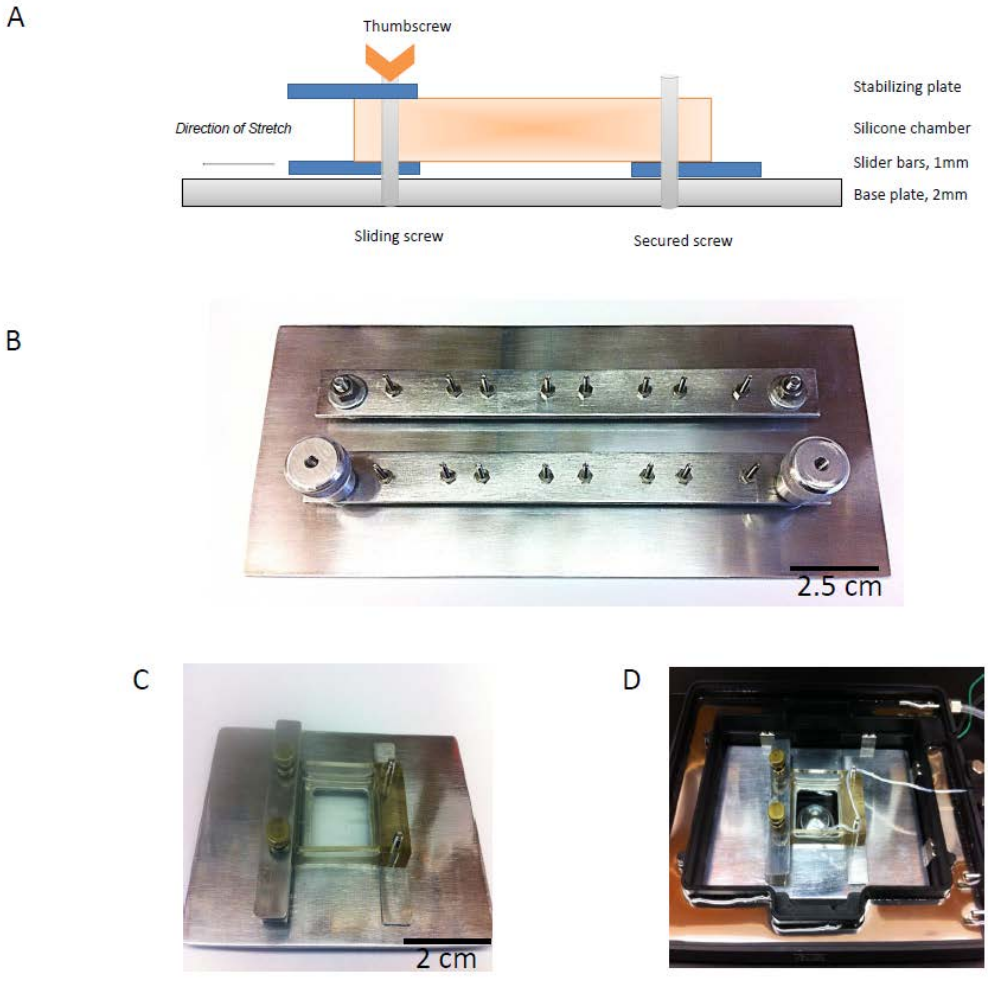

To characterize the device, I first measured the change in length experienced by the mounted chamber. In my design, the moving end of the chamber is displaced 5 mm, theoretically increasing the length of the chamber from 3.2 cm to 3.7 cm, which provides a 15.6% uniaxial stretch. To determine the actual stretch experienced by the chamber, I marked 1 cm vertical lines onto the cell culture area of the chamber with a marker and moved the sliding bar 5 mm. To illustrate this displacement, a ruler was mounted underneath the chamber (Figure 3-2). Using a camera mounted at a fixed distance above the chamber, the chamber was photographed in the unstretched and stretched positions. The resulting images were imported into Nikon elements and calibrated using the known dimensions of the chamber. The length of the cell culture chamber is 3.23 cm in the unstretched state and 3.69 cm in the stretched state, resulting in a 14.2% stretch across the chamber (Figure 3-2). Attempts to analyze the drawn lines using Elements software augmented manual error because the lines appeared as streaks or dots at high magnification. Instead, to analyze the change in length of the lines drawn on the chamber, I printed large-scale versions of the unstretched and stretched chamber images and measured the line change manually using a ruler. This approach showed that lines experienced an average stretch of 13.8 ± 1.5%.

Figure 3-2: Quantitation of the length change imposed on a silicone chamber using the manual device. Purchased, silicone-based cell culture chambers were marked with 5 mm black marker lines and mounted onto the large manual stretch device. Using a camera mounted at a fixed distance above the chamber, the chamber was imaged in the unstretched position. Then the slider bar was moved 5 mm to the stretched position and the chamber was imaged again. The resulting images were imported into Nikon elements and calibrated using the known dimensions of the chamber. The total length of the chamber increases from 3.23 cm in the unstretched state to 3.69 cm in the stretched state, a 14.2% change. Manual measurement of the lines on enlarged images showed that the lines increased in length 13.8 ± 1.5%.

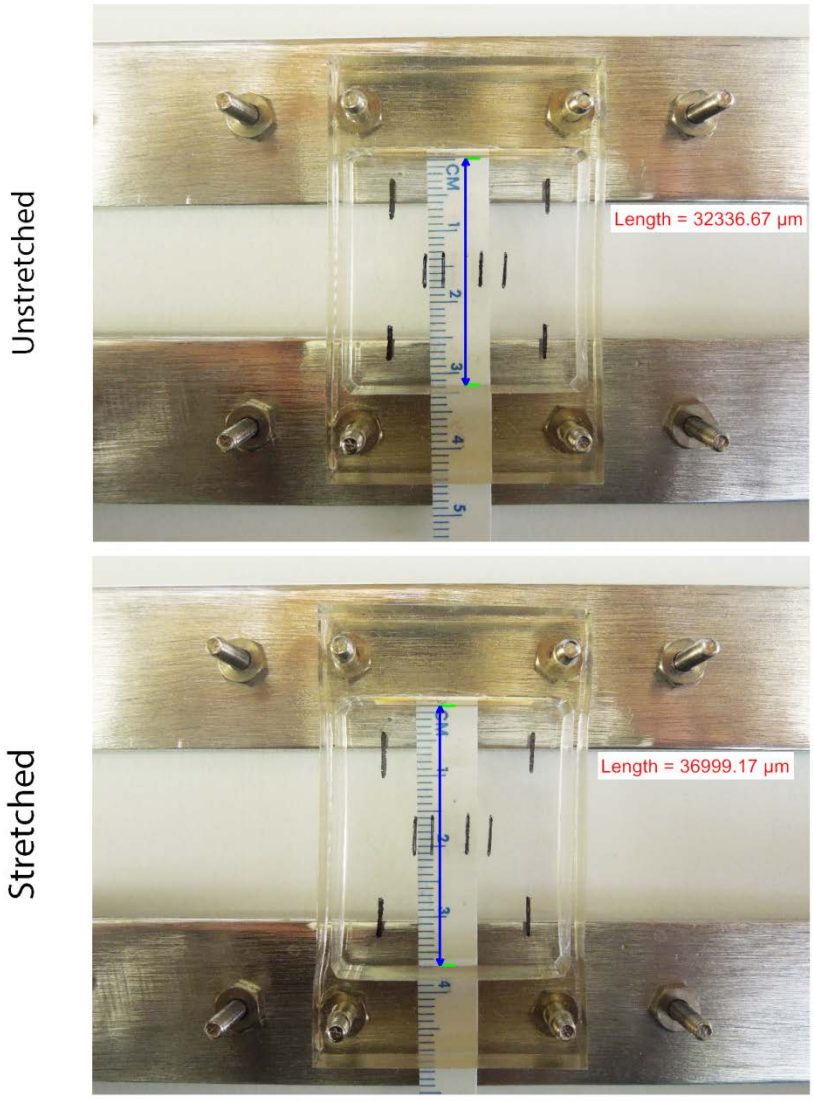

To demonstrate that tension generated using the manual device was transmitted to cells, I modified a published protocol (Sawada and Sheetz, 2002) to create Triton-insoluble cytoskeletons in order to create *Vcl*-null cytoskeletons. Key modifications in the published protocol included 1) the addition of a reversible, cell-impermeable crosslinker (DTSSP) to bind the cells to the fibronectin-coated substrate and 2) using digitonin as opposed to Triton as the permeabilization agent (Figure 3-4).

I then mounted a chamber with crosslinked cytoskeletons on the small-scale manual device. Images were taken of cytoskeletons in the unstretched, stretched and released positions. Quantification of 20 cytoskeletons in the various mechanical states showed that adherent cytoskeletons on average experienced a 13.8 ± 1.2% uniaxial stretch (Figure 3-3). When released from stretch, cytoskeletons returned to within 0.32% of their original length. The data collected using adherent cytoskeletons stretched with the small device is in agreement with the data collected on the total stretch experienced by the silicone chamber (Figure 3-2), and indicates that the tension generated on silicone chambers using the manual devices is transmitted to adherent cells.

Figure 3-3: Manual device applies stretch to cytoskeletons. *Vcl*-null MEFs were crosslinked to a fibronectin-coated silicone-based cell culture chamber, permeabilized with 0.003% digitonin, washed, and fixed again with 0.4% PFA. The resulting cytoskeletons were imaged in the unstretched, stretched, and released positions. The resulting images were analyzed for uniaxial length changes in the direction of applied stretch. A) *Vcl*-null cytoskeleton in three different mechanical states applied by the manual device. Red bars = 10 μm. B) 20 cells were analyzed for percent stretch applied by the manual device. Average cell stretch was 13.8 ± 1.2%. With release, cells returned to their unstretched length with a return accuracy of 0.32%.

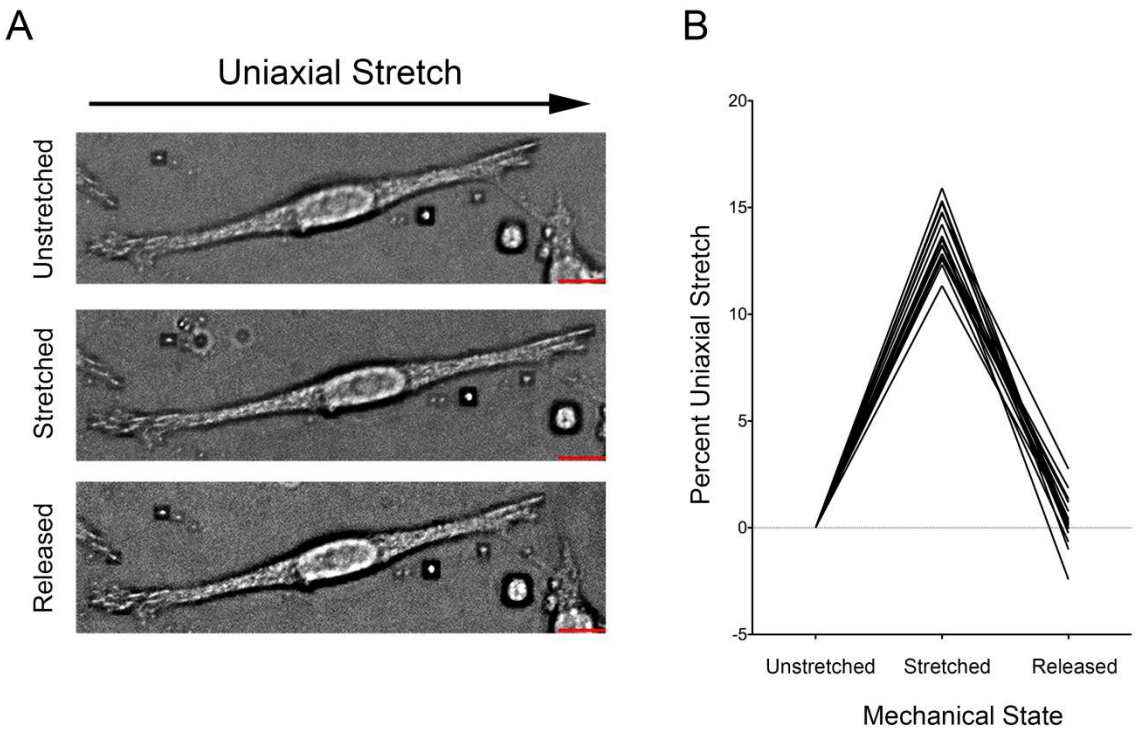

To show that my manual device was comparable to commercially available devices, I chose to reproduce a published assay showing stretch-dependent binding of cytosolic proteins to Triton-insoluble cytoskeletons (Sawada and Sheetz, 2002). To do this, I modified the published protocol to be compatible with digitonin-insoluble *Vcl*-null cytoskeletons prepared from live cells crosslinked to fibronectin-coated substrate with a reversible, cell-impermeable crosslinker. (Figure 3-4).

Figure 3-4: Protocol for stretch-dependent binding of exogenous proteins to digitonin-insoluble cytoskeletons. *Vcl*-null cells were cultured on a fibronectin-coated silicone substrate and allowed to grow for 48 hrs to reach 80-90% confluency. After washing with DPBS, the cells were crosslinked to the fibronectin substrate using the reversible, cell impermeable crosslinker DTSSP. Crosslinked cells were then washed into the stretch assay buffer (SAB) and digitonin-insoluble cytoskeletons were created by treatment with 0.003% digitonin at RT for 2 min in SAB with protease inhibitors (SAB+). To probe for stretch-dependent binding of exogenous proteins, cytoskeletons were stretched 15% uniaxially before adding exogenous proteins diluted in SAB+. The cytoskeletons were stretched for 5 min at 37°C. After washing, stretched cytoskeletons and bound proteins were collected by scraping the samples from the silicone substrate using 0.1% Triton in SAB+.

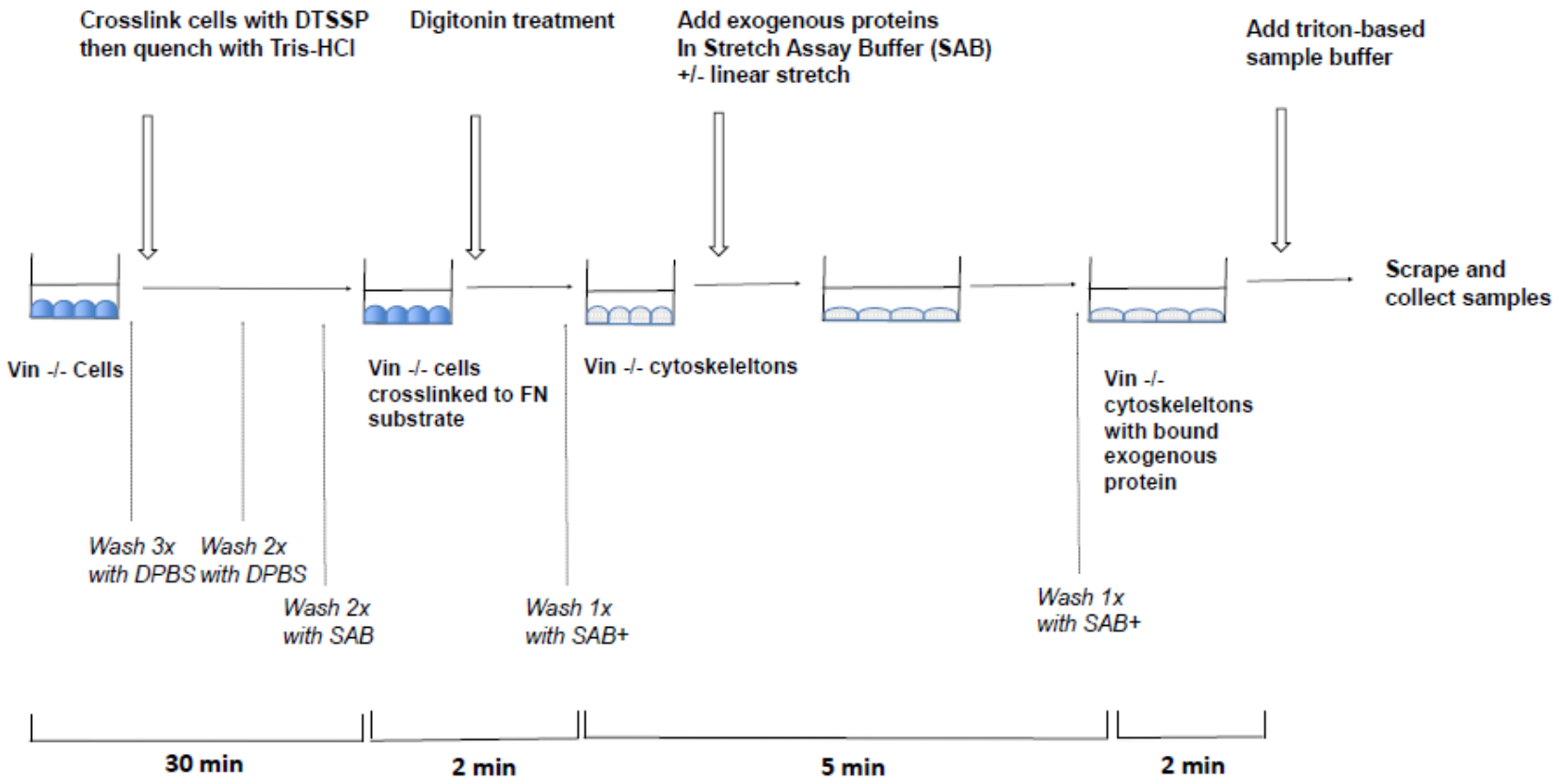
Crosslink cells with DTSSP
then quench with Tris-HCl
Digitonin treatment
Add exogenous proteins
In Stretch Assay Buffer (SAB)
+/- linear stretch
Add triton-based
sample buffer
Scrape and
collect samples
Vin -/- Cells
Vin -/- cells
crosslinked to FN
substrate
Vin -/- cytoskeleltons
Vin -/-
cytoskeleltons
with bound
exogenous
protein
Wash 3x
with DPBS
Wash 2x
with DPBS
Wash 2x
with SAB
Wash 1x
with SAB+
Wash 1x
with SAB+
30 min
2 min
5 min
2 min

As a control, I tested the binding of exogenous paxillin from cell lysates to *Vcl*-null cytoskeletons. Paxillin has been previously shown to bind in a stretch-dependent manner to Triton-insoluble cytoskeletons (Sawada and Sheetz, 2002). Additionally, I decided to test the binding of bacterially expressed and purified vinculin domain 1 (VD1) to stretched cytoskeletons. VD1 interacts with talin (Price *et al.*, 1989) and is sufficient to co-immunoprecipitate with talin *in vitro* (Gilmore *et al.*, 1992). Furthermore, it has been shown that mechanical stretch applied directly to a portion of talin rod unmasks cryptic vinculin binding sites and increases the binding of VD1 to talin (del Rio *et al.*, 2009). From this data, I hypothesized VD1 would show stretch-dependent binding to cytoskeletons because uniaxial stretch would uncover cryptic binding sites in cytoskeletal talin for VD1.

My experiments using digitonin-insoluble cytoskeletons began by looking at the stretch-dependent binding of paxillin and VD1 on the Strex Machine. Using the commercial device, I was able to reproduce the previously published result that paxillin has stretch-dependent binding to cytoskeletons. Furthermore, VD1 also showed stretch-dependent binding to cytoskeletons. The results became the basis for another project, which will be discussed in detail in Chapter 4. Because this preliminary data encouraged me to pursue further data on the interaction of VD1 with the cytoskeleton, I chose VD1 as the exogenous protein with which to compare my manual device to the Strex machine. Using VD1 as a model for binding of exogenous proteins to cytoskeletons, my data showed that the performance of the Strex machine and my manual device was nearly identical (Figure 3-5a). More recently, I attempted to show that there is similar

performance between the manual device and the Strex machine using paxillin as the model protein. Unfortunately, I have only collected positive data for that once (Figure 3-5b) and the digital blot file has since been corrupted.

Figure 3-5: Commercial and manual devices are comparable for detecting the stretch-dependent binding of exogenous proteins by Western blot. Digitonin-insoluble *Vcl*-null cytoskeletons were created as previously described. One mL of 1-μM recombinant VD1 in SAB+ or 100-nM YFP-paxillin in HEK lysate diluted in SAB+ were incubated with either unstretched or stretched cytoskeletons for 5 min at 37°C. After washes, cytoskeletons with bound protein were scraped from the FN-coated silicone substrate, resolved on a 4-12% acrylamide gel, and transferred to nitrocellulose for Western blotting. Western blots were scanned and quantified using a Licor infrared imaging system. All data was normalized to an actin loading control. U = unstretched, S = stretched. A) Comparison of stretch-dependent binding on the Strex machine versus manual device using 1-μM recombinant VD1 purified from bacteria. B) Comparison of stretch-dependent binding on the Strex machine versus manual device using 100-nM YFP-paxillin in HEK lysate. There is near identical performance between the commercial and manual devices. Bars indicate S.E.M, n = 3.

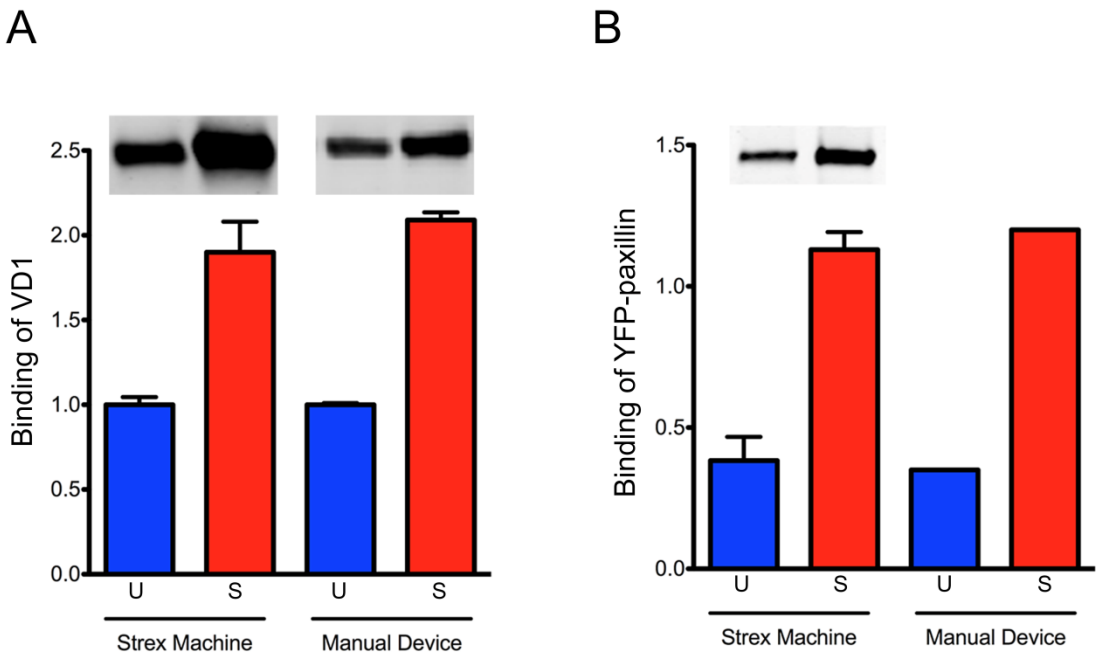

These characterization steps (Figures 3-2, 3-3, and 3-5) were considered evidence that the manual device was able to apply uniaxial stretch to an adherent cell in a manner comparable to a commercial Strex device. I then began testing the smaller device designed to fit into a Tokai onstage incubator for feasibility of use during live cell imaging. Ideally, my system would allow real-time microscopy of live cells in the unstretched, stretched, and released state. This system would allow me to use *Vcl*-null cells transfected with mutants of vinculin to pursue information about the role of vinculin, its autoinhibition, and its ligand binding abilities on focal adhesion growth in response to external force. Testing of the device highlighted several design limitations when used in conjunction with live microscopy. First, stretching the chamber uniaxially changes the focal plane (z-plane) and viewing field (x, y coordinates) during stretch. I accommodated these changes by noting the coordinates of fiduciary landmarks introduced to the culture chamber (usually an intentionally introduced orienting scratch wound) and characterizing the typical xyz shift of the chambers with stretch (data not shown). Secondly, imaging of live cells required the use of an extra-long working distance (ELWD) phase objective due to both the light dispersing properties of silicone and the shifting z-plane of the chamber. When the device was developed, I had access to a 40x ELWD objective, so that is the magnification at which I conducted my live cell experiments.

Vcl-null mouse embryonic fibroblast (MEF) cells were transfected with YFP-paxillin, eGFP-vinculin, eGFP-Vh, or eGFP-T12. For each construct, timelapse control cells were imaged at 0 min, 5 min, and 10 min. To analyze the effect of stretch, cells were imaged

immediately before stretching (U), after 5 min of 13.8% uniaxial stretch (S), and after having been released from stretch for 5 min (R). The timelapse control and stretched cell data sets were unpaired. The collected images were converted into quantifiable binaries of the peripheral focal adhesions of cells (Figure 3-6). Visual inspection of some initial image sequences indicated that YFP-paxillin-expressing *Vcl*-null cells show increased focal adhesion number or size with stretch (Figure 3-7) as has been previously published (Sawada 2002). Indeed, across several experiments, individual cells showed evidence of either increased focal adhesion number or focal adhesion size.

Figure 3-6: Manual stretch device allows the quantification of focal adhesion changes with time or mechanical stretch. *Vcl*-null mouse embryonic fibroblasts (MEF) cells were transfected with eGFP-tagged constructs and allowed to recover for 48 hrs before experimentation. Cells were imaged with a 40x ELWD phase objective. The images were then segmented and converted into binaries reflecting the dimensions of peripheral adhesions and quantified using Nikon NIS-Elements. Red bars = 5 μm. A) YFP-paxillin transfected *Vcl*-null MEF in the unstretched, stretched, and released mechanical state. B) eGFP-vinculin transfected *Vcl*-null MEF in the unstretched, stretched, and released mechanical state.

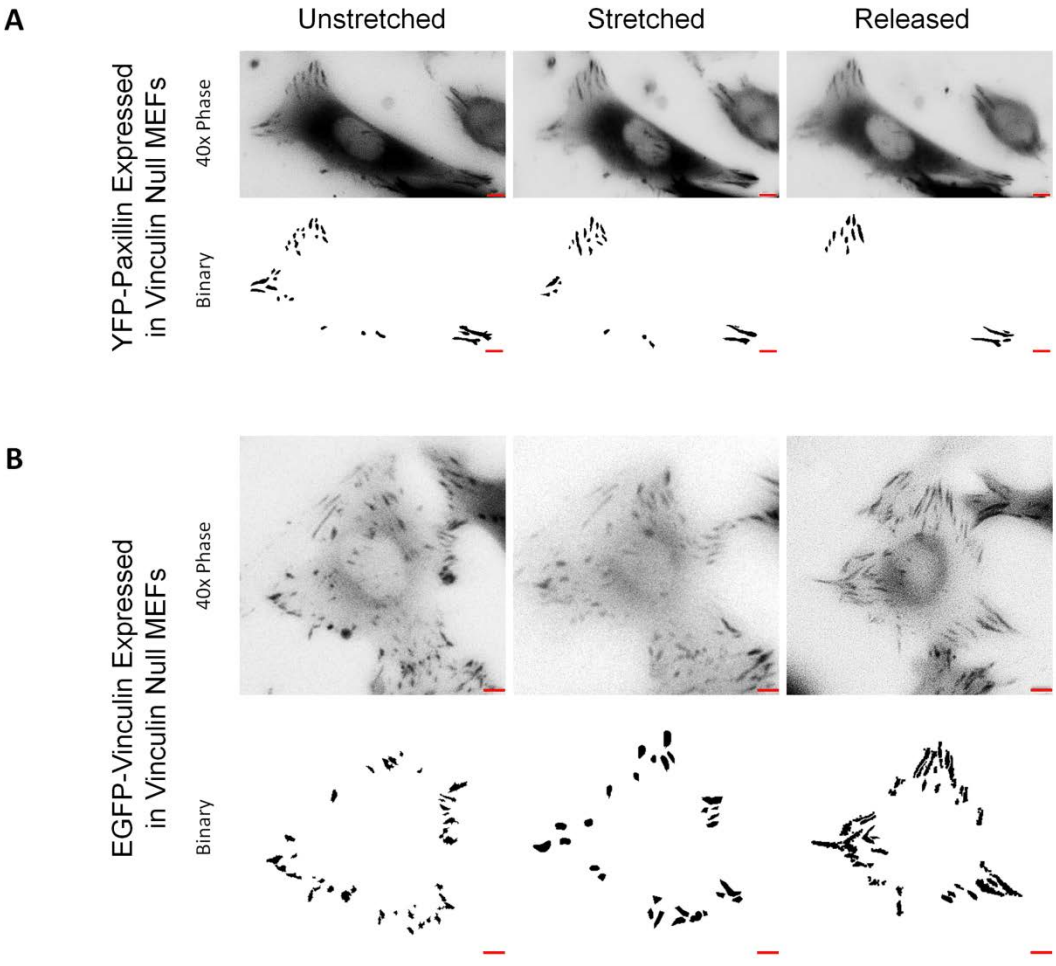

Figure 3-7: Visual inspection of images of stretched cells encourage the conclusion that acute uniaxial stretch causes focal adhesion growth. *Vcl*-null cells transfected with YFP-paxillin as a marker of focal adhesions were imaged with 40x ELWD phase objects in their unstretched, stretched, and released states. Red bar = 5 μm. Cell 1 shows a typical timelapse image set indicating that focal adhesion number increases with stretch. Cell 2 shows a typical timelapse image set indicating that some focal adhesions may increase in size with stretch and shrink upon release.

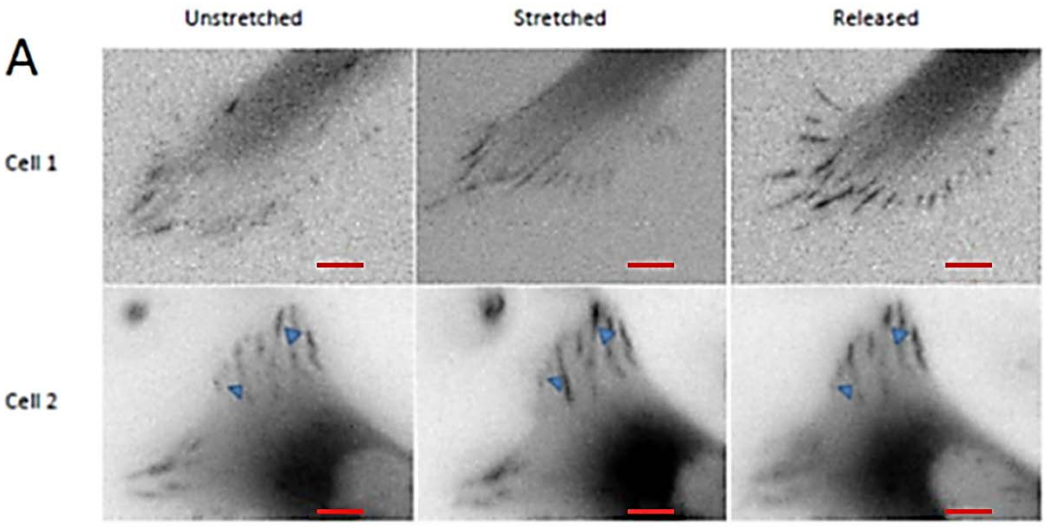

To determine if there was a significant, stretch-dependent change, I analyzed the peripheral focal adhesions of 5 randomly chosen timelapse control cells and 5 stretched cells. Peripheral focal adhesions were examined because the vast majority of transfected cells contained peripheral focal adhesions in their protrusions, while relatively few had any central adhesions. All images were segmented, and the areas of peripheral focal adhesions were quantified using Nikon Elements software. Several transformations were attempted on the data before determining that the square root transformation results in a sufficiently normal distribution of data points to enable comparison of the data groups by methods such as ANOVA that require approximately normal data distributions.

Additionally, while all YPF-paxillin-expressing cells showed some evidence of focal adhesion change with stretch, I focused our initial analysis on the 5 stretched cells that showed the greatest response. This was done in hopes of capturing any trends in focal adhesion change that may be present. The timelapse cells appeared to have a consistent amount of focal adhesion change across all cells imaged, and so 5 timelapse control cells were chosen at random.

Quantification of all peripheral focal adhesions in YFP-paxillin-expressing *Vcl*-null cells showed only one cell (Cell 5) with significant stretch-dependent changes in peripheral focal adhesion area and length (Figure 3-8a), despite visual inspection of the data having suggested focal adhesion change in all five stretched cells. A comparison of the number of focal adhesions at each timepoint in the experiment between timelapse control and stretched cells showed 2 out of 5 cells (Cells 4 and 5) having significantly increased

numbers of focal adhesions (Figure 3-8b). While limited by sample size, this data remained encouraging because the only cells showing significant change in focal adhesion area and number over time had been stretched.

Figure 3-8: There was no difference in FA area, length, or number over time, with or without a stretch and release protocol, in YFP-paxillin-expressing *Vcl*-null **cells.** A) Cells imaged at 0 min, 5 min, and 10 min were used as timelapse controls compared to cells imaged in the unstretched (U), stretched (S), and released (R) states. Live images were converted into binaries of peripheral focal adhesions and analyzed for changes in focal adhesion area and length. A square root transformation was applied to the resulting data to allow analysis by ANOVA. * implies $p<0.01$, ** implies $p<0.001$. B) Total number of focal adhesions at each timepoint for a given cell (timelapse control or stretched)

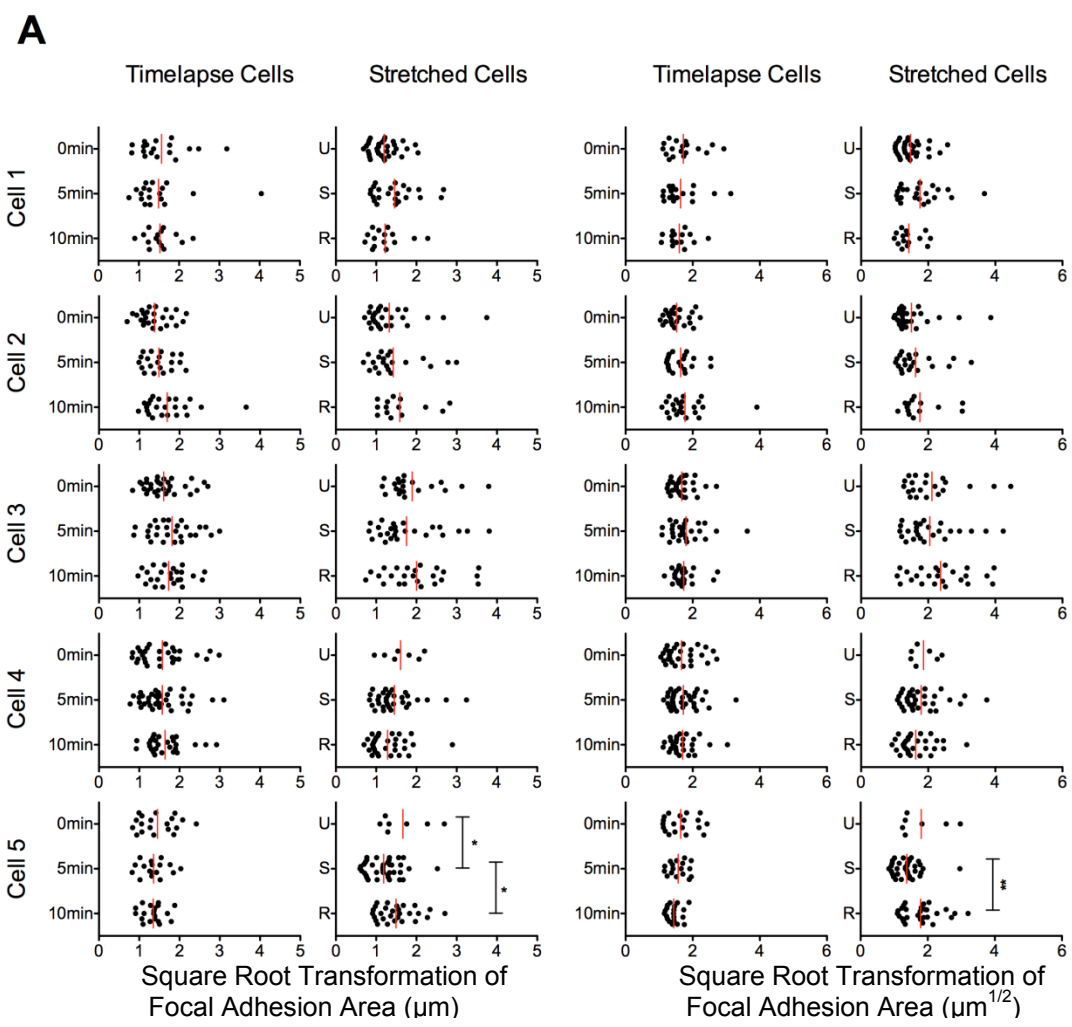
A
Timelapse Cells
Stretched Cells
Timelapse Cells
Stretched Cells
Cell 1
Cell 2
Cell 3
Cell 4
Cell 5
0min
5min
10min
U
S
R
Square Root Transformation of Focal Adhesion Area (μm)
Square Root Transformation of Focal Adhesion Area (μm1/2)

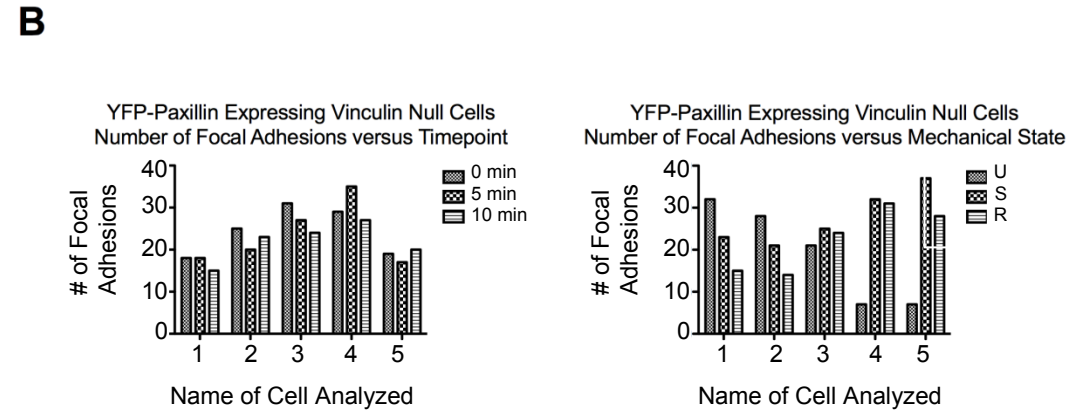
B
YFP-Paxillin Expressing Vinculin Null Cells
Number of Focal Adhesions versus Timepoint
# of Focal Adhesions
0 min
5 min
10 min
Name of Cell Analyzed
YFP-Paxillin Expressing Vinculin Null Cells
Number of Focal Adhesions versus Mechanical State
# of Focal Adhesions
U
S
R
Name of Cell Analyzed

Although both paxillin and vinculin are focal adhesion proteins and accepted focal adhesion markers, I hypothesized that different focal adhesion proteins may respond differently to uniaxial stretch. It was possible that eGFP-vinculin containing focal adhesions would respond differently to uniaxial stretch. Therefore, I decided to analyze similar images collected for eGFP-vinculin. Additionally, I hypothesized that *Vcl*-null cells expressing a truncation mutant of vinculin previously shown to increase focal adhesion number (Xu *et al.*, 1998) and increase cell adhesion strength (Dumbauld, 2013) would respond differently to uniaxial stretch compared to *Vcl*-null cells expressing full-length vinculin. I also expressed eGFP-T12 in *Vcl*-null cells to determine whether an autoinhibition mutant of vinculin would affect the focal adhesion response to external force. However, these images were not analyzed because these cells showed a propensity for detaching from the substrate after release from stretch. The images of eGFP-vinculin and eGFP-Vh transfected cells showed no change in focal adhesion area, length, or number that occurred in greater frequency in stretched cells than in timelapse control cells (Figures 3-9 and 3-10).

Figure 3-9: There was no difference in FA area, length, or number over time, with or without a stretch and release protocol, in EGFP-vinculin-expressing *Vcl*-null **cells.**
A) Cells imaged at 0 min, 5 min, and 10 min were used as timelapse controls compared to cells imaged in the unstretched (U), stretched (S), and released (R) states. Live images were converted into binaries of peripheral focal adhesions and analyzed for changes in focal adhesion area and length. A square root transformation was applied to the resulting data to allow analysis by ANOVA. * implies $p<0.01$, ** implies $p<0.001$. B) Total number of focal adhesions at each timepoint for a given cell (timelapse control or stretched)

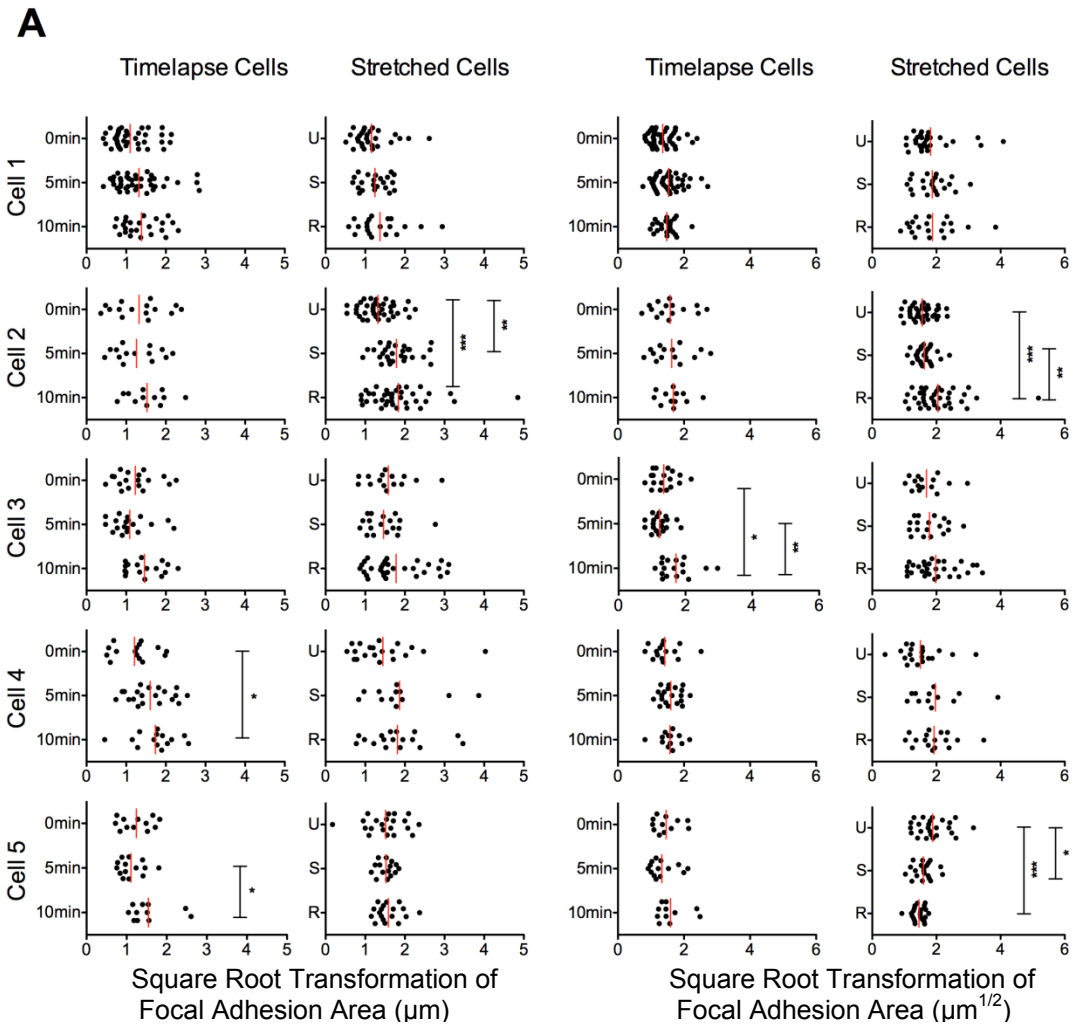
A
Timelapse Cells
Stretched Cells
Timelapse Cells
Stretched Cells
Cell 1
Cell 2
Cell 3
Cell 4
Cell 5
0min
5min
10min
U
S
R
Square Root Transformation of Focal Adhesion Area (µm)
Square Root Transformation of Focal Adhesion Area (µm^1/2)

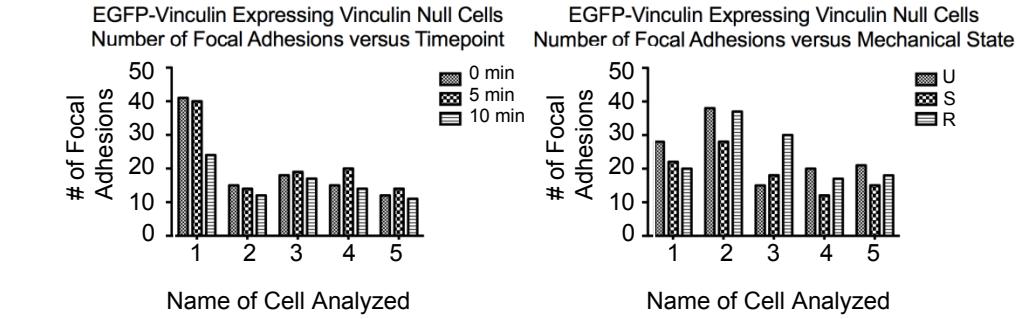
B
EGFP-Vinculin Expressing Vinculin Null Cells
Number of Focal Adhesions versus Timepoint
# of Focal Adhesions
0 min
5 min
10 min
Name of Cell Analyzed
EGFP-Vinculin Expressing Vinculin Null Cells
Number of Focal Adhesions versus Mechanical State
# of Focal Adhesions
U
S
R
Name of Cell Analyzed

Figure 3-10: There was no difference in FA area, length, or number over time, with or without a stretch and release protocol, in EGFP-Vh-expressing *Vcl*-null cells. A) Cells imaged at 0 min, 5 min, and 10 min were used as timelapse controls compared to cells imaged in the unstretched (U), stretched (S), and released (R) states. Live images were converted into binaries of peripheral focal adhesions and analyzed for changes in focal adhesion area and length. A square root transformation was applied to the resulting data to allow analysis by ANOVA. * implies $p<0.01$, ** implies $p<0.001$. B) Total number of focal adhesions at each timepoint for a given cell (timelapse control or stretched)

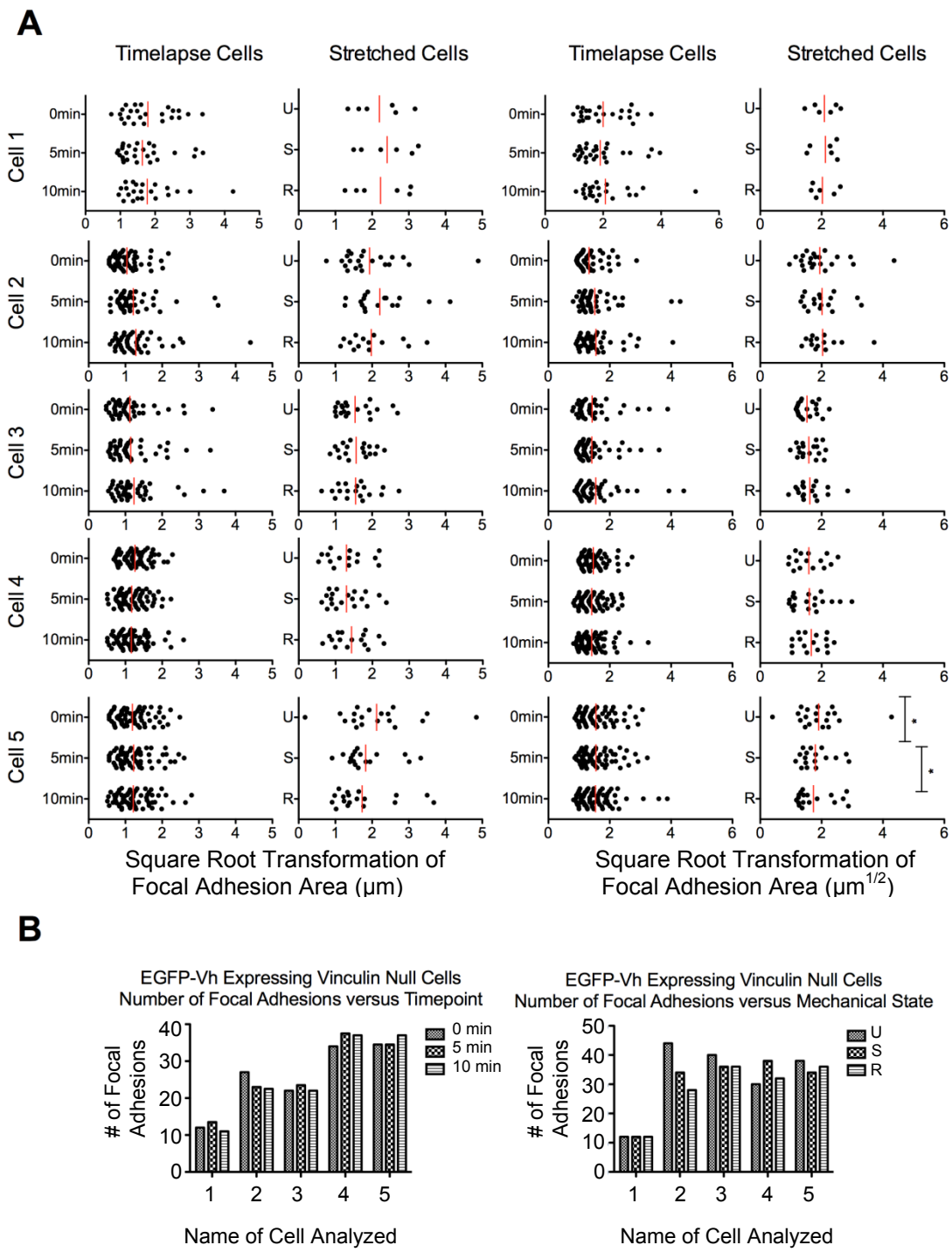
A
Timelapse Cells
Stretched Cells
Timelapse Cells
Stretched Cells
Cell 1
Cell 2
Cell 3
Cell 4
Cell 5
0min
5min
10min
U
S
R
Square Root Transformation of Focal Adhesion Area (μm)
Square Root Transformation of Focal Adhesion Area (μm^1/2)
B
EGFP-Vh Expressing Vinculin Null Cells
Number of Focal Adhesions versus Timepoint
# of Focal Adhesions
0 min
5 min
10 min
Name of Cell Analyzed
EGFP-Vh Expressing Vinculin Null Cells
Number of Focal Adhesions versus Mechanical State
# of Focal Adhesions
U
S
R
Name of Cell Analyzed

I hypothesized that focal adhesion change may be dependent on the angle between the focal adhesion and the direction of uniaxial stretch, with perhaps only focal adhesions oriented in a particular way to the direction of external force being able to undergo a reinforcement response. To analyze this, the focal adhesions for eGFP-vinculin transfected *Vcl*-null cells were segregated according to whether they were parallel or perpendicular to the direction of stretch. Segregating the data according to the angle of the focal adhesion yielded no trends with regard to parallel versus perpendicular focal adhesions (Figure 3-11), and those cells that showed significance were the same ones that showed significance when all peripheral focal adhesions were pooled (Figure 3-11 compared to Figure 3-9a). In one instance (Cell 3), the segregation of focal adhesions by angle actually caused the loss of any significant changes in focal adhesion length.

Figure 3-11: The angle of a focal adhesion relative to the direction of stretch has no effect on focal adhesion length. The peripheral focal adhesions from 5 stretched EGFP-vinculin-expressing *Vcl*-null cells were further analyzed. Focal adhesions were categorized as parallel to the direction of stretch or perpendicular to the direction of stretch. A square root transformation was applied to the resulting data to allow analysis by ANOVA. Only cells that showed significant length changes in the pooled data showed significant changes when the data was categorized by angle. Significant change did not correlate with the focal adhesion being parallel or perpendicular to the angle of stretch. * implies $p<0.01$, ** implies $p<0.001$.

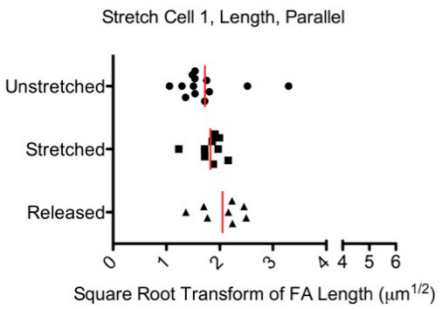
Stretch Cell 1, Length, Parallel
Unstretched
Stretched
Released
0 1 2 3 4 4 5 6
Square Root Transform of FA Length (μm^1/2)

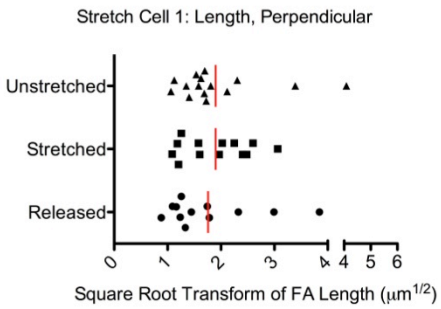
Stretch Cell 1: Length, Perpendicular
Unstretched
Stretched
Released
0 1 2 3 4 4 5 6
Square Root Transform of FA Length (μm^1/2)

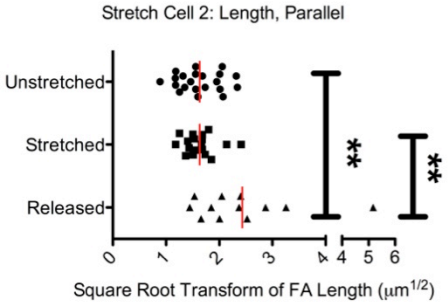
Stretch Cell 2: Length, Parallel
Unstretched
Stretched
Released
**
**
0 1 2 3 4 4 5 6
Square Root Transform of FA Length (μm^1/2)

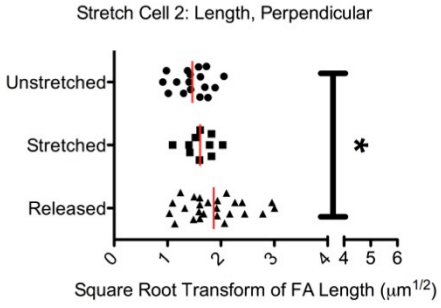
Stretch Cell 2: Length, Perpendicular
Unstretched
Stretched
Released
*
0 1 2 3 4 4 5 6
Square Root Transform of FA Length (μm^1/2)

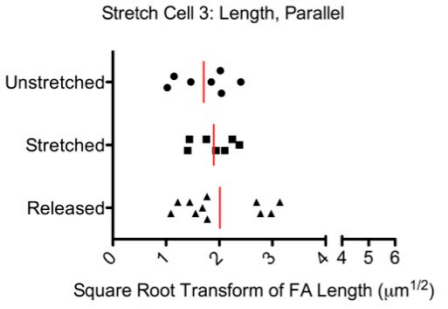
Stretch Cell 3: Length, Parallel
Unstretched
Stretched
Released
0 1 2 3 4 4 5 6
Square Root Transform of FA Length (μm^1/2)

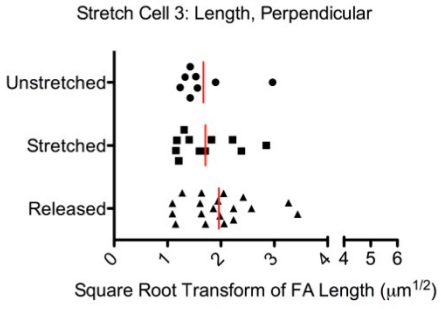
Stretch Cell 3: Length, Perpendicular
Unstretched
Stretched
Released
0 1 2 3 4 4 5 6
Square Root Transform of FA Length (μm^1/2)

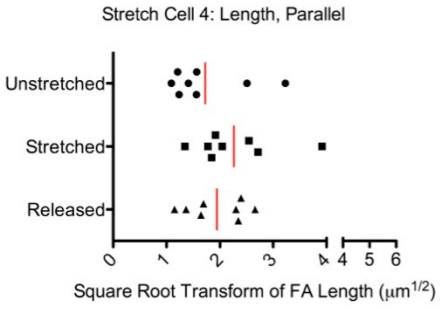
Stretch Cell 4: Length, Parallel
Unstretched
Stretched
Released
0 1 2 3 4 4 5 6
Square Root Transform of FA Length (μm^1/2)

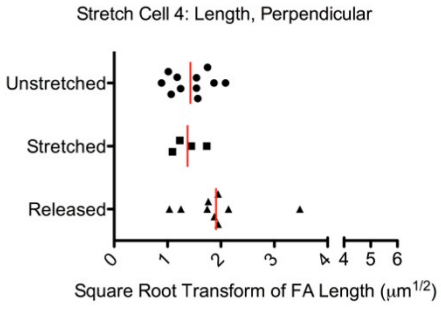
Stretch Cell 4: Length, Perpendicular
Unstretched
Stretched
Released
0 1 2 3 4 4 5 6
Square Root Transform of FA Length (μm^1/2)

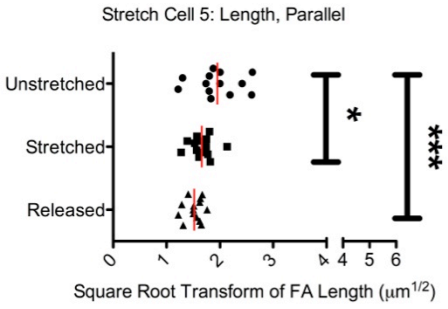
Stretch Cell 5: Length, Parallel
Unstretched
Stretched
Released
*
***
0 1 2 3 4 4 5 6
Square Root Transform of FA Length (μm^1/2)

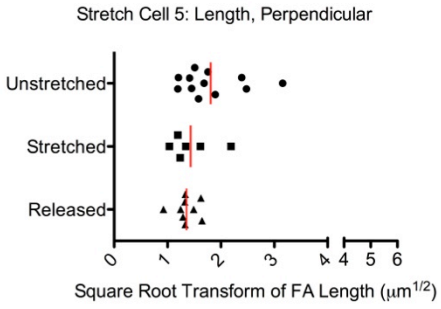
Stretch Cell 5: Length, Perpendicular
Unstretched
Stretched
Released
0 1 2 3 4 4 5 6
Square Root Transform of FA Length (μm^1/2)

The lack of significant trends in focal adhesion area or length with stretch led me to investigate whether the cells were responding with another type of global change. For instance, perhaps the cells were changing the total surface area of the cell immobilized to the substrate instead of changing the size of individual focal adhesions. To determine if any such trends were present, eGFP-vinculin transfected cells were analyzed individually for changes in total cell area, perimeter, and circularity with time. To do this, the values of each metric were plotted with time (Figure 3-12) both linear and nonlinear regressions were performed on each plot to yield a slope quantifying the degree of change experienced. The slope values for timelapse control cells (n=4) versus stretched cells (n=5) were not significantly different using any metric. Therefore, while individual cells could show impressive changes in area, perimeter, or circularity with stretch, there were no significant, stretch-dependent trends in these changes

Figure 3-12: Timelapse control cells show no increased change in morphology over stretched cells. Timelapse control cells (n=4) and stretched cells (n=5) were analyzed for changes in total cell area, perimeter, and circularity. While individual stretched cells may have shown significant changes in any one of these parameters, there is no correlation between the introduction of stretch and change in cell morphology.

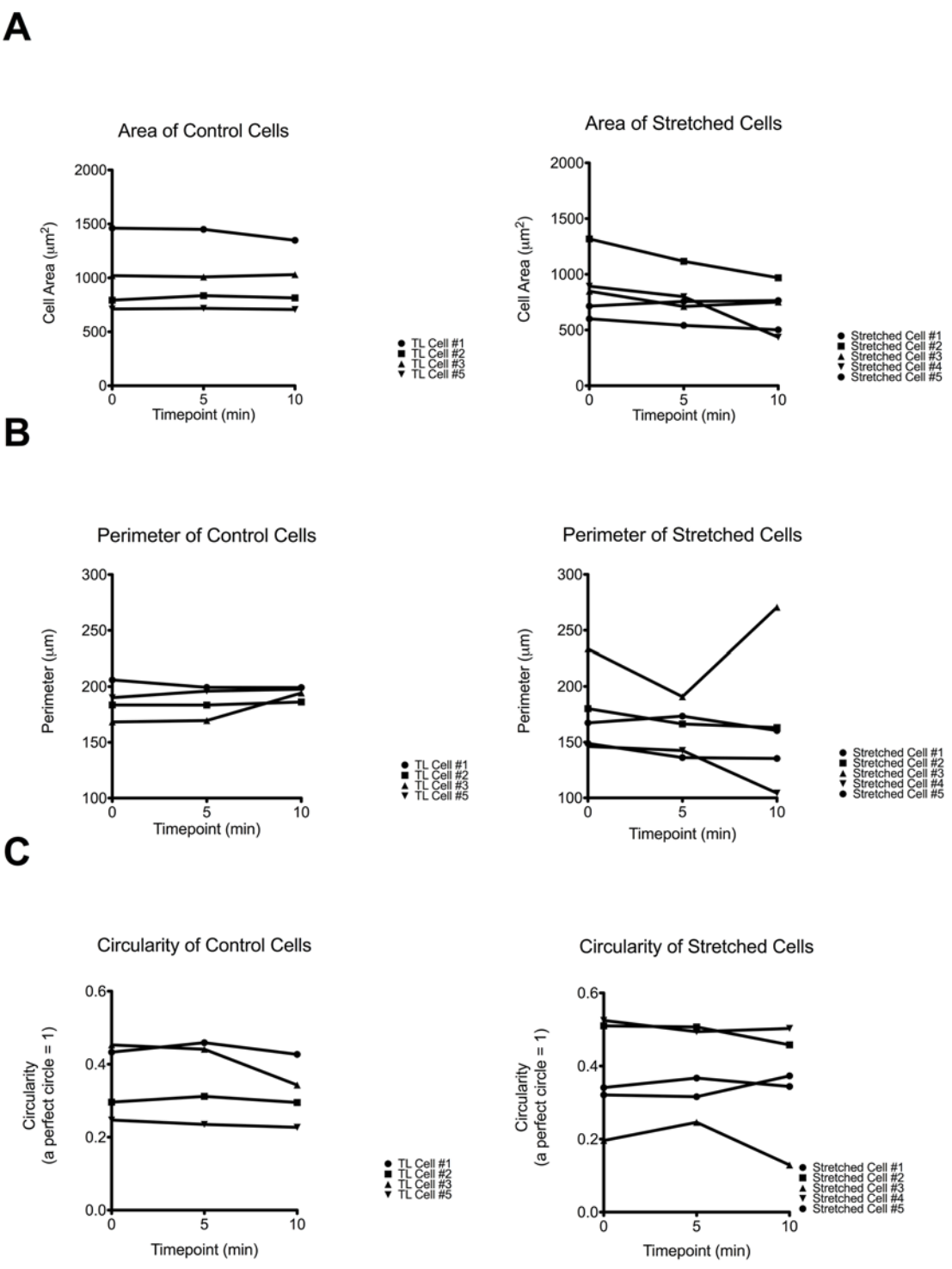
A
Area of Control Cells
Cell Area (μm²)
2000
1500
1000
500
0
0
5
10
Timepoint (min)
TL Cell #1
TL Cell #2
TL Cell #3
TL Cell #5
Area of Stretched Cells
Cell Area (μm²)
Timepoint (min)
Stretched Cell #1
Stretched Cell #2
Stretched Cell #3
Stretched Cell #4
Stretched Cell #5
B
Perimeter of Control Cells
Perimeter (μm)
300
250
200
150
100
Timepoint (min)
TL Cell #1
TL Cell #2
TL Cell #3
TL Cell #5
Perimeter of Stretched Cells
Perimeter (μm)
Timepoint (min)
Stretched Cell #1
Stretched Cell #2
Stretched Cell #3
Stretched Cell #4
Stretched Cell #5
C
Circularity of Control Cells
Circularity
(a perfect circle = 1)
0.6
0.4
0.2
0.0
Timepoint (min)
TL Cell #1
TL Cell #2
TL Cell #3
TL Cell #5
Circularity of Stretched Cells
Circularity
(a perfect circle = 1)
Timepoint (min)
Stretched Cell #1
Stretched Cell #2
Stretched Cell #3
Stretched Cell #4
Stretched Cell #5

Discussion:

The lack of focal adhesion response with the application of uniaxial stretch was, at first, very puzzling. I had characterized my device and shown that not only was it capable of applying stretch to silicone-based cell culture chambers, but that the stretch generated was transmitted to cytoskeletons adherent to the silicone. Previous to my work, the literature showed a correlation between focal adhesion size and traction force, and several more recent studies had shown that the application of external force was correlated with increased focal adhesion size. It remained unclear to me what aspects of my assay could have led to the application of external force having no effect on focal adhesions.

Upon consideration of the conditions of my assay, I realized that all of my observations were on adherent spread cells that had been plated at least 48 hrs to allow the cells to recover from electroporation. Furthermore, due to the technical limitations of my setup, I was imaging focal adhesions at 40x. This information indicated that I had been observing the effects of external force on established, likely mature, focal adhesions and may have missed the responses of smaller, immature focal adhesions. Knowing this, I began to question what was currently known about the responses of nascent focal adhesions versus established, mature focal adhesions to external force.

I reviewed previous studies on the effects of external force on focal adhesion size to look for indications as to what populations of focal adhesions had been studied. Surprisingly, no single study has explored the effect of external force on different subpopulations of

focal adhesions using the same assay. However, there are published results showing that application of external force causes increased focal adhesion size may have been conducted using assays that weighed the observations towards the responses of nascent focal adhesions. For example, in Riveline's seminal study, his methods section indicates that all of his experiments were conducted in serum-free media. It is unclear from the paper why serum-free conditions were necessary, but it has been established that serum-free cell culture conditions limit focal adhesion maturation due to a lack of lysophosphatidic acid, a growth factor that activates rho-dependent focal adhesion maturation (Ridley and Hall, 1992; Choi *et al.*, 2008). This indicates that Riveline's observations of the response of focal adhesions to external force may have actually been limited to the responses of nascent focal adhesions to external force. It also suggests why he saw stretch-dependent changes in focal adhesions in 18 out of 18 cells tested (Riveline *et al.*, 2001).

Similarly, Galbraith showed that external force results in focal adhesion growth (Galbraith *et al.*, 2002). However, the conditions of her assay depend on the formation of nascent focal adhesions on the dorsum of a cell. In her assay, 1 μm, fibronectin-coated beads are placed at the lamellipodia of fibroblasts to establish an initial ECM-membrane contact. In the absence of external force, this bead then moves toward the center of the cell as the cell membrane continues to protrude and migration continues. To exert external force, Galbraith used an optical trap to prevent the cell from using these initial contacts to move the beads in a retrograde fashion. In her assay, she saw that in response to this external force, the ECM-membrane contacts recruited vinculin and increased in

size. Again, here is a study well accepted to show a link between the application of external force and focal adhesion size that likely was observing the responses of nascent focal adhesions. In Galbraith's assay, the responses of established, ventral focal adhesions were not measured.

While no single study has looked at the effects of nascent versus mature focal adhesions using a single assay, there are two pieces of data in the literature that indicate that the two subpopulations of focal adhesions may respond differently to external force. Sniadecki monitored the focal adhesion response of spread, adherent fibroblasts plated onto magnetically controlled microposts (Sniadecki *et al.*, 2007). In his assay, he found that a single actuation of a magnetic post was not sufficient external force to cause significant changes in focal adhesion size. Rather, multiple actuations of the magnetic posts applied over a ten min period were necessary to cause significant changes in focal adhesion size. Additionally, his data does not indicate whether the degree of focal adhesion growth reported (an average 2-fold growth in focal adhesion area) was a global response or occurred only in a subset of focal adhesions.

Finally, Stricker measured the traction forces generated by the established focal adhesions of spread cells when their polyacrylamide growth substrate was stretched (Stricker *et al.*, 2011). In his results, he presents the data for two established focal adhesions that show that established focal adhesions are capable of generating large increases in traction force without showing proportional increases in focal adhesion size.

In this study I present an assay to introduce external stress to a cell by stretching the extracellular substrate, an approach similar in many ways to both Sawada (Sawada and Sheetz, 2002) and Stricker's (Stricker *et al.*, 2011) work. I verified that the device delivers stretch to the silicone-based cell culture chamber (Figure 3-2), and that this stretch is transmitted to adherent cytoskeletons (Figure 3-3). Adherent cytoskeletons experienced a 13.8 ± 1.3% uniaxial stretch. Furthermore, I showed that, when using Western blotting to quantify the binding of an exogenous protein, my device performed similarly to a commercially available machine designed to apply stretch to cells. A small-scale model of this device was designed to function on a microscope stage during live cell imaging, allowing data to be collected on the response of focal adhesions containing eGFP-tagged proteins before, during, and after the application of uniaxial stretch.

Of course, there are caveats to the use of this device, especially as applies to live imaging. First, the need to manually introduce stretch limits the time resolution of timelapse studies. This is due to 1) the time needed to secure the screws maintaining stretch and 2) the resulting change in z-plane that is introduced when the chamber itself is stretched. In my experience, I found that the most consistent timepoints could be collected when they were spaced at least five min apart. If changes in a protein or structure of interest occur more quickly than this, any changes due to stretch will not be observed using this device. However, previous studies have used similarly spaced timepoints (Riveline *et al.*, 2001; Sawada and Sheetz, 2002), so I do not believe that the spacing of my timepoints was the reason I did not detect similar changes in focal

adhesion size and number.

Second, the elasticity of the substrate comes at the cost of an optically clear substrate. The different refractive indexes of PDMS (the silicone basis of commercially available stretch chambers) versus German coverglass (1.4 vs 1.515) (MIT Material Properties Database) leads to greater dispersion of light when attempting to image samples on silicone substrates using an inverted microscope and prevents the use of TIRF and confocal microscopy that are accessible when using glass substrates. I addressed this short-coming by conducting my studies using an available, lower magnification ELWD phase objective. This allowed me image focal adhesions as they were being stretched, but limited the detail that I could observe.

The technical limitation of changing xyz coordinates between timepoints imposed several limitations on the analysis of the collected data. First, while many cells could be imaged, very few cells remained in focus throughout the entirety of the experiment. Second, the changing z-planes inherent in these experiments make it impossible to compare focal adhesion intensity accurately. Finally, the moving x-y coordinates meant that the images taken between the unstretched, stretched, and released states are not perfectly registered, making it impossible to definitively identify a single focal adhesion throughout the entirety of the experiment. As a result, in our analysis of the collected data, we had to include all focal adhesions in each cell instead of tracking particularly interesting ones, such as nascent focal adhesions. This limited our analysis to average focal adhesion size

and number in the unstretched, stretched, and released state rather than allowing timecourse information on the response of individual focal adhesions to external force.

The collected data on visual inspection suggested that acute uniaxial stretch was causing focal adhesion growth and changes in focal adhesion number (Figure 3-7). However, after quantitation it became obvious that neither the act of stretching the cell or releasing the cell from stretch had a discernible effect on average focal adhesion area or number (Figures 3-8, 3-9, and 3-10). Furthermore, there was no significant difference in focal adhesion size or number when stretched cells were compared to unpaired, timelapse controls. From this I can only conclude that visual analysis of focal adhesion change can be misleading unless the changes seen are easily calculated by eye and occur in the majority of focal adhesions present.

My study focuses on the response of mature focal adhesions to acute, uniaxial stretch. *Vcl*-null cells were plated 48 hrs before study and allowed to grow to 80% confluency, allowing ample time for focal adhesion development and maturation. In light of my results and what I now know about the subpopulations of focal adhesions likely observed in previous studies, I believe that I observed no significant changes in focal adhesions because my observations were on established, mature focal adhesions. There are two publications that examine the effect of external stretch on mature focal adhesions in living cells. Sawada's data only presents the response of a single cell and lacks timelapse controls (Sawada and Sheetz, 2002). Stricker's data shows that external stretch causes increases in traction stress in focal adhesions, but does not always result in increased

focal adhesion size (Stricker *et al.*, 2011). My data shows that individual cells undergoing stretch may show significant focal adhesion responses, but there is no trend for established focal adhesions in stretched cells to show a greater change in focal adhesion size than the focal adhesions of control cells.

I believe that, currently, studies on the effects of external force on focal adhesion growth do not take into account that focal adhesions mature along a continuum from nascent to mature focal adhesions. It is possible that different subpopulations of focal adhesions respond differently to external force. Furthermore, the role for vinculin in regulating the focal adhesion response to force may be different in these different subpopulations. My study and analysis suggests that effects of external force on focal adhesions should be studied in a single system that allows the observation of focal adhesions along the maturation continuum from nascent adhesions, through focal complexes, and finally mature adhesions. My assay could be modified to do this by 1) correcting the discussed shortcomings of the current method for applying stretch and 2) varying the conditions of the experiment to limit focal adhesion maturation.

Suggested mechanical revisions to the device include incorporation of two sliding bars rather than one (Figure 3-1) in order to minimize xyz shift of the viewing field and thereby increase the time resolution of timelapse studies. Additionally, the introduction of pressure clamps to secure any sliding bars (as opposed to thumbscrews) would allow for imaging of samples sooner after the introduction of stretch. Both of these

modifications could be made easily and inexpensively, expanding the potential uses of this manual device.

The conditions of the assay could be modified to limit focal adhesion maturation by developing a system that uses short-term serum starvation of cells transfected with eGFP-tagged focal adhesion markers. An alternative approach would be to introduce inhibitors that affect key signaling proteins in focal adhesion maturation. For example, microinjection of fibroblasts with the exoenzyme C3 transferase from *Clostridium botulinum* has been shown to inhibit rho-signaling (Ridley and Hall, 1992), a key activator of focal adhesion maturation. Additionally, cells could be incubated with Y27632, a compound that inhibits Rho-Kinase (ROCK), a signaling protein downstream of Rho that affects myosin activity (Uehata *et al.*, 1997).

References:

Balaban, N.Q., U.S. Schwarz, D. Riveline, P. Goichberg, G. Tzur, I. Sabanay, D. Mahalu, S. Safran, A. Bershadsky, L. Addadi, and B. Geiger. 2001. Force and focal adhesion assembly: a close relationship studied using elastic micropatterned substrates. *Nature cell biology*. 3:466-472.

Beningo, K.A., M. Dembo, I. Kaverina, J.V. Small, and Y.L. Wang. 2001. Nascent focal adhesions are responsible for the generation of strong propulsive forces in migrating fibroblasts. *The Journal of cell biology*. 153:881-888.

Choi, C.K., M. Vicente-Manzanares, J. Zareno, L.A. Whitmore, A. Mogilner, and A.R. Horwitz. 2008. Actin and alpha-actinin orchestrate the assembly and maturation of nascent adhesions in a myosin II motor-independent manner. *Nature cell biology*. 10:1039-1050.

Choquet, D., D.P. Felsenfeld, and M.P. Sheetz. 1997. Extracellular matrix rigidity causes strengthening of integrin-cytoskeleton linkages. *Cell*. 88:39-48.

Cohen, D.M., H. Chen, R.P. Johnson, B. Choudhury, and S.W. Craig. 2005. Two distinct head-tail interfaces cooperate to suppress activation of vinculin by talin. *The Journal of biological chemistry*. 280:17109-17117.

del Rio, A., R. Perez-Jimenez, R. Liu, P. Roca-Cusachs, J.M. Fernandez, and M.P. Sheetz. 2009. Stretching single talin rod molecules activates vinculin binding. *Science (New York, N.Y.* 323:638-641.

DeMali, K.A., C.A. Barlow, and K. Burridge. 2002. Recruitment of the Arp2/3 complex to vinculin: coupling membrane protrusion to matrix adhesion. *The Journal of cell biology*. 159:881-891.

DePasquale, J.A., and C.S. Izzard. 1987. Evidence for an actin-containing cytoplasmic precursor of the focal contact and the timing of incorporation of vinculin at the focal contact. *The Journal of cell biology*. 105:2803-2809.

Dumbauld, D.W., T.T. Lee, A. Singh, J. Scrimgeour, C.A. Gersbach, E.A. Zamir, J. Fu, C.S. Chen, J.E. Curtis, S.W. Craig, and A.J. Garcia. 2013. How vinculin regulates force transmission. *Proceedings of the National Academy of Sciences of the United States of America*. 110:9788-9793.

Ezzell, R.M., W.H. Goldmann, N. Wang, N. Parashurama, and D.E. Ingber. 1997. Vinculin promotes cell spreading by mechanically coupling integrins to the cytoskeleton. *Experimental cell research*. 231:14-26.

Galbraith, C.G., K.M. Yamada, and M.P. Sheetz. 2002. The relationship between force and focal complex development. *The Journal of cell biology*. 159:695-705.

Gilmore, A.P., P. Jackson, G.T. Waites, and D.R. Critchley. 1992. Further characterisation of the talin-binding site in the cytoskeletal protein vinculin. *Journal of cell science*. 103 (Pt 3):719-731.

Goffin, J.M., P. Pittet, G. Csucs, J.W. Lussi, J.J. Meister, and B. Hinz. 2006. Focal adhesion size controls tension-dependent recruitment of alpha-smooth muscle actin to stress fibers. *The Journal of cell biology*. 172:259-268.

Harris, A.K., D. Stopak, and P. Wild. 1981. Fibroblast traction as a mechanism for collagen morphogenesis. *Nature*. 290:249-251.

Humphries, J.D., P. Wang, C. Streuli, B. Geiger, M.J. Humphries, and C. Ballestrem. 2007. Vinculin controls focal adhesion formation by direct interactions with talin and actin. *The Journal of cell biology*. 179:1043-1057.

Izzard, C.S. 1988. A precursor of the focal contact in cultured fibroblasts. *Cell motility and the cytoskeleton*. 10:137-142.

Lee, J., M. Leonard, T. Oliver, A. Ishihara, and K. Jacobson. 1994. Traction forces generated by locomoting keratocytes. *The Journal of cell biology*. 127:1957-1964.

Oliver, T., M. Dembo, and K. Jacobson. 1995. Traction forces in locomoting cells. *Cell motility and the cytoskeleton*. 31:225-240.

Palecek, S.P., J.C. Loftus, M.H. Ginsberg, D.A. Lauffenburger, and A.F. Horwitz. 1997. Integrin-ligand binding properties govern cell migration speed through cell-substratum adhesiveness. *Nature*. 385:537-540.

Pelham, R.J., Jr., and Y. Wang. 1997. Cell locomotion and focal adhesions are regulated by substrate flexibility. *Proceedings of the National Academy of Sciences of the United States of America*. 94:13661-13665.

Price, G.J., P. Jones, M.D. Davison, B. Patel, R. Bendori, B. Geiger, and D.R. Critchley. 1989. Primary sequence and domain structure of chicken vinculin. *The Biochemical journal*. 259:453-461.

Ridley, A.J., and A. Hall. 1992. The small GTP-binding protein rho regulates the assembly of focal adhesions and actin stress fibers in response to growth factors. *Cell*. 70:389-399.

Riveline, D., E. Zamir, N.Q. Balaban, U.S. Schwarz, T. Ishizaki, S. Narumiya, Z. Kam, B. Geiger, and A.D. Bershadsky. 2001. Focal contacts as mechanosensors: externally applied local mechanical force induces growth of focal contacts by an mDia1-dependent and ROCK-independent mechanism. *The Journal of cell biology*. 153:1175-1186.

Rodriguez Fernandez, J.L., B. Geiger, D. Salomon, and A. Ben-Ze'ev. 1993. Suppression of vinculin expression by antisense transfection confers changes in cell

morphology, motility, and anchorage-dependent growth of 3T3 cells. *The Journal of cell biology*. 122:1285-1294.

Sawada, Y., and M.P. Sheetz. 2002. Force transduction by Triton cytoskeletons. *The Journal of cell biology*. 156:609-615.

Sniadecki, N.J., A. Anguelouch, M.T. Yang, C.M. Lamb, Z. Liu, S.B. Kirschner, Y. Liu, D.H. Reich, and C.S. Chen. 2007. Magnetic microposts as an approach to apply forces to living cells. *Proceedings of the National Academy of Sciences of the United States of America*. 104:14553-14558.

Stopak, D., N.K. Wessells, and A.K. Harris. 1985. Morphogenetic rearrangement of injected collagen in developing chicken limb buds. *Proceedings of the National Academy of Sciences of the United States of America*. 82:2804-2808.

Stricker, J., Y. Aratyn-Schaus, P.W. Oakes, and M.L. Gardel. 2011. Spatiotemporal constraints on the force-dependent growth of focal adhesions. *Biophysical journal*. 100:2883-2893.

Tan, J.L., J. Tien, D.M. Pirone, D.S. Gray, K. Bhadriraju, and C.S. Chen. 2003. Cells lying on a bed of microneedles: an approach to isolate mechanical force. *Proceedings of the National Academy of Sciences of the United States of America*. 100:1484-1489.

Uehata, M., T. Ishizaki, H. Satoh, T. Ono, T. Kawahara, T. Morishita, H. Tamakawa, K. Yamagami, J. Inui, M. Maekawa, and S. Narumiya. 1997. Calcium sensitization of smooth muscle mediated by a Rho-associated protein kinase in hypertension. *Nature*. 389:990-994.

Xu, W., J.L. Coll, and E.D. Adamson. 1998. Rescue of the mutant phenotype by reexpression of full-length vinculin in null F9 cells; effects on cell locomotion by domain deleted vinculin. *Journal of cell science*. 111 (Pt 11):1535-1544.

Chapter 4:

Role of Vinculin Autoinhibition in the Recruitment of Vinculin to Uniaxially Stretched Cytoskeletons

Abstract:

A published study has shown that several focal adhesion proteins show stretch-dependent binding when added exogenously to Triton-insoluble cytoskeletons. However, in that study, full-length vinculin did not respond in a similar manner. Since vinculin is autoinhibited, I hypothesized that if vinculin were activated before being exposed to stretched cytoskeletons, it would also be able to bind in a stretch-dependent manner. A previously published study has also shown a portion of talin rod can be mechanically stretched to uncover cryptic binding sites for vinculin. From this data, I hypothesized that perhaps mechanical stretch of the cytoskeleton was sufficient to uncover cryptic binding sites in talin rod for vinculin and increase the recruitment of vinculin to focal adhesions. To determine the effect of activation on vinculin's ability to bind cytoskeletons in a stretch-dependent manner, I first developed a method for creating digitonin-insoluble *Vcl*-null cytoskeletons. As a positive control, digitonin-insoluble cytoskeletons were also incubated with paxillin, which has been previously shown to bind in a stretch-dependent manner to cytoskeletons. Initial experiments showed that exogenous paxillin bound to digitonin-insoluble cytoskeletons in a stretch-dependent manner, as previously reported. Then, digitonin-insoluble cytoskeletons were incubated with exogenous vinculin and various vinculin truncation mutants. Full-length, autoinhibited vinculin did not bind cytoskeletons in a stretch-dependent manner, as previously reported. However, domain 1 of vinculin (VD1), when expressed alone, showed stretch-dependent binding to digitonin-insoluble cytoskeletons. Incubation of digitonin-insoluble cytoskeletons with VD1 containing a well characterized mutation that

ablates vinculin-talin and vinculin-alpha-actinin interactions reduced stretch-dependent binding. This result indicated that the stretch-dependent binding of VD1 was due to interactions between VD1 and talin or alpha-actinin. However, subsequent imaging studies showed that exogenous VD1 did not localize to focal adhesions in this assay. Instead, VD1 showed a generalized punctate binding pattern to cytoskeletons not consistent with any known localization of vinculin. The stretch-dependent binding of VD1 was not reproduced using a truncation mutant of vinculin, vinculin head (Vh), which contains domains 1 through 4. I interpret my results from this study as indicating that the method I developed for creating digitonin-insoluble cytoskeletons was sufficient for reproducing the result that paxillin binds in a stretch-dependent manner to cytoskeletons, but lacked a critical localization factor that would make this my assay an appropriate system to study how vinculin's autoinhibition and direct stretch applied to the cytoskeleton affect the recruitment of vinculin to focal adhesions.

Introduction:

A key question in mechanotransduction is how the actomyosin cytoskeleton mediates both intracellular forces and external forces to affect cellular function and signaling. Through focal adhesions, there is a structural coupling between the extracellular matrix (ECM), integrins, and actin filaments. This suggests that focal adhesions could play a key role as mechanosensors that respond to changes in intracellular or extracellular force. Several studies have demonstrated that there is a positive, linear correlation between focal adhesion size and the traction force a focal adhesion can exert on the extracellular matrix (Balaban *et al.*, 2001; Tan *et al.*, 2003; Goffin *et al.*, 2006) for many, but not all, focal adhesions. Furthermore, studies have shown that focal adhesions increase in size in response to external forces through the recruitment of additional focal adhesion proteins (Riveline *et al.*, 2001; Galbraith *et al.*, 2002; Sawada and Sheetz, 2002; Sniadecki *et al.*, 2007). However, the mechanism of how these focal adhesion proteins are recruited remains unclear.

Several studies have shown that direct application of force to purified domains of focal adhesion proteins exposes cryptic phosphorylation or ligand-binding sites. When amino acids 115-420 of p130Cas are bound to a latex substrate and stretched, there is a positive, linear correlation between the extent to which the latex is stretched and the amount of p130Cas115-420 phosphorylation (Sawada *et al.*, 2006). Similarly, when amino acids 482-889 of talin rod are mechanically stretched using magnetic tweezers, the binding of

vinculin head to talin482-889 increases with the amount of force applied to talin482-889 (del Rio *et al.*, 2009).

Together, these two studies indicate that some focal adhesions proteins may be able respond to changes in cytoskeletal tension by altering their ligand binding abilities. One could hypothesize that increased cytoskeletal tension results in increased ligand binding abilities in some focal adhesion proteins. If so, this would be a potential mechanism by which focal adhesion proteins are recruited when external forces are applied to a cell. This hypothesis could be extended to propose that increased cytoskeletal tension may uncover cryptic binding sites on talin for vinculin, leading to increased talin:vinculin interactions. If so, application of external force to a cell would result in increased talin:vinculin interaction, providing a potential mechanism for vinculin recruitment to focal adhesions when external force is applied to cells.

An alternative hypothesis to explain these findings could be the application of catch bond theory (Kramers, 1940; Bell 1978; Dembo *et al.*, 1988), and is supported by the several systems where it has been shown that intramolecular bond lifetimes can increase with force. Catch bonds have been confirmed experimentally for other adhesion proteins including actin binding to myosin (Guo *et al.*, 2006), fibronectin binding to integrin (Kong *et al.*, 2009), and P-selectin/L-selectin binding to P-selectin glycoprotein ligand 1 (Fritz et al., 1998; Evans et al., 2001; Marshall et al., 2003; Yago *et al.*, 2004; Barsegov et al., 2005). Using the catch bond theory, it has been proposed that the molecules involved undergo a structural conformation change that allows for firmer attachment

(Lou *et al.*, 2007, Yakovenko *et al.*, 2008). Likewise, one could hypothesize that increased cytoskeletal tension results in firmer attachment between vinculin and talin, allowing increased time for recruitment of additional focal adhesion proteins. This could be an alternative potential mechanism for the recruitment of to focal adhesions when external force is applied to cells.

Biaxial stretch of cytoskeletons has been used as a model to determine the stretch-dependent binding of exogenous proteins to cytoskeletons. These experiments found that paxillin and focal adhesion kinase (FAK) bind Triton-insoluble cytoskeletons in a stretch-dependent manner (Sawada and Sheetz, 2002). Both of these proteins are ligands for vinculin, are present in nascent focal adhesions, and remain present throughout focal adhesion maturation (Choi *et al.*, 2008). Interestingly, vinculin itself does not bind to Triton-insoluble cytoskeletons in a stretch-dependent manner (Sawada and Sheetz, 2002). Based on this data, I hypothesized that vinculin did not bind in a stretch-dependent manner because full-length vinculin is autoinhibited and unable to bind ligands. If an activated form of vinculin were incubated with Triton-insoluble cytoskeletons, the application of stretch to those cytoskeletons would cause activated vinculin to also be bound in a stretch-dependent manner. Furthermore, I hypothesized that the stretch-dependent binding of activated vinculin would occur because stretch applied to cytoskeletons would be sufficient to uncover previously cryptic binding sites on cytoskeletal talin for activated vinculin.

In this study, I build on my previous work where I developed digitonin-insoluble cytoskeletons created from *Vcl*-null mouse embryonic fibroblasts (MEFs). To determine whether my digitonin-insoluble cytoskeletons were appropriate for observing the stretch-dependent binding of exogenous proteins, I incubated digitonin-insoluble cytoskeletons with paxillin and probed for stretch-dependent binding. Using digitonin-insoluble cytoskeletons, I was able to reproduce the previously published result that paxillin binds in a stretch-dependent manner to cytoskeletons. I then tested the hypothesis that vinculin's ability to bind to a cytoskeleton is dependent on the accessibility of the talin-binding site on vinculin head. To do this, I incubated digitonin-insoluble *Vcl*-null cytoskeletons with full-length vinculin and mutants of vinculin lacking a tail domain (and therefore incapable of autoinhibition). Additionally, I tested the hypothesis that stretching a cytoskeleton would be sufficient to uncover previously cryptic binding sites on talin for vinculin. To do this, I incubated digitonin-insoluble *Vcl*-null cytoskeletons with mutants of vinculin containing an A50I point mutation that ablates binding of vinculin to talin and alpha-actinin (Bakolitsa *et al.*, 2004).

My results showed full-length vinculin shows no stretch-dependent binding to digitonin-insoluble cytoskeletons. This result is in agreement with previous studies (Sawada and Sheetz, 2002). However, it was found that domain 1 of vinculin (AA1-258) binds to digitonin-insoluble cytoskeletons in a stretch-dependent manner. This stretch-dependent binding is ablated when VD1 contains an A50I point mutation. These results prompted me to conduct imaging studies to determine the localization of VD1 in digitonin-insoluble cytoskeletons. Confocal microscopy showed that VD1 bound to cytoskeletons

binds in a punctate pattern unlike any known localization of vinculin. Furthermore, VD1 bound to cytoskeletons does not localize to focal adhesions. Attempts to recreate the stretch-dependent binding of VD1 using another truncation mutant of vinculin, vinculin head (Vh), did not reproduce the results found with VD1. My results lead to me conclude that the stretch-dependent binding of VD1 may reflect a spurious binding ability of this 30 kDa domain of vinculin and does not reflect a physiologic ability of activated vinculin to interact with cytoskeletal proteins in a stretch-dependent manner.

Methods:

Cell culture: *Vcl*-null mouse embryo fibroblasts (MEFs), a kind gift from Eileen Adamson, have been previously described (Xu *et al.*, 1998). Cells were maintained using phenol-free, high glucose Dulbecco's Modified Eagle Medium (DMEM, Gibco 31053) supplemented with 10% FBS (Hyclone) and 2 mM glutamine (Gibco 25030). HEK293 cells were provided by Dr. Peter Devreotes at Johns Hopkins University and were maintained in DMEM supplemented with 10% FBS (Hyclone). Cells were cultured at 37°C and 5% CO_2 on tissue culture plastic coated with 0.1% gelatin. For transfer onto other growth substrates, cells were enzymatically lifted from the culture dish using 0.04% trypsin (Gibco 15090).

Protein Transfection and/or Isolation: *EGFP-Vinculin (1-1066), EGFP-VD1, EGFP-VD1A50I, EGFP-Vh, EGFPVhA50I, and YFP-Paxillin:* HEK 293 cells were seeded on 0.1% gelatin-coated 100 mm dishes at 3 x 10^6 per plate; transfection was performed the

next day with 3 μg of plasmid DNA using Lipofectamine/Plus reagent (Invitrogen). HEK 293 cells were lysed 2-5 days after transfection with Stretch Assay Buffer (SAB) (20 mM HEPES, 150 mM NaCl, 4 mM $MgCl_2$, 0.05 mM $CaCl_2$, 0.5 mM ATP, 1 mM PMSF, 1 mM DTT, 0.02% BSA) with 2x protease inhibitor cocktail I (PIC I) and protease inhibitor cocktail II (PIC II)) from 1000x stocks . 1000x PIC I stock contained 1 mg/mL leupeptin, 2 mg/mL antipain, 10 mg/mL benzamidine, 10 KIU/mL aprotinin in H_2O. 1000x PIC II contained 1 mg/mL chymostatin, and 1 mg/mL pepstatin in dimethyl sulfoxide. Lysates were evaluated for fluorescence using a fluorimeter and a standard curve for EGFP/YFP concentration. *His-VD1, His-VD1A50I, His-Vh, His-VhA50I*: pET expression vectors were transformed into BL21(DE3) (Stratagene) competent cells. Bacterial cultures were grown to an OD_{600} of 0.6 in LB medium + 1% glucose at 37°C, and then induced with 0.5 mm isopropyl-1-thio-β-d-galactopyranoside (IPTG) for 4 hrs at 37°C. His-tagged VD1 and VD1A50I were isolated using nickel affinity chromatography with Ni-NTA resin (Qiagen) as described previously (Steimle *et al.*, 1999). *Thrombin cleavage of His-VD1 and His-VD1A50I:* His-tagged proteins were cleaved with biotinylated thrombin (Novagen, 1U per 3mg His-tagged protein) for 22 hrs at 4°C to remove their N-terminal His_6 tags. Proteins were dialyzed into Fusion Protein Storage (FPS) buffer (10 mM Tris, pH 7.5, 100 mM NaCl, 0.1 mM EDTA, 0.1 mM EGTA, 0.02% azide, 0.1% β-mercaptoethanol), supplemented with 2x PIC I and PIC II, and snap frozen in liquid nitrogen. Chicken gizzard vinculin was isolated as previously described (Johnson and Craig, 1994).

Cytoskeletal stretch assay: Silicone stretch chambers (B-Bridge) were coated with human plasma fibronectin at 20 μg/ml in Dulbecco's phosphate-buffered saline (DPBS, Gibco 33016) and plated with $2.5x10^5$ *Vcl*-null cells in DMEM supplemented with 10% FBS (Hyclone), 2 mM glutamine (Gibco 25030), penicillin (5 μg/mL), and gentamycin (20 μg/mL). After 2 days (~80% confluency), the cells were rinsed twice with warm DPBS (37°C) and crosslinked to the fibronectin substrate using the cell impermeable reversible crosslinker 3,3´-Dithiobis(sulfosuccinimidylpropionate) (Sigma) at 1 mM dissolved in DPBS for 15 min at 37°C. The cells were rinsed 2x and the crosslinking reaction quenched with 50 mM Tris-HCl in DPBS pH 7.5 for 15 min at 37°C. The cells were then rinsed 2x with Stretch Assay Buffer (SAB) (20 mM HEPES, 150 mM NaCl, 4 mM $MgCl_2$, 0.05 mM $CaCl_2$, 0.5 mM ATP, 1 mM PMSF, 1 mM DTT, 0.02% BSA) before being incubated with 0.003% digitonin in SAB+ (SAB buffer supplemented with 2x PIC I and 2x PIC II) to create digitonin-insoluble cytoskeletons. The resulting cytoskeletons were rinsed once with SAB+ and stretched 15% uniaxially on a Strex mechanical strain instrument (B-Bridge). Exogenous proteins diluted in SAB+ were immediately added and the system was stretched for 5 min at 37°C. Stretched cytoskeletons were then rinsed with SAB+ before adding 100 μL of 0.1% Triton X-100 diluted in SAB+. Samples were scraped from the silicone substrate using the rounded edge of a pipette tip and stored at 0°C.

Co-immunoprecipitation for talin-VD1 interaction: 100 μL of Ni-NTA beads were coupled to His-TnRAvi (AA 432-884, 5 VBSs) and His-TnR1655 (1655-1882, no VBSs) for 1.5 hrs at room temperature in 1 mL of 100-μM protein solutions for a final concentration of 1 mM talin rod construct on Ni-NTA beads. 1 mM TnR coupled to Ni-

NTA beads (TnRAvi: 200 μg on 4 μL of beads, TnR1655: 242 μg on 4 μL of beads) was incubated with a 3-μM solution of thrombin-cleaved VD1 (Tc-VD1) in a 100 μL reaction. All necessary dilutions were done in SAB+. After incubations ranging from 2-60 min, the beads were rinsed 2x with SAB+ and bound complexes were eluted with 2x laemmli sample buffer. After washing, the samples were eluted with Laemmeli sample buffer and run on 4-12% Bis-Tris gels in MES buffer. Gels were imaged using the 700 nm detector on a Licor Infrared Scanner.

Immunoblotting: Western blots were developed with species-specific infrared secondary antibodies (Li-Cor) per the manufacturer's instructions. Murine monoclonal G-11 anti-vinculin was obtained from Sigma and used at a 1:250 dilution. Murine monoclonal C4 anti-actin was a gift from Dr. Jim Lessard. Affinity purified rabbit C22 anti-talin was raised against C-terminal 22 amino acids of talin rod. C4 and C22 were used at a 1:4000 dilution.

Microscopy: *Vcl*-null cells were plated onto either poly-L-lysine treated coverslips coated with 20 μg/mL human plasma fibronectin or fibronectin-coated stretch chambers and allowed to reach ~80% confluency. Cytoskeletons were created as described above and fixed using 4% paraformaldyhyde in ddH_2O pH 7.3 at room temperature for 30 min and blocked using 2% goat serum. G-11 anti-vinculin was used at 1:50 and C22 anti-talin at 1:4000. Coverslips were mounted in Prolong Gold Anti-Fade solution with DAPI. Confocal images were acquired on an upright LSM 510 (Carl Zeiss, Germany) microscope using Zeiss AIM software. Digital images were imported into Adobe

Photoshop for figure preparation. All other images were acquired on a Nikon Eclipse Ti using Elements software.

Results:

I have previously described how I developed an assay to test the binding of exogenous eGFP-tagged proteins to digitonin-insoluble cytoskeletons (Chapter 3, Figure 3-4). I characterized this assay by determining whether digitonin-insoluble cytoskeletons created from *Vcl*-null MEFs could reproduce the published finding that paxillin binds in a stretch-dependent manner to cytoskeletons. To do this, I incubated *Vcl*-null digitonin-insoluble cytoskeletons with 100-nM YFP-paxillin created by transfecting HEK cells. Using Western blots, I determined the binding of YFP-paxillin to unstretched and stretched *Vcl*-null digitonin-insoluble cytoskeletons that had been stretched 15% uniaxially using a commercial Strex machine. Over three experiments, I found that YFP-paxillin bound in a stretch-dependent manner to digitonin-insoluble cytoskeletons, with stretch inducing a 3-fold increase in the binding of YFP-Paxillin (Figure 4-1). Since YFP-paxillin bound in a stretch-dependent manner, I concluded that my assay created cytoskeletons similar to those used in a previous study to identify focal adhesion proteins that bound in a stretch-dependent manner (Sawada and Sheetz, 2002). I then decided to use this assay to test the hypothesis that vinculin's ability to bind to a cytoskeleton is dependent on the accessibility of the talin-binding site on vinculin head.

My first experiment in this study was to determine whether full-length vinculin showed stretch-dependent binding to *Vcl*-null digitonin-insoluble cytoskeletons using my assay. To do, this I incubated *Vcl*-null digitonin-insoluble cytoskeletons with 100-nM eGFP-vinculin created by transfecting HEK cells. Using Western blots, I determined the binding of eGFP-vinculin to unstretched and stretched *Vcl*-null digitonin-insoluble cytoskeletons that had been stretched 15% uniaxially using a commercial Strex machine. Over three experiments, I found that eGFP-vinculin did not bind in a stretch-dependent manner to digitonin-insoluble cytoskeletons (Figure 4-1). This result was in agreement with the results of a previous study showing that full-length vinculin does not bind in a stretch-dependent manner to Triton-insoluble cytoskeletons (Sawada and Sheetz, 2002).

Figure 4-1: Initial results on the binding of exogenous proteins to digitonin-insoluble cytoskeletons replicated previously published results regarding YFP-paxillin and full-length vinculin. *Vcl*-null cells were plated on fibronectin-coated, silicone-based cell culture chambers and allowed to recover for 48 hrs. Digitonin-insoluble cytoskeletons were then created and incubated with exogenous proteins diluted in SAB+ at 37°C for 5 min. Cytoskeletons were either left unstretched or stretched 15% uniaxially using a commercial Strex machine. Samples were scraped from the chambers in a 0.1% Triton solution and western blots were quantified using infrared densitometry. A) Representative Western blots showing binding of exogenous proteins to digitonin-insoluble cytoskeletons in the unstretched and stretched mechanical states. B) Quantitation of Western blots for each exogenous protein. Three experiments were quantified for each protein. Bars indicate the S.E.M. In addition to replicating previously published results, these findings suggest that vinculin's ability to bind to talin or alpha-actinin (demonstrated by the VD1A50I mutation data) play a role in the stretch-dependent binding of VD1 to cytoskeletons.

A

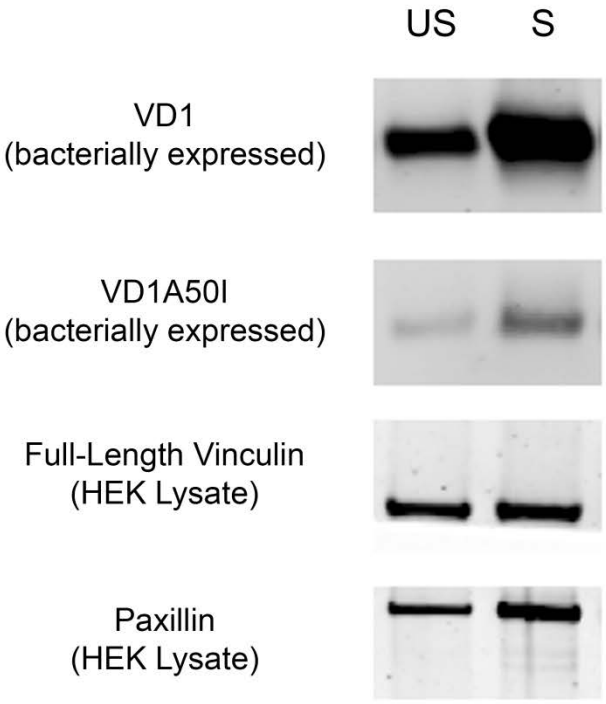

B

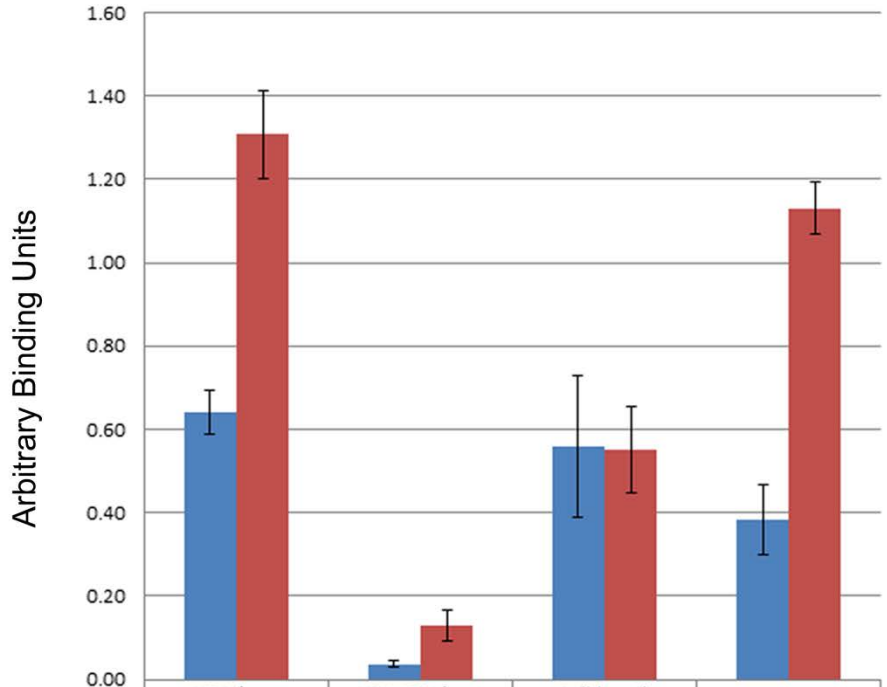

	VD1 from bacterial purification	VD1A50I from bacterial purification	Full-length Vinculin from HEK Lysate	Paxillin from HEK Lysate
Unstretched	0.64	0.04	0.56	0.38
Stretched	1.31	0.13	0.55	1.13

I then decided to test the hypothesis that vinculin's ability to bind to a cytoskeleton is dependent on the accessibility of the talin-binding site on vinculin head. To do this, I wished to use a truncation mutant of vinculin that contains only domain 1 (VD1) and is therefore incapable of autoinhibition and contains a talin-binding site. However, before I could analyze the binding of VD1 to unstretched and stretched cytoskeletons, I first wanted to determine whether recombinant VD1 is capable of binding talin under the conditions of my assay. The Craig lab has unpublished data showing that 0.5-1-μM purified recombinant VD1 purified from bacteria is capable of co-immunoprecipitating 90% of 100-nM eGFP-talin from transfected HEK cell lysate. However, these experiments had also shown that successful co-immunoprecipitation of the majority of eGFP-talin in HEK lysates required overnight incubation at 37°C. I interpreted this data as indicating that since VD1 has a high affinity for talin in solution, exogenous recombinant VD1 purified from bacteria might be capable of binding accessible talin in *Vcl*-null digitonin-insoluble cytoskeletons. However, it was unclear on what timescale this interaction could occur.

To determine whether recombinant VD1 in solution might be capable of binding immobilized talin present in *Vcl*-null digitonin-insoluble cytoskeletons, and the time period needed for this binding, I attempted to co-immunoprecipitate soluble recombinant VD1 purified from bacteria with TnRAvi, a portion of talin rod (AA482-911) that contains 5 vinculin binding sites that are cryptic within full-length talin rod. As a negative control, I attempted to co-immunoprecipitate soluble, recombinant VD1 purified from bacteria with TnR1655, a portion of talin rod (AA1655-1882) that contains no

vinculin binding sites. Ni-NTA beads were coupled with these talin rod constructs at high concentration (1 mM) to mimic the localization of talin in focal adhesions. In each of these co-immunoprecipitationss, 1-mM TnR coupled to Ni-NTA beads (200 μg TnR construct in 4 μL of beads) were incubated with 3-μM VD1 in stretch assay buffer with protease inhibitors (SAB+) at 37°C. My results show that co-immunoprecipitation of VD1 with TnRAvi occurs within 2 min of incubation (Figure 4-2). There was no detectable co-immunoprecipitation of VD1 with TnR1655. I interpreted this to mean that 3-μM soluble recombinant VD1 would be capable of binding any available vinculin binding sites on cytoskeletal talin on the time scale of a minute. I chose to allow soluble recombinant VD1 to incubate with cytoskeletons for 5 min in the hopes of maximizing potential binding between VD1 and cytoskeletal talin. This incubation time was also similar to the incubation times used by Sawada (2 min) to determine the stretch-dependent binding of exogenous paxillin and FAK to Triton-insoluble cytoskeletons (Sawada and Sheetz, 2002).

Figure 4-2: VD1 is capable of binding to talin rod constructs with available vinculin binding sites. 100 µL of Ni-NTA beads were coupled to His-TnRAvi (AA 432-884, 5 VBSs) and His-TnR1655 (1655-1882, no VBSs) for 1.5 hrs at room temperature in 1 mL of 100-µM protein solutions for a final concentration of 1-mM talin rod construct on Ni-NTA beads. 1-mM TnR (200 µg TnRAvi on 4 µL of beads; 242 µg TnR1655 on 4 µL of beads) was incubated with a 3-µM solution of thrombin-cleaved recombinant VD1 (Tc-VD1) purified from bacteria in a 100 µL reaction at 37°C. After washes, the samples were eluted with Laemmeli sample buffer and run on 4-12% Bis-Tris gels in MES buffer. The gel was stained with Coomassie blue and imaged using the 700 nm detector on a Licor Infrared Scanner. Lanes: 1) Benchmark ladder 2) Protein standards for TnRAvi and VD1, 3) 2 min co-immunoprecipitation between TnAvi and VD1, 4) Negative control. Co-immunoprecipitation between Tn1655 and VD1.

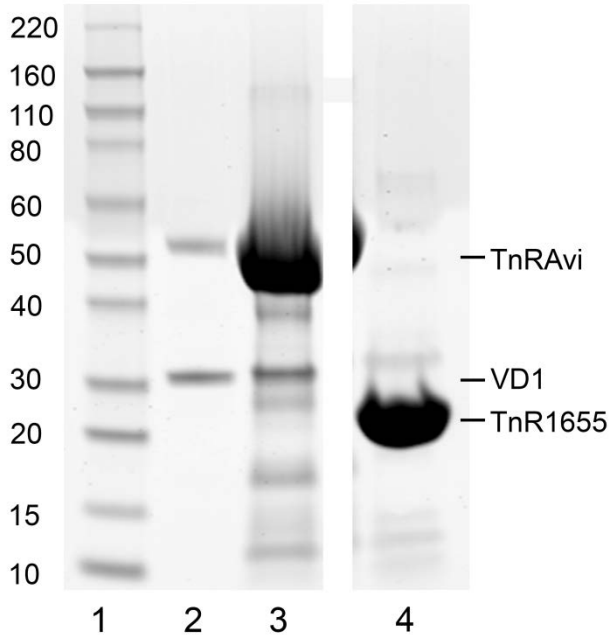

I then proceeded to incubate *Vcl*-null digitonin-insoluble cytoskeletons with 3-μM recombinant VD1 purified from bacteria. A preliminary experiment showed that 3-μM and 1-μM recombinant VD1 purified from bacteria demonstrated similar stretch-dependent binding to unstretched and stretched *Vcl*-null digitonin-insoluble cytoskeletons that had been stretched 15% uniaxially using a commercial Strex machine (data not shown). To conserve protein, I proceeded to repeat the experiments using 1-μM recombinant VD1 purified from bacteria. Over three experiments, I found that 1-μM recombinant VD1 purified from bacteria bound in a stretch-dependent manner to digitonin-insoluble cytoskeletons, with stretch inducing a 2-fold increase in the binding of recombinant VD1 (Figure 4-1).

I then probed the binding of a vinculin mutant, VD1A50I, that is domain 1 of vinculin containing a mutation that ablates vinculin:talin and vinculin:alpha-actinin interactions (Bakolitsa *et al.*, 2004). Using VD1A50I would allow me to determine whether the stretch-dependent binding of VD1 was occurring through binding to either talin or alpha-actinin. I incubated *Vcl*-null digitonin-insoluble cytoskeletons with 1-μM recombinant VD1A50I purified from bacteria. Using Western blots, I determined the binding of 1-μM recombinant VD1A50I to unstretched and stretched *Vcl*-null digitonin-insoluble cytoskeletons that had been stretched 15% uniaxially using a commercial Strex machine. Over three experiments, I found that recombinant VD1A50I did not bind in a stretch-dependent manner to digitonin-insoluble cytoskeletons (Figure 4-1). Additionally, the binding of recombinant VD1A50I was lower than the binding of recombinant VD1. I interpreted these results to mean that recombinant VD1 was binding to cytoskeletons

through its talin/alpha-actinin binding site, and that the application of stretch was potentially uncovering cryptic binding sites on cytoskeletal talin for vinculin.

However, there were caveats to comparing the stretch-dependent binding of vinculin versus VD1 to digitonin-insoluble cytoskeletons. In this initial study, paxillin and vinculin were isolated from HEK lysates and exposed to cytoskeletons at 100-nM while VD1 and VD1A50I were purified from bacteria and used at 1-μM concentrations. These different protein sources reflect technical limitations in our ability to easily purify these four different proteins using the same method. Paxillin cannot be isolated from bacterial cultures. Purification of full length vinculin from bacteria often yields numerous breakdown products. VD1 and VD1A50I are very difficult to transfect into mammalian cells (low transfection rate), and transfected cells yield lysates with extremely low concentrations of eGFP-VD1 or eGFPVD1A50I. Before committing to other more difficult methods of protein purification to address these issues, I decided to determine where the recombinant VD1 purified from bacteria bound in *Vcl*-null digitonin-insoluble cytoskeletons. This would allow me to determine whether the stretch-dependent binding of vinculin was specific and whether the VD1 was binding to already formed focal adhesions in the digitonin-insoluble cytoskeletons.

To determine the localization of VD1 when incubated with digitonin-insoluble cytoskeletons, I created two sets of samples. First, *Vcl*-null cells were plated onto fibronectin-coated coverslips and digitonin-insoluble cytoskeletons were created as previously described. These coverslips were then incubated with 1-μM recombinant

VD1 purified from bacteria for 5 min at 37°C. As a control, I created *Vcl*-null digitonin-insoluble cytoskeletons on coverslips that were incubated in SAB+ buffer with no recombinant VD1 protein. These coverslips were immunostained for endogenous talin and VD1. Attempts to image these coverslips using widefield microscopy proved difficult because the VD1 signal was blurry and no single z-plane yielded clear images of the VD1 localization. I interpreted this as indicating that the VD1 signal may have a 3-dimensional aspect and that VD1 may be binding throughout the entirety of the digitonin-insoluble cytoskeletons. The coverslips were then imaged with confocal microscopy (Figure 4-3).

Figure 4-3: Confocal micrographs show that VD1 does not localize to the focal adhesions of digitonin-insoluble cytoskeletons. (A-F) *Vcl*-null digitonin-insoluble cytoskeletons were made on fibronectin-coated coverslips as previously described. (A-C) *Vcl*-null digitonin-insoluble cytoskeletons were incubated with 1-μM recombinant VD1 purified from bacteria in SAB+. (D-F) *Vcl*-null digitonin-insoluble cytoskeletons were incubated with SAB+ containing no recombinant VD1. Vinculin was detected with murine monoclonal G-11 anti-vinculin (1:250). Talin was detected with affinity-purified rabbit C22 anti-talin (1:2000). Murine anti-vinculin was detected with 488 donkey anti-mouse Ig (DaMIg) secondary antibody. Rabbit C22 anti-talin was detected with RRX DaRIg. The nucleus was stained with DAPI. All images were taken with a 60x DIC objective, N.A. = 1.4. Red bar = 30 μm. (A-C) Control stainings for murine monoclonal G-11 anti-vinculin and 488 donkey anti-mouse Ig secondary antibody. (A) Incubation with murine monoclonal G-11 anti-vinculin (G-11) alone results in some background staining and autofluorescence (B) Incubation with 488 donkey anti-mouse Ig secondary antibody alone indicates that *Vcl*-null digitonin-insoluble cytoskeletons have some autofluorescence (C) *Vcl*-null digitonin-insoluble cytoskeletons immunostained for both endogenous talin (red) and VD1 (green) show that there is some background fluorescence in cytoskeletons alone. Negative control. (D-F) Staining for localization of exogenous recombinant VD1 on *Vcl*-null digitonin-insoluble cytoskeletons. (D) Incubation with murine monoclonal G-11 anti-vinculin (G-11) alone results in some background staining and autofluorescence. (E) Incubation with 488 donkey anti-mouse Ig secondary antibody alone indicates that *Vcl*-null digitonin-insoluble cytoskeletons show very little background secondary staining. (F) *Vcl*-null digitonin-insoluble cytoskeletons incubated with 1-μM recombinant VD1 immunostained for both endogenous talin (red) and VD1 (green) show that exogenous recombinant VD1 binds specifically to cytoskeletons and does not colocalize with talin.

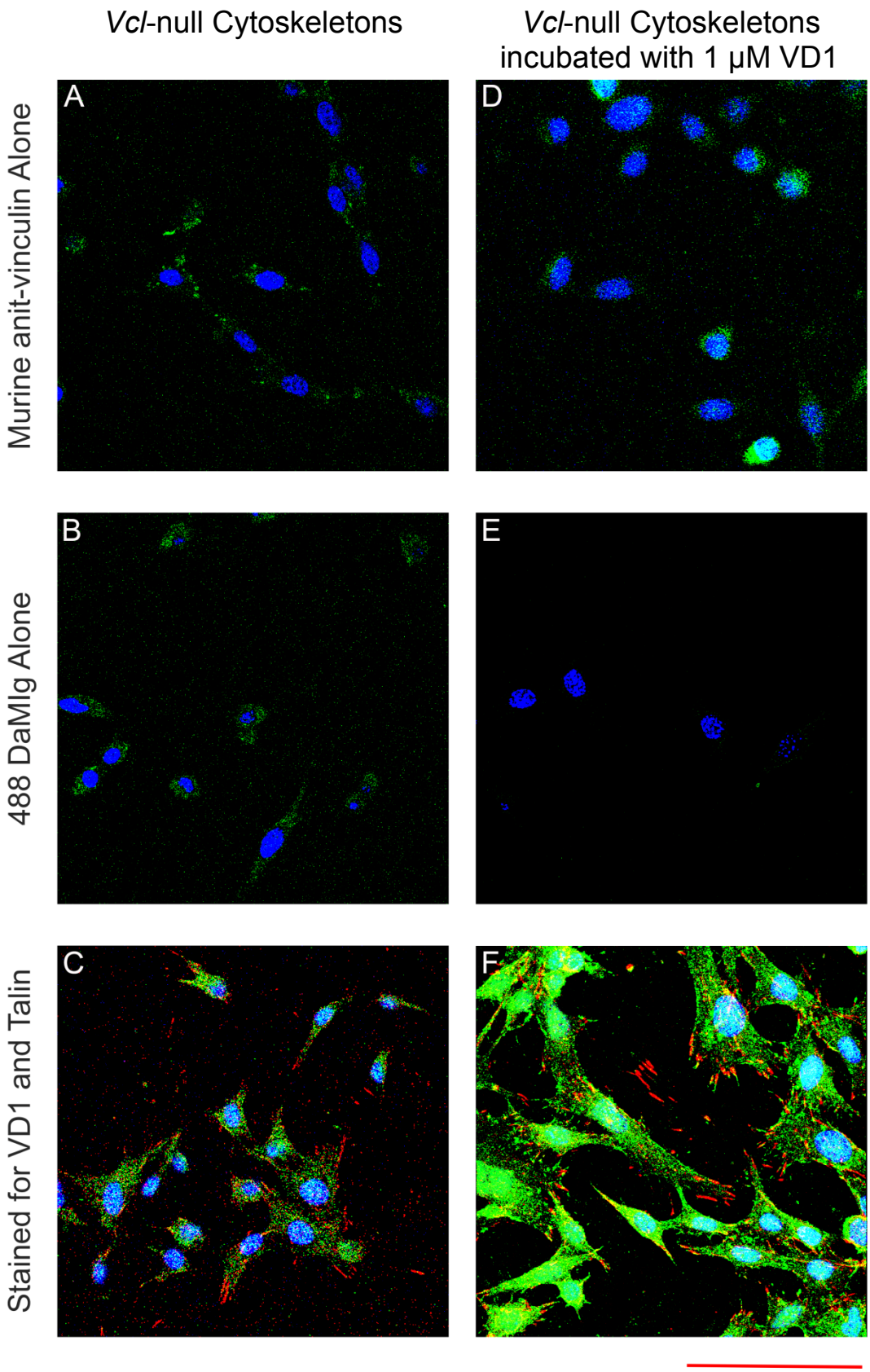
Vcl-null Cytoskeletons
Vcl-null Cytoskeletons incubated with 1 μM VD1
Murine anit-vinculin Alone
488 DaMIg Alone
Stained for VD1 and Talin
A
B
C
D
E
F

Figure 4-4: Confocal micrograph showing the punctate, cytoskeletal binding of exogenous VD1 to *Vcl*-null cytoskeletons. This is an enlarged picture of Figure 4-3F. *Vcl*-null digitonin-insoluble cytoskeletons were made on fibronectin-coated coverslips as previously described and then incubated with 1-μM recombinant VD1 purified from bacteria in SAB+ for 5 min at 37°C. Vinculin was detected with murine monoclonal G-11 anti-vinculin (1:250). Talin was detected with affinity-purified rabbit C22 anti-talin (1:2000). Murine anti-vinculin was detected with 488 donkey anti-mouse Ig secondary antibody. Rabbit C22 anti-talin was detected with RRX DaRIg. The nucleus was stained with DAPI. All images were taken with a 60x DIC objective, N.A. = 1.4. Red bar = 30 μm. Exogenous recombinant VD1 binds to cytoskeletons and the not fibronectin-coated coverglass. The binding pattern of exogenous recombinant VD1 is punctate and not consistent with any known localization of vinculin. VD1 largely does not colocalize with talin.

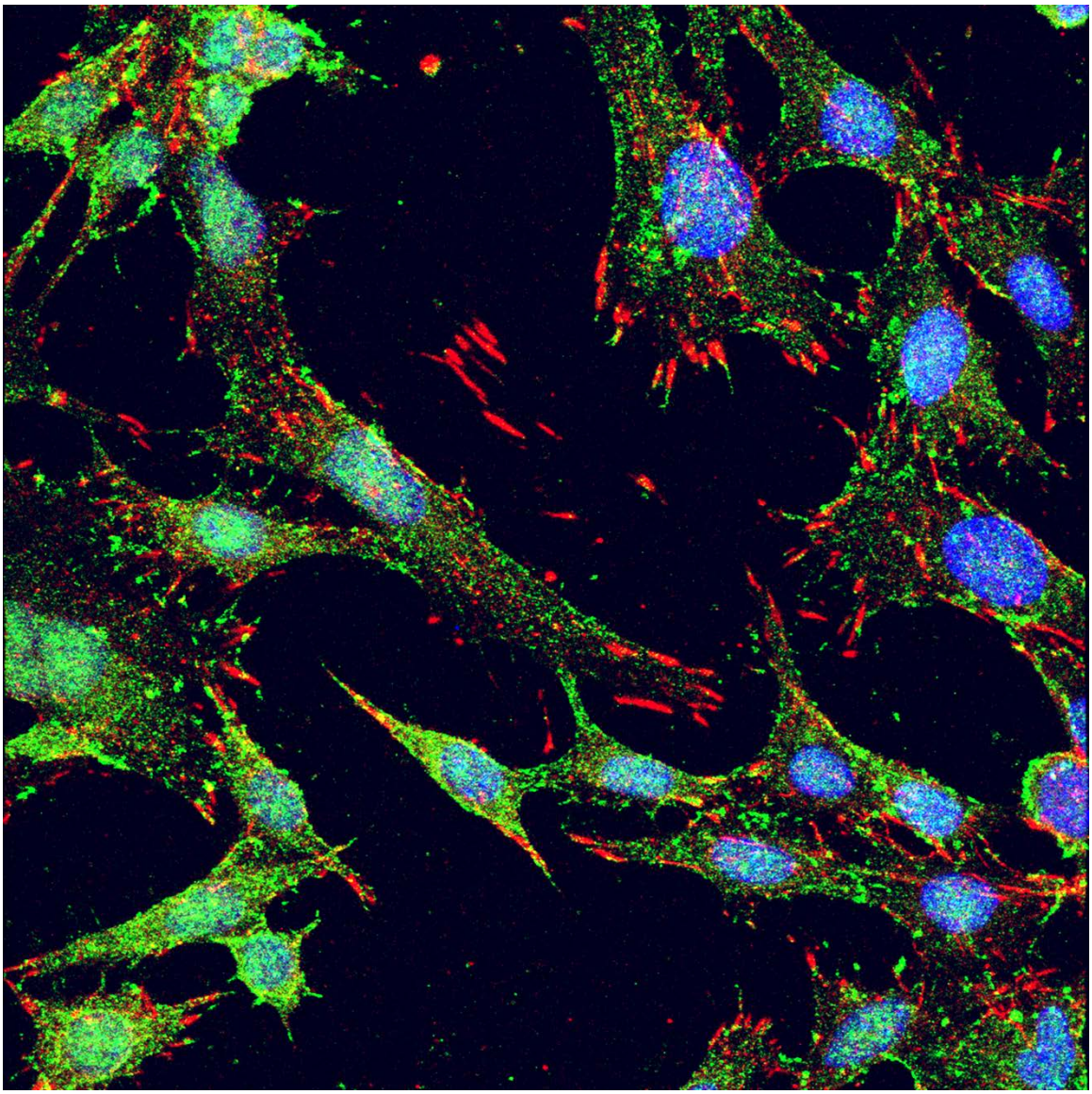

These confocal images showed that recombinant VD1 bound to cytoskeletons with no detectable binding to the fibronectin-coated coverslips. However, the binding of recombinant VD1 was punctate and did not correspond with any known localization pattern of vinculin. Although a very minor amount of VD1 did co-localize with talin, it is likely that this was due to random coincidence. Since these images were taken using cytoskeletons adherent to coverslips, I decided to image cytoskeletons adherent to silicone-based cell culture chambers and determine if VD1 colocalization with talin increased with stretch. Attempts to compare the localization of VD1 in unstretched and stretched cytoskeletons uncovered the technical limitation that confocal microscopy cannot be performed through these silicone substrates with sufficient resolution to clearly image focal adhesions (Figure 4-5). The different refractive indexes of PDMS (the silicone base of commercially available stretch chambers) versus German coverglass (1.4 versus 1.515) (MIT, 2012) leads to a greater dispersion of light and low-quality images. However, these images also showed stretch-dependent binding of VD1 to digitonin-insoluble cytoskeletons.

Figure 4-5: Confocal microscopy of unstretched and stretched *Vcl*-null cytoskeletons incubated with exogenous 1-μM VD1. *Vcl*-null cytoskeletons were made on fibronectin-coated silicone-based cell culture chambers as previously described and then incubated with 1-μM recombinant VD1 purified from bacteria in SAB+ for 5 min at 37°C. Vinculin was detected with murine monoclonal G-11 anti-vinculin (1:250). Talin was detected with affinity-purified rabbit C22 anti-talin (1:2000). Murine anti-vinculin was detected with 488 donkey anti-mouse Ig secondary antibody. Rabbit C22 anti-talin was detected with RRX DaRIg. The nucleus was stained with DAPI. All images were taken with a 60x DIC objective, N.A. = 1.4. Red bar = 20 μm. Cytoskeletons were imaged through silicone to determine the differences in VD1 localization between unstretched and stretched cytoskeletons. However, a larger pinhole than optimal pinhole size was required to image through silicone, resulting in lower resolution using the same magnification objective. (A) Unstretched *Vcl*-null cytoskeleton incubated with VD1. (B) Stretched *Vcl*-null cytoskeleton incubated with VD1.

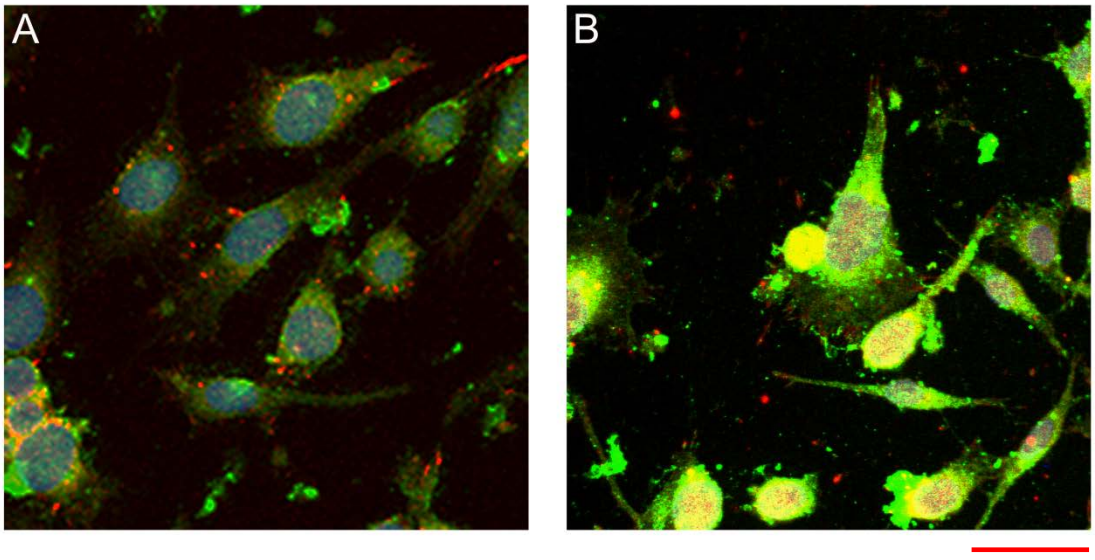

These images (Figures 4-3, 4-4, and 4-5) showed that exogenous recombinant VD1 did not localize to the focal adhesions of digitonin-insoluble cytoskeletons. This prompted me to image the localization of full-length vinculin bound to digitonin-insoluble cytoskeletons (Figure 4-6). To do so, *Vcl*-null cells were plated onto German glass coverslips and *Vcl*-null digitonin-insoluble cytoskeletons were created as previously described. These coverslips were then incubated with 100-nM eGFP-vinculin from transfected HEK lysate for 5 min at 37°C. As a control, I created digitonin-insoluble cytoskeletons from *Vcl*-null cells that had been transiently transfected with eGFP-vinculin. These coverslips were immunostained for endogenous talin and VD1. The coverslips were then imaged using widefield fluorescence (Figure 4-6). These images showed that eGFP-vinculin transfected into *Vcl*-null cells colocalizes with talin and is found in focal adhesions. However, exogenous eGFP-vinculin from transfected HEK cell lysate binds to cytoskeletons but does localize to focal adhesions.

Figure 4-6: Unlike transiently transfected eGFP-vinculin, exogenous eGFP-vinculin from HEK lysate does not localize to focal adhesions when incubated with digitonin-insoluble cytoskeletons. (A-C) *Vcl*-null cells transiently transfected with eGFP-vinculin were converted to digitonin-insoluble cytoskeletons as previously described. (D-F) *Vcl*-null digitonin-insoluble cytoskeletons were made on fibronectin-coated coverslips as previously described and then incubated with 100-nM eGFP-vinculin from transfected HEK cell lysate in SAB+ for 5 min at 37°C. Vinculin was detected with murine monoclonal G-11 anti-vinculin (1:250). Talin was detected with affinity-purified rabbit C22 anti-talin (1:2000). Murine anti-vinculin was detected with 488 donkey anti-mouse Ig secondary antibody. Rabbit C22 anti-talin was detected with RRX DaRIg. The nucleus was stained with DAPI. All images were taken with a 40x ELWD Phase objective, N.A. = 0.6. Red bar = 20 μm. (A-C) *Vcl*-null cells transiently transfected with eGFP-vinculin. (A) *Vcl*-null cells with transiently transfected eGFP-vinculin show endogenous talin in focal adhesions. (B) *Vcl*-null cells with transiently transfected eGFP-vinculin show endogenous talin in focal adhesions. (C) Overlay of the endogenous talin and transfected eGFP-vinculin signals show that talin and eGFP-vinculin colocalize. (D) Endogenous talin in *Vcl*-null cytoskeletons localizes to focal adhesions. (E) Exogenous eGFP-vinculin isolated from transfected HEK cell lysate binds to cytoskeletons but does not localize to focal adhesions. (F) Overlay of the endogenous talin and exogenous eGFP-vinculin signals shows that endogenous talin and exogenous eGFP-vinculin do not colocalize.

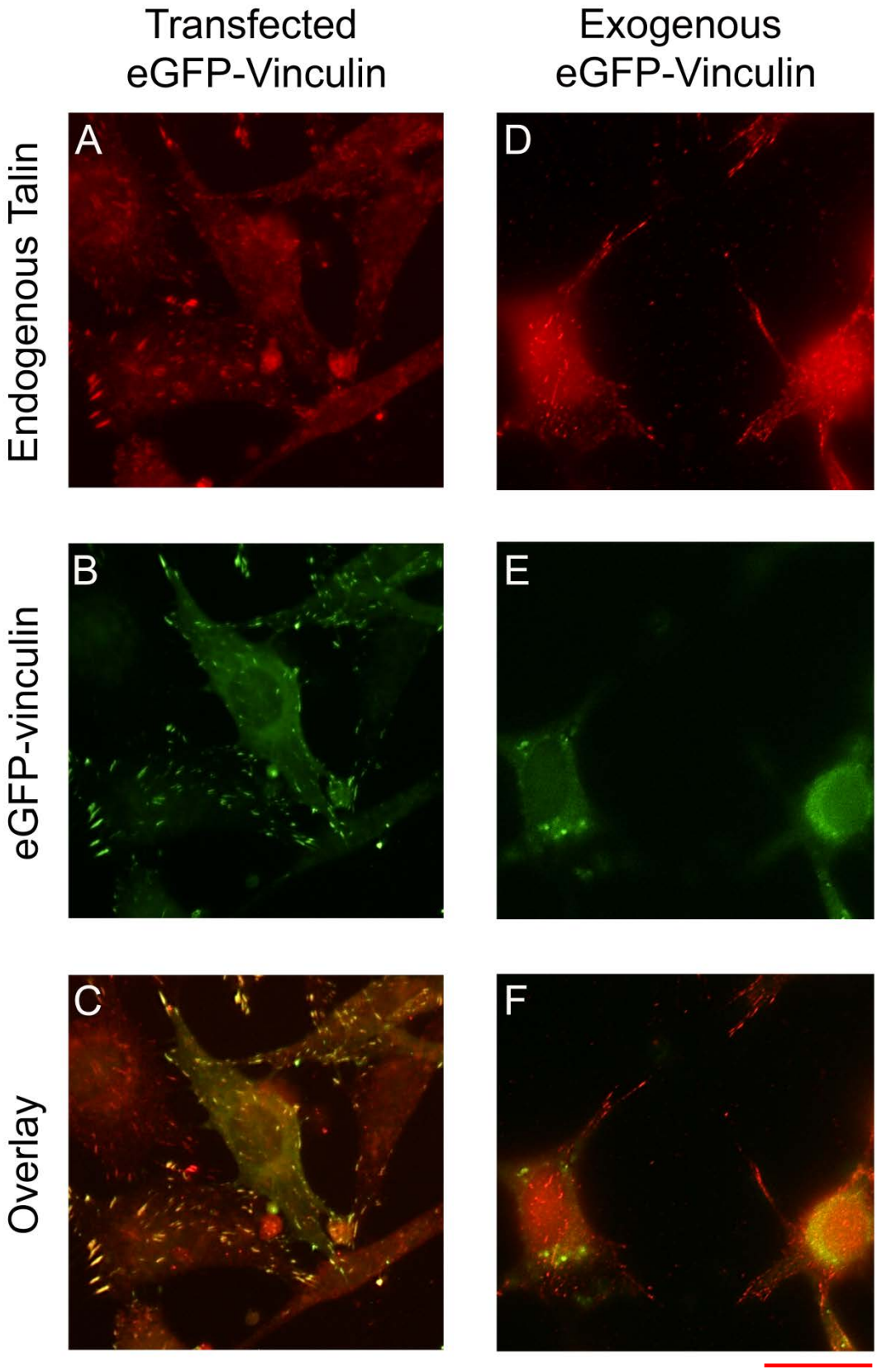
Transfected
eGFP-Vinculin
Exogenous
eGFP-Vinculin
Endogenous Talin
eGFP-vinculin
Overlay
A
B
C
D
E
F

The images showing the localization of exogenous recombinant VD1 (Figure 4-4) and exogenous eGFP-vinculin from transfected HEK cell lysate (Figure 4-6, D-F) made me suspect that my initial findings showing stretch-dependent binding of VD1 to *Vcl*-null cytoskeletons was an artifact of the conditions of my assay and some spurious ability of VD1 to interact with cytoskeletons. To confirm my earlier findings with VD1 and VD1A50I, I attempted to express both VD1 and VD1A50I in HEK cells in order to repeat the binding assays. However, I found that it was not possible to collect eGFP-VD1 or eGFP-VD1A50I lysates with concentrations near 100 nM. As an alternative, I expressed vinculin head (Vh, AA 1-851) and a mutant of vinculin head also containing the A50I mutation (VhA50I) in HEK cells. I considered Vh an acceptable substitution for VD1 since it is also a truncation mutant of vinculin capable of binding talin and alpha-actinin that lacks the tail domain. As a result, Vh is incapable of autoinhibition.

To determine whether eGFP-tagged vinculin-truncation mutants would also show stretch-dependent binding to digitonin-insoluble cytoskeletons, a panel of stretch experiments was completed in triplicate (Figure 4-7). These experiments compared the binding of exogenous full-length vinculin to the binding of exogenous Vh and VhA50I using proteins from bacterial purifications, HEK lysates, and in one experiment, vinculin and vinculin head isolated from chicken gizzard. These experiments showed no stretch-dependent binding of vinculin head (Vh) and no change in binding between Vh and VhA50I. Of all the experiments I conducted on the stretch-dependent binding of exogenous proteins to digitonin-insoluble cytoskeletons, only two showed stretch dependence: paxillin (which is a previously published result) and VD1. This indicated

that the stretch-dependent binding of VD1 observed earlier, while replicable, likely does not reflect an actual biological function of activated vinculin.

Figure 4-7: The stretch-dependent binding of recombinant VD1 purified from bacteria likely does not reflect a biological function of activated vinculin. *Vcl*-null cells were plated on fibronectin-coated, silicone-based cell culture chambers and allowed to recover for 48 hrs. Digitonin-insoluble cytoskeletons were then created and incubated with exogenous proteins diluted in SAB+ at 37°C for 5 min. Cytoskeletons were either left unstretched or were stretched 15% uniaxially using a commercial Strex machine. Samples were scraped from the chambers in a 0.1% Triton solution and western blots were quantified using infrared densitometry. The prefix "Tc-" indicates a recombinant protein purified from bacteria and thrombin cleaved to remove the 6xHis-tag. All proteins purified from bacteria were used at a concentration of 1 μM diluted in SAB+. The prefix "EGFP-" indicates proteins present in transfected HEK cell lysate and these proteins were used at a concentration of 100 nM, as determined by fluorimetry and standard curves generated with eGFP standards. Chicken gizzard vinculin had some break down during purification, but the relative binding of full-length vinculin versus vinculin head could be distinguished and compared on western blot. Data for eGFP-vinculin, YFP-paxillin, Tc-VD1, Tc-VD1A50I, and chicken gizzard vinculin were collected using a commercial Strex machine that stretched the silicone-based cell culture chambers 15%. All other experiments were stretched on a previously characterized manual device that stretched the silicone-based cell culture chambers 14.1%. All experiments were repeated 3 times with the exception of the assay performed with chicken gizzard vinculin. Bars indicate the S.E.M.

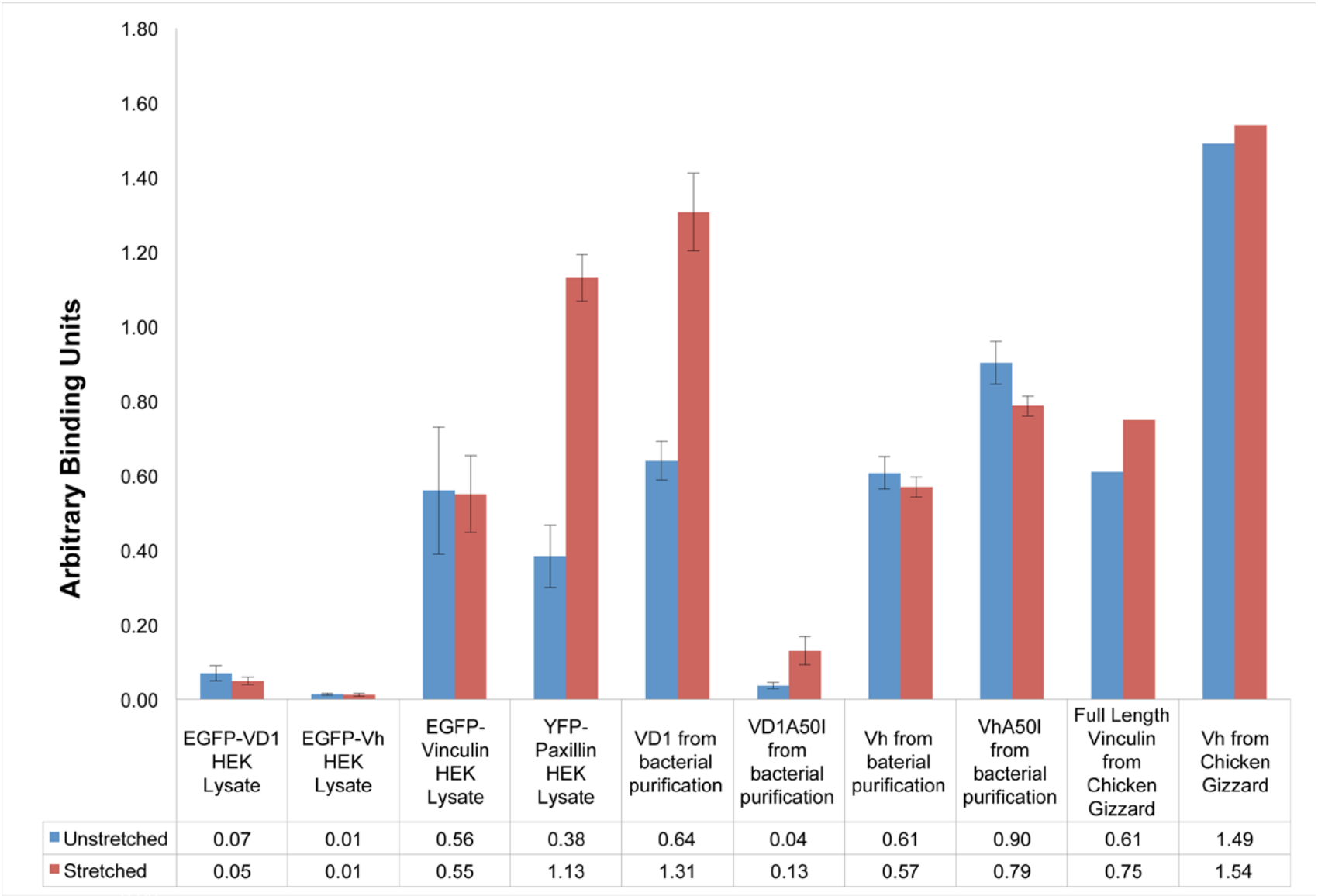

	EGFP-VD1 HEK Lysate	EGFP-Vh HEK Lysate	EGFP-Vinculin HEK Lysate	YFP-Paxillin HEK Lysate	VD1 from bacterial purification	VD1A50I from bacterial purification	Vh from baterial purification	VhA50I from bacterial purification	Full Length Vinculin from Chicken Gizzard	Vh from Chicken Gizzard
Unstretched	0.07	0.01	0.56	0.38	0.64	0.04	0.61	0.90	0.61	1.49
Stretched	0.05	0.01	0.55	1.13	1.31	0.13	0.57	0.79	0.75	1.54

Discussion:

Prior to this work, a previous study had shown that full-length vinculin did not bind in a stretch-dependent manner to cytoskeletons while paxillin and FAK, two other focal adhesion proteins, did. I began this study hoping to determine whether activated vinculin could bind in a stretch-dependent manner to cytoskeletons. To pursue this question, I created *Vcl*-null digitonin-insoluble cytoskeletons and incubated them with YFP-paxillin from transfected HEK cell lysate. These experiments reproduced the previously published finding that YFP-paxillin binds to cytoskeletons in a stretch-dependent manner. I interpreted this as evidence that my method of creating *Vcl*-null digitonin-insoluble cytoskeletons and introducing uniaxial stretch (both from commercial and manual devices) was sufficient to probe the binding of vinculin and various vinculin mutants to cytoskeletons. I followed my experiments with YFP-paxillin with experiments exploring the stretch-dependent binding of eGFP-vinculin from transfected HEK cell lysate. I also explored the binding of recombinant VD1 and VDA50I, two truncation mutants of vinculin that lack the tail domain of vinculin and are therefore incapable of autoinhibition. VD1A50I was used a control to determine whether any stretch-dependent binding of VD1 to cytoskeletons could be occurring through VD1:talin or VD1:alpha-actinin interactions.

Initial data in this study supported my hypothesis, with exogenous VD1 showing increased binding with stretch while exogenous vinculin showed no stretch-dependent binding (Figure 4-1). However, imaging studies showed that VD1 bound to

cytoskeletons in a punctate pattern that is not consistent with any known localization pattern of vinculin. Furthermore, VD1 did not localize to focal adhesions. Experiments using another truncation mutant of vinculin (Vh and VhA50I, AA 1-851) incapable of autoinhibition also showed no stretch-dependent binding. Based on these results, I suspect that while the stretch-dependent binding of VD1 is replicable, it is likely related to a spurious binding ability of VD1. VD1 crystalizes (Izard *et al.*, 2004) and is an intact subdomain of vinculin head capable of binding both Vt and talin (Gilmore *et al.*, 1992; Bakolitsa *et al.*, 2004). However, the Craig lab has unpublished data showing that VD1 has a tendency to aggregate in solution. This may occur because of the exposed hydrophobic surfaces on VD1 that are usually buried when full-length vinculin is autoinhibited or when full-length vinculin interacts with its ligands (Bakolitsa *et al.*, 2004). Perhaps this tendency to self-associate in some way mediated the stretch-dependent-binding of VD1 to cytoskeletons. It is possible that the VD1:VD1 interaction is stronger than the VD1:talin interaction, although there are no published studies on this. Aggregation of VD1 would explain the punctate binding pattern of VD1 to cytoskeletons (Figure 4-4). Due to the availability of alternative autoinhibition mutants of vinculin, we did not take steps to characterize the extent or source of VD1-mutant aggregation or why VD1 bound in a stretch-dependent manner to *Vcl*-null digitonin-insoluble cytoskeletons while Vh did not.

I acknowledge that the developed system is very much *in vitro* and heavily dependent on the buffer conditions for each step. However, the conditions were sufficient to replicate previously published data showing paxillin's increased binding to stretched

cytoskeletons. Based on those results, it seemed reasonable to use this same cytoskeletal system to study the role of vinculin autoinhibition in regulating vinculin's binding to cytoskeletons. In fact, I considered my system an improvement over the published cytoskeletal assay to detect stretch-dependent binding because my assay probes the binding of vinculin using cytoskeletons generated from *Vcl*-null mouse embryonic fibroblasts (MEFs). This ensures that any effect would be due only to the response of exogenous vinculin. Indeed, this system showed that exogenous proteins bound to only digitonin-insoluble cytoskeletons and not to the fibronectin-coated substrates (Figures 4-3 thru 4-6). I am interpreting these results as evidence that while the cytoskeletons I generated may have been intact enough to prompt paxillin binding, the process of cell permeabilization and the creation of the cytoskeletons might have a) washed away a key localization factor for vinculin or b) uncovered less specific or different vinculin ligands, prompting diffuse binding of vinculin and abrogating any localization to talin-containing focal adhesions.

References:

Bakolitsa, C., D.M. Cohen, L.A. Bankston, A.A. Bobkov, G.W. Cadwell, L. Jennings, D.R. Critchley, S.W. Craig, and R.C. Liddington. 2004. Structural basis for vinculin activation at sites of cell adhesion. *Nature*. 430:583-586.

Balaban, N.Q., U.S. Schwarz, D. Riveline, P. Goichberg, G. Tzur, I. Sabanay, D. Mahalu, S. Safran, A. Bershadsky, L. Addadi, and B. Geiger. 2001. Force and focal adhesion assembly: a close relationship studied using elastic micropatterned substrates. *Nature cell biology*. 3:466-472.

Barsegov, D.T. 2005. Dynamics of unbinding of cell adhesion molecules: transition from catch to slip bonds. *Proceedings of the National Academy of Sciences of the United States of America*. 102:1835-1839.

Bell, G.I. 1978. Models for the specific adhesion of cells to cells. Science. 200: 618-627.

Choi, C.K., M. Vicente-Manzanares, J. Zareno, L.A. Whitmore, A. Mogilner, and A.R. Horwitz. 2008. Actin and alpha-actinin orchestrate the assembly and maturation of nascent adhesions in a myosin II motor-independent manner. *Nature cell biology*. 10:1039-1050.

del Rio, A., R. Perez-Jimenez, R. Liu, P. Roca-Cusachs, J.M. Fernandez, and M.P. Sheetz. 2009. Stretching single talin rod molecules activates vinculin binding. *Science (New York, N.Y.* 323:638-641.

Dembo, D.C., D.C. Torney, D. Hammer. 1988. The reaction-limited kinectics of membrane-to-surface adhesion and detachment. Proceedings of the Royal Academy of Sciences B: Biological Sciences. 234: 55-83.

Dumbauld, D.W., T.T. Lee, A. Singh, J. Scrimgeour, C.A. Gersbach, E.A. Zamir, J. Fu, C.S. Chen, J.E. Curtis, S.W. Craig, and A.J. Garcia. 2013. How vinculin regulates force transmission. *Proceedings of the National Academy of Sciences of the United States of America*. 110:9788-9793.

Evans, A.L., S. Simon. 2001. Chemically distinct transition states govern rapid dissociation of single L-selectin bonds under force. *Proceedings of the National Academy of Sciences of the United States of America*. 98: 3784-3789.

Fritz, A.G., D.A. Katopodis. 1998. Force-mediated kinetics of single P-selectin/ligand complexes observed by atomic force microscopy. *Proceedings of the National Academy of Sciences of the United States of America*. 95:12283-12288.

Galbraith, C.G., K.M. Yamada, and M.P. Sheetz. 2002. The relationship between force and focal complex development. *The Journal of cell biology*. 159:695-705.

Gilmore, A.P., P. Jackson, G.T. Waites, and D.R. Critchley. 1992. Further characterisation of the talin-binding site in the cytoskeletal protein vinculin. *Journal of cell science*. 103 (Pt 3):719-731.

Goffin, J.M., P. Pittet, G. Csucs, J.W. Lussi, J.J. Meister, and B. Hinz. 2006. Focal adhesion size controls tension-dependent recruitment of alpha-smooth muscle actin to stress fibers. *The Journal of cell biology*. 172:259-268.

Guo, B., W.H. Guilford. 2006. Mechanics of actomyosin bonds in different nucleotide states are tuned to muscle contraction. *Proceedings of the National Academy of Sciences of the United States of America*. 103:9844–9849.

Izard, T., G. Evans, R.A. Borgon, C.L. Rush, G. Bricogne, and P.R. Bois. 2004. Vinculin activation by talin through helical bundle conversion. *Nature*. 427:171-175.

Johnson, R.P., and S.W. Craig. 1994. An intramolecular association between the head and tail domains of vinculin modulates talin binding. *The Journal of biological chemistry*. 269:12611-12619.

Kong, F., A.J. García, C. Zhu. 2009. Demonstration of catch bonds between an integrin and its ligand. Journal of Cell Biology. 185:1275-1284.

Kramers, H.A. 1940. Brownian motion in a field of force and the diffusion model of chemical reactions. *Physica.* 7:284-304.

Lou, J.Z., C. Zhu. 2007. A structure-based sliding-rebinding mechanism for catch bonds. *Biophysical Journal.* 92:1471-1485.

Marshall, B.T., M. Long, C. Zhu. 2003. Direct observation of catch bonds involving cell-adhesion molecules. *Nature.* 423:190-193.

MIT. 2012. Materials Project Database.

Riveline, D., E. Zamir, N.Q. Balaban, U.S. Schwarz, T. Ishizaki, S. Narumiya, Z. Kam, B. Geiger, and A.D. Bershadsky. 2001. Focal contacts as mechanosensors: externally applied local mechanical force induces growth of focal contacts by an mDia1-dependent and ROCK-independent mechanism. *The Journal of cell biology*. 153:1175-1186.

Sawada, Y., and M.P. Sheetz. 2002. Force transduction by Triton cytoskeletons. *The Journal of cell biology*. 156:609-615.

Sawada, Y., M. Tamada, B.J. Dubin-Thaler, O. Cherniavskaya, R. Sakai, S. Tanaka, and M.P. Sheetz. 2006. Force sensing by mechanical extension of the Src family kinase substrate p130Cas. *Cell*. 127:1015-1026.

Sniadecki, N.J., A. Anguelouch, M.T. Yang, C.M. Lamb, Z. Liu, S.B. Kirschner, Y. Liu, D.H. Reich, and C.S. Chen. 2007. Magnetic microposts as an approach to apply

forces to living cells. *Proceedings of the National Academy of Sciences of the United States of America*. 104:14553-14558.

Steimle, P.A., J.D. Hoffert, N.B. Adey, and S.W. Craig. 1999. Polyphosphoinositides inhibit the interaction of vinculin with actin filaments. *The Journal of biological chemistry*. 274:18414-18420.

Tan, J.L., J. Tien, D.M. Pirone, D.S. Gray, K. Bhadriraju, and C.S. Chen. 2003. Cells lying on a bed of microneedles: an approach to isolate mechanical force. *Proceedings of the National Academy of Sciences of the United States of America*. 100:1484-1489.

Xu, W., H. Baribault, and E.D. Adamson. 1998. Vinculin knockout results in heart and brain defects during embryonic development. *Development (Cambridge, England)*. 125:327-337.

Yago, T., J.H. Wu, R.P. McEver. 2004. Catch bonds govern adhesion through L-selectin at threshold shear. Journal of Cell Biology. 166: 913–923.

Yakovenko, O., S. Sharma, W.E. Thomas. FimH forms catch bonds that are enhanced by mechanical force due to allosteric regulation. *Journal of Biological Chemistry*. 283:11596-11605.

Chapter 5:

Future Directions

In my opinion, future work based on the experiments presented in this thesis should be based on the work presented in "Chapter 3: The Role of Vinculin Autoinhibition in the Recruitment of Vinculin to Uniaxially Stretched Cytoskeletons". However, in order to proceed with this work, several limitations to my system would have to be overcome. In this chapter, I will present both the understood and the predicted barriers to advancing this work, as well as several potential alterations in experimental approach that may be interesting to the reader.

First and foremost, the reader should understand by this point that the device as presented is manually stretched and secured. While this approach was both cost-effective and sufficient for the questions I posed, its simplicity inherently limits future researchers from further exploring the role of vinculin in the cellular response to external stretch. As previously explained, the act of stretching the silicone chamber causes a change in the coordinates and focal plane of the cells initially photographed. The delay caused by compensating for this position change lead to me to collect images at 5 min intervals to ensure that the same timepoints could be collected during each experiment. Additionally, the slight shift in images limited the evaluation of each data image to only peripheral focal adhesions instead of the much-preferred approach of tracking the evolution of individual focal adhesions.

Ideally, a future system would eliminate both of these shortcomings and allow the constant photography of focal adhesions before stretch, during sustained stretch, and after the release of stretch so that the evolution of vinculin in focal adhesions can be further

studied. Current Nikon Elements software allows pre-programming of objective positioning as well as settings for both the camera and image capture. It may be worth the time investment for future researchers to characterize the exact shift of their stretch substrates before data collection and compensate for these movements in order to meet the above-specified goals. An alternative approach would involve designing a simple device that introduces stretch from both ends of the silicone chamber, ideally resulting in minimal x,y movement of the chamber. This would involve a relatively simple modification of the current device design. Once accomplished, the microscope user would only have to compensate for changes in the z-position of the sample. This simple change from a one-sided to a two-sided stretch system alone would result in higher time resolutions and the preservation of additional focal adhesions for analysis. A final alternative approach would be to alter the source of stretch completely by developing an approach similar to that of Riveline *et al.* (Riveline *et al.*, 2001), where a fibronectin-coated pipette is placed on top of a cell and moved laterally to introduce external stretch. Such a system would have to be extensively characterized because it is a complete departure from my approach. However, it is an alternative worth consideration because 1) modification of the silicone-based stretch device as described above may still not yield high enough time resolutions and 2) such an approach would allow the use of total internal reflection (TIRF) microscopy.

An additional shortcoming of my previous approach was my dependence on the *Vcl*-null cell-line for my experiments. The benefit of this cell-line is that a true negative control is available for all experiments. However, this cell-line is difficult to both culture and

transfect, and our lab (in collaboration with others) has been unable to make stable cell-lines permanently expressing all of the desired vinculin mutants. As an alternative, I began using a transient transfection protocol based on an electroporation approach used by our collaborators (Dumbauld *et al.*, 2013). However, this approach still results in large amounts of cell death, low transfection rates, and attempts to co-transfect multiple constructs are rarely successful. Development of a method to express multiple fluorescently-tagged protein constructs in *Vcl*-null cells would allow one to image the evolution of a focal adhesion in response to external stretch, instead of limiting the work to only collecting data on the response of vinculin.

Finally, I would propose that future researchers build upon the work of Peng *et al.* (Peng *et al.*, 2011), a group of researchers who published a drug cocktail composed of jasplakinolide, latrunculin B, and Y27632 that inhibits actin disassembly, actin polymerization, and myosin II-based rearrangements, respectively. Their work showed that this cocktail, referred to as JLY, functions within seconds to preserve cell morphology and inhibit dynamic actin changes in neutrophil-like HL-60 cells, human fibrosarcoma HT1060 cells, and mouse NIH 3T3 fibroblast cells. Most interestingly, they also showed that while actin dynamics are arrested, JLY does not inhibit the ability of cells to respond to external stimuli. Neutrophil-like HL-60 cells treated with JLY had no changes in basal calcium levels or the magnitude or kinetics of calcium release. Furthermore, the JLY cocktail was used to show that actin dynamics are essential for the spatial persistence of Rac activity at the leading edge during random migration.

Together, these results generate some interesting questions about how JLY could be used study the response of vinculin to external stretch. Of course, despite having been shown to be effective in mouse NIH 3T3 human fibroblasts, the effects of the JLY cocktail would have to be characterized in the *Vcl*-null cell-line, as well as in each cell-line expressing one of the various vinculin constructs. The ability to co-transfect each cell-line expressing a vinculin construct with YFP-actin would allow one to also follow actin dynamics throughout the application of stretch. Then, the researcher would be able to design an assay to determine whether any observed changes in vinculin-containing focal adhesions in response to stretch were also dependent on functional actin dynamics. One could hypothesize that since vinculin tail binds actin (see Chapter 1), actin dynamics would be necessary to ensure additional vinculin could be activated in order to respond to the stress imposed on the cell by external stretch. An alternative hypothesis could argue that, by freezing actin dynamics, actin would remain bound to vinculin tail, leaving vinculin active and capable of binding additional partners, strengthening the focal adhesion complex.

The caveat to this line of research is that any vinculin-dependent, stretch-dependent changes are happening on a timescale comparable to the effects of the JLY cocktail. While Peng *et al.* reported their JLY cocktail having an effect "within seconds", most of their reported data is on the timescale of minutes. Therefore, if stretch-dependent changes are occurring on the timescale of seconds or less, these changes may occur before the JLY cocktail takes effect. This would render the JLY cocktail inappropriate for studying the role of actin dynamics during the application of external stretch.

References:

Dumbauld, D.W., T.T. Lee, A. Singh, J. Scrimgeour, C.A. Gersbach, E.A. Zamir, J. Fu, C.S. Chen, J.E. Curtis, S.W. Craig, and A.J. Garcia. 2013. How vinculin regulates force transmission. *Proceedings of the National Academy of Sciences of the United States of America*. 110:9788-9793.

Peng, G., S. Wilson, O. Weiner. 2011. A pharmacological cocktail for arresting actin dynamics in living cells. *Molecular Biology of the Cell.* 22: 3986-3994.

Riveline, D., E. Zamir, N.Q. Balaban, U.S. Schwarz, T. Ishizaki, S. Narumiya, Z. Kam, B. Geiger, and A.D. Bershadsky. 2001. Focal contacts as mechanosensors: externally applied local mechanical force induces growth of focal contacts by an mDia1-dependent and ROCK-independent mechanism. *The Journal of cell biology*. 153:1175-1186.

CURRICULUM VITAE

Leilani Sharpe
501 St. Paul Street, Apt. 1512, Baltimore, MD 21202
Cell: (443) 554-0454
leilani.sharpe@jhmi.edu

Educational History:

M.D. Expected	2014	Johns Hopkins University School of Medicine
Ph.D. Expected	2014	Biochemistry, Cell, and Molecular Biology Program Johns Hopkins School of Medicine Mentor: Susan W. Craig, Ph.D.
B.S.	2004	Biochemistry and Genetics University of Washington
B.S.	2004	Analytical Chemistry University of Washington
A.A.	2001	Associate of Arts South Puget Sound Community College

Other Professional Experience:

Graduate student 2007-2009 Laboratory of Fizan Abdullah
Department of Pediatric Surgery, Johns Hopkins School of Medicine
Development of a PDMS scaffold to support differentiation of primary alveolar cells in microculture.

Research Rotation 2007 Laboratory of Ben Ho Park
Department of Pathobiology, Johns Hopkins School of Medicine
Interdisciplinary project the role of Notch-3 in the oncogenesis of breast cancer.

Research rotation 2005 Laboratory of Subroto Chatterjee
Department of Biochemistry, Johns Hopkins School of Medicine
Interdisciplinary project to determine the role of apo-1 in apoptosis and lipid synthesis in macrophages.

Undergraduate research 2003-2004 Laboratory of Brian Reid
Human Biology Division, Fred Hutchinson Cancer Research Center
Interdisciplinary project to determine whether the extent of Barrett's Esophagus metaplasia was associated with decreased patient survival.

Undergraduate research 2001-2003 Laboratory of David Kimmelman
Department of Developmental Biology, University of Washington
Determination of the role of FGF-16 in migration of neural crest cells from somite 16 using a zebrafish model.

Scholarships, Fellowships, or other external funding:

2004-2014	Medical Scientist Training Program (MSTP) Fellow	Johns Hopkins
2001-2003	Diversity Enhancement Scholarship Recipient	Costco-University of Washington

Academic and other honors at Hopkins and elsewhere:

2011 Otology/Neuro-Otology Special Intern Roosevelt Hospital

Publications:

Camp M., Chang D.C., Zhang Y., Arnold M., **Sharpe L.** Gabre-Kidan A., Bathurst M.A., Abdullah F. Provider density and health system facility factors and their relationship to rates of pediatric perforated appendicitis in US counties. *Arch Surg.* Dec 2010. 145:1139-44. PMID 21173286.

Abdullah, F., Gabre-Kidan, A., Zhang, Y., **Sharpe, L.,** Chang, D.C. Report of 2,087,915 surgical admissions in U.S. children: inpatient mortality rates by procedure and specialty. *World J Surg*. Dec 2009. 33:2714-21. PMID 19795164.

Nalayanda, D.D., Puleo, C., Fulton, W.B., **Sharpe, L.M.**, Wang, T.H., Abdullah, F. An open-access microfluidic model for lung-specific functional studies at an air-liquid interface. *Biomed Microdevices*. May 2009. 11:1081-9. PMID 19484389.

Presentations:

Sharpe, L.M., Nalayanda, D.D., Abdullah, F. Micro-culture of murine fetal pulmonary cells in a multi-chamber varying flow microfluidic chip. *Biomedical Engineering Society Annual Meeting*. 2007.

Posters:

Sharpe, L.M., Nalayanda, D.D., Abdullah, F. Engineering an artificial alveolar-capillary membrane: A novel continuously perfused model within microchannels. *American Pediatric Surgery Association Annual Meeting*. 2009.

Service and leadership:

2004 – 2013	University of Washington GenOM Project, Alumni STEM diversity mentor
2004 – 2013	Student National Medical Organization (SNMA)
2009 - 2013	Junior Biological Scientists, STEM Mentor and Instructor
2009 - 2012	Johns Hopkins Biomedical Scholars Association, Instructor
2004 - 2009	US Dream Academy, Mentor and Instructor

Non-academic pursuits:

I am a classically trained operatic soprano and still train at the New York studio of Dr. Jean Ronald LaFond. I love exploring new and different kinds of music and connecting new works to those with which I am already familiar. Often very disparate works can be linked by a common theme. Finding these themes and seeing how they carry over from one style of music to another makes unfamiliar works more approachable and a joy to learn more about. In particular, I am fascinated by the history of how American popular music transitioned from the opera, to the operetta, and into the foundations of the modern American "pop" musical. They use very different methods to portray similar stories of ambition, love, and achievement.